Synthesis and application of hydroxyapatite and fluoroapatite to scorodite encapsulation

Lydia Katsarou

Department of Mining and Materials Engineering

McGill University

Montreal

Canada

August 2011

A thesis submitted to McGill University in partial fulfilment of the requirements of the degree of Master of Engineering

Abstract

Recent research has investigated the precipitation of crystalline scorodite ($FeAsO_4 \cdot 2H_2O$) as a method to stabilise arsenic for disposal due to its good stability performance according to EPA's TCLP test. It has been determined, however, that scorodite releases arsenic in significant concentrations under alkaline pH or under anoxic conditions. With the objective of enhancing the stability of scorodite, its encapsulation with minerals inert to pH and redox potential variations is considered in this work. Such encapsulation materials are hydroxyapatite (HAP-$Ca_5(PO_4)_3OH$) and fluoroapatite (FAP-$Ca_5(PO_4)_3F$), the two most stable of the calcium phosphates. The work described in this thesis includes: 1) the preparation of hydroxyapatite and fluoroapatite powders and their characterisation, 2) the synthesis of crystalline scorodite under atmospheric conditions and its characterisation, 3) the encapsulation of scorodite with hydroxyapatite and fluoroapatite, and 4) the long term stability testing of the encapsulated solids. Hydroxyapatite and fluoroapatite were prepared first by homogeneous precipitation from a metastable solution, to which "Ca" and "PO_4" source reagents of different concentrations were added at variable rates. The crystallinity of the produced materials was found to increase with temperature. Crystalline scorodite was produced by seeded crystallisation in ambient pressure. For the encapsulation of the scorodite particles various methods of direct precipitation by controlled supersaturation were attempted, by adjusting the pH and adding/mixing feed solutions of individual calcium and phosphate source reagents. Heterogeneous deposition of HAP on scorodite proved rather difficult. Optimum results were obtained via prior conditioning of the scorodite substrate in a calcium solution and employment of low agitation regime and high (37 ºC rather than 22 ºC) temperature. The stability tests were done in oxic and anoxic environments and their results demonstrated that the encapsulated solids had enhanced stability, since the release of arsenic was lower than it was for naked scorodite. The presence of gypsum was found to help reduce the release of arsenic further as well as phosphorus under oxic, but not anoxic conditions due to possible interaction with the sulphite ions used as reducing agent.

Résumé

Des recherches récentes ont caractérisé la précipitation de la scorodite ($FeAsO4{\cdot}2H2O$) comme méthode de stabilisation de l'arsenic à cause de la bonne stabilité de ce composé lorsque mesuré par le test TCLP de l'EPA. Par contre, ces travaux ont montré que la scorodite relâche plus d'arsenic dans des solutions basiques ou dans des conditions anoxiques. Ce projet se concentre donc sur la stabilisation de la scorodite par son encapsulation par des minéraux inertes aux variations de pH et d'ORP. Les deux matériaux considérés pour l'encapsulation sont hydroxyapatite (HAP-$Ca_5(PO_4)_3OH$) et fluorapatite (FAP-$Ca_5(PO_4)_3F$), les deux phosphates de calcium les plus stables. Les résultats décrits dans cette thèse incluent : 1) la préparation de poudre d' hydroxyapatite, de fluorapatite et leurs caractérisations; 2) la synthèse de scorodite cristalline sous air et sa caractérisation; 3) l'encapsulation de scorodite avec l'hydroxyapatite et la fluorapatite; 4) l'évaluation de la stabilité à long terme des solides encapsulés. L'hydroxyapatite et la fluorapatite ont été préparées à partir d'une solution métastable dans laquelle des réactifs contenant du calcium et des phosphates ont été ajoutés à différents rythmes. Les résultats ont montrés que la cristallinité des composés produits augmente avec la température. La scorodite cristalline fut produite par cristallisation amorcée à pression ambiante. L'encapsulation par différentes techniques de précipitation directes fut investiguée en variant le pH et le taux d'addition des réactifs. La déposition hétérogène d'hydroxyapatite sur la scorodite fut difficile à réaliser. Les meilleurs résultats furent obtenus par l'addition de scorodite dans une solution de calcium, une faible agitation et une haute température (37 ºC au lieu de 22 ºC). Les tests de stabilité effectués en présence et en absence d'oxygène ont montré que les solides encapsulés avaient une plus grande stabilité (moins de rejet d'arsenic que ceux non encapsulés). La présence de gypse avait aussi comme effet de diminuer le rejet d'arsenic et de phosphore en présence d'oxygène seulement, probablement à cause d'une interaction avec les sulfites utilisés comme agents réducteurs.

Acknowledgments

I would like to thank Professor George Demopoulos for his enthusiasm when I decided to apply and his help and support throughout my studies as my supervisor. Thank you for your time and your understanding.

I am also thankful to all the members of the McGill hydrometallurgy group. Especially Sonia, Jessica, Levente, Renaud, Derek, Cecile, Cesar, Nicolas, Guobin. I am grateful to Ranjan Roy and Andrew Golsztajn for their help with the ICP, Monique Riendeau for the help on different characterisation techniques, Mario Gomez for the help on Raman, Benedetto Marelli for the help with the FTIR, Petr Fiurasek for the TGA, Line Mongeon for helping me with the SEM.

This work was supported by the Natural Sciences and Engineering Research Council of Canada (NSERC) and Teck Metals, for which I am deeply thankful.

The support and help from my family is highly acknowledged, and I would also like to thank my friends and the McGill International Student Network for making my stay in Montreal interesting and pleasant.

Table of Contents

Abstract i

Résumé ii

Acknowledgments iii

Table of Contents iv

List of figures vii

List of tables xi

Chapter 1. Introduction 1

Chapter 2. Literature Review 4

2.1 The arsenic problem 4

2.2 Arsenic removal and fixation 5

2.2.1 Scorodite Synthesis 6

2.2.2 Stability of Scorodite 6

2.2.2.1 Oxic environment 6

2.2.2.2 Anoxic environment 8

2.3 Crystallisation theory 8

2.3.1 Nucleation 10

2.3.1.1 Primary homogeneous nucleation 11

2.3.1.2 Primary heterogeneous nucleation 12

2.3.1.3 Supersaturation control 12

2.3.2 Crystal growth 13

2.4 Encapsulation 14

2.5 Calcium Phosphates-Apatites 14

2.5.1 Solubility and stability 15

2.5.2 Synthesis of hydroxyapatite and fluoroapatite 19

2.5.3 Substitution of OH^- with F^- and the effect on solubility 22

2.6 Previous use of calcium phosphates for coating purposes 23

2.6.1 Scorodite encapsulation studies 24

Chapter 3. Experimental 26

3.1 Chemicals 26

3.2 Experimental Setup 27

3.3 Chemical analysis 30

3.4 Preparation of scorodite 33
3.4.1 Preparation of Scorodite Seed 33
3.4.1.1 Characterisation 33
3.4.2 Production of Scorodite under Atmospheric Pressure Conditions 36
3.4.2.1 Characterisation 39
3.5 Stability Testing 42
Chapter 4. Results and Discussion 43
4.1 Homogeneous precipitation of hydroxyapatite and fluoroapatite 43
4.1.1 Hydroxyapatite precipitation 43
4.1.1.1 Characterisation 44
4.1.2 Determination of the metastable zone of hydroxyapatite 49
4.1.3 Fluoroapatite precipitation 51
4.1.4 Characterisation 51
4.1.5 Determination of the metastable zone of fluoroapatite 53
4.1.6 Substitution of OH^- with F^- 54
4.2 Encapsulation 56
4.2.1 Procedures 57
4.2.1.1 Conditioning of scorodite 57
4.2.1.2 Nucleation step 57
4.2.1.3 Growth step 58
4.2.1.4 “Nancollas” step 58
4.2.2 Encapsulation of scorodite with hydroxyapatite 59
4.2.2.1 Nucleation 59
4.2.2.2 Combined Nucleation & Growth 64
4.2.3 Encapsulation of scorodite with fluoroapatite 71
4.2.3.1 Nucleation 71
4.2.3.2 Growth 73
4.3 Stability testing 74
4.3.1 Stability of HAP 74
4.3.2 Stability of HAP-encapsulated scorodite 77
4.3.2.1 Oxic Environment 77
4.3.2.2 Anoxic Environment 79

4.3.3 Stability of FAP-encapsulated scorodite 82
4.3.3.1 Oxic Environment 82
4.3.3.2 Anoxic Environment 83
Chapter 5. Conclusions 85
Chapter 6. References 87
Appendix A. OLI Software Calculations 93
Appendix B. TGA curves 96
Appendix C. Encapsulation data tables 98
Appendix D. Stability testing data 99
Appendix E. pH and e_h variation graphs for stability tests 112
Appendix F. Onomatology and organisation of the experiments 120

List of figures

Figure 1: Comparison of the final arsenic concentrations from different studies [8-10, 40-42] of scorodite stability at 22-25 °C [9]. 7
Figure 2: Solubility-supersaturation diagram explaining the stable metastable and labile zones for a salt with inverse solubility (adapted from [43]). 9
Figure 3: Classification of nucleation mechanisms (adapted from [45]). 10
Figure 4: Overall free energy change resulting from an embryo nucleating homogeneously from solution, according to equation (2.4) (reproduced from [47]). 11
Figure 5: Generalised nucleation rate diagram showing the dominant areas for homogeneous, heterogeneous and surface nucleation (reproduced from [48]). 13
Figure 6: Solubility isotherms of calcium orthophosphate phases in the system $Ca(OH)_2$-H_3PO_4-H_2O at 37 °C (Taken from [59]). 16
Figure 7: Solubility isotherms of calcium phosphate phases in the ternary system Ca^{2+}-PO_4^{3-}-H_2O at 25 °C (taken from [12]). 16
Figure 8: Solubility Isotherms for hydroxyapatite, fluoroapatite and calcium fluoride at fluoride concentrations in solution of 1 and 10 mg/L, respectively. For FAP and CaF_2 the solid lines represent the saturation calcium concentrations at 10 mg/L fluoride and the dashed lines are the corresponding calcium levels at 1 mg/L fluoride (adapted from [55]). 17
Figure 9: Left: ADI 1010 Bio Controller, Lower left: ADI 1025 Bio Console, middle: Applikon Bioreactor, right: Haake oil bath and temperature controller. 27
Figure 10: Volume of addition over time for two pump drive rotation speeds. for pump 1 and for pump 2 28
Figure 11: Schematic diagram of experimental setup. 29
Figure 12: XRD spectrum of hydrothermally precipitated scorodite. 34
Figure 13: SEM images of hydrothermally precipitated scorodite. 34
Figure 14: Particle size analysis of hydrothermally precipitated scorodite. 35
Figure 15: On the left Raman spectrum and on the right FTIR spectrum of hydrothermally precipitated scorodite. 35
Figure 16: Thermogravimetric analysis of hydrothermally precipitated scorodite. 36
Figure 17: Temperature and pH during atmospheric scorodite precipitation. 37
Figure 18: Arsenic concentration for the filtering washing and repulping steps for atmospherically precipitated scorodite. F1 is the filtration right after the synthesis, and steps RP1, RP2 and RP3 give higher concentrations due to the repulping step before the filtration. 38
Figure 19: XRD spectrum of the atmospherically precipitated scorodite. 39
Figure 20: SEM images of the atmospherically precipitated scorodite particles. 39
Figure 21: Particle size distribution of atmospherically precipitated scorodite. 40
Figure 22: On the left FTIR spectrum and on the right Raman spectrum of the atmospherically precipitated scorodite. 40
Figure 23: Thermogravimetric analysis for the atmospherically precipitated scorodite. 41
Figure 24: XRD patterns of the homogeneously precipitated hydroxyapatite powders for different concentrations at 22 °C. 45

Figure 25: XRD patterns of homogeneously precipitated hydroxyapatite powders at different temperatures. 45
Figure 26: SEM images of hydroxyapatite product HAP 4: 170 mmol/L P. 46
Figure 27: SEM images of hydroxyapatite product HAP 3: 330 mmol/L P. 46
Figure 28: SEM images of hydroxyapatite product HAP 7: 330 mmol/L P, 50 °C. 47
Figure 29: SEM images of hydroxyapatite product HAP 8: 330 mmol/L, 80 °C. 47
Figure 30: FTIR spectra of homogeneously precipitated hydroxyapatite powders. 48
Figure 31: A closer look at the FTIR spectra of two hydroxyapatite powders where the OH^- vibrations are noticeable. On the left HAP 3 and on the right HAP 7. 49
Figure 32: Metastable zone width for the $CaCl_2$-NaH_2PO_4-NaOH system at 22±1 °C. 50
Figure 33: Metastable zone width for the $CaCl_2$-NaH_2PO_4-NaOH system at 40±1 °C. 50
Figure 34: XRD spectrum of fluoroapatite precipitated powder. 52
Figure 35: SEM images of fluoroapatite precipitated powder. 52
Figure 36: FTIR spectrum of fluoroapatite precipitated powder. 53
Figure 37: Metastable zone width for the $CaCl_2$-NaH_2PO_4-NaF system at 22±1 °C. 53
Figure 38: XRD spectrum of fluoride substituted hydroxyapatite. 55
Figure 39: Schematic representation of particle and coating cross-section as per the calculation 56
Figure 40: Concentrations of P, Ca, As, Fe during the first (nucleation) step of deposition of ENCH 3. 60
Figure 41: SEM cross-section images of resulting solids after ENCH 3 encapsulation steps. 60
Figure 42: Concentrations of P, Ca, As during the first and fourth nucleation steps of ENCH 4. 61
Figure 43 : SEM cross-section images of resulting solids after ENCH 4 encapsulation experiments. 62
Figure 44: Concentrations of P and Ca during three nucleation experiments at different temperatures and agitation speeds, ENCH 6, 7 and 8. 63
Figure 45: Concentration profiles for nucleation steps 1, 4 and 9 and the growth step of the ENCH 10 series. 65
Figure 46: SEM cross-section images of resulting solids from ENCH 10 encapsulation experiments. 66
Figure 47: FTIR spectra of ENCH 10 solids and hydroxyapatite and scorodite reference patterns. 66
Figure 48 : Concentration profiles during a typical nucleation step and the Nancollas growth step of Test ENCH 11. 67
Figure 49: SEM images of resulting solids from ENCH 11 encapsulation tests. 68
Figure 50: P removal (%) at the end of each nucleation step for ENCH 10 and ENCH 11 series. 69
Figure 51: SEM cross-section images of resulting solids from ENCH 13 encapsulation test. 70
Figure 52: SEM images of resulting solids from ENCH 13 encapsulation experiment. 70
Figure 53: Backscattered electron image of a partially coated particle's cross-section and elemental mapping of the particle and the coating. 71
Figure 54: Concentration profiles during nucleation steps 1 and 2 of ENCF 1. 72

Figure 55: SEM images after nucleation step 1 of ENCF 1. On the left particles “as-is” and on the right cross-section of the particles. 73
Figure 56: Backscattered electron image of particles coated with fluoroapatite from ENCF 3 and elemental mapping of the particles and their coating. 74
Figure 57: Ca and P release from reference HAP, HAP 3 and HAP 3/gypsum in pH 8 oxic environment. 75
Figure 58: Ca and P release from reference HAP, HAP 3 and HAP 3/gypsum in pH 8 anoxic (150 mV) environment 75
Figure 59: Oxic tests at pH 7, 8 and 9 for reference scorodite and ENCH 10 solids with and without gypsum saturated water. 77
Figure 60: Release of Ca and P from ENCH 10 solids at pH 7, 8 and 9 with and without gypsum. 78
Figure 61: Arsenic release from scorodite and ENCH 10 solids at pH 7 and 150 mV. 79
Figure 62: Arsenic release from scorodite and ENCH 10 solids at pH 9 and 150 mV. 79
Figure 63: Arsenic release under anoxic conditions (pH 8 and 150 mV) for various materials. .. 80
Figure 64: Release of Ca and P under anoxic conditions (pH 8 150 mV) for various materials. (The value for Ca ENCH 13 at the 40-day mark was exceptionally high and is omitted so that the rest of the values are viewed properly.) 81
Figure 65: Oxic tests at pH 9 for reference scorodite and ENCF 3 solids. 82
Figure 66: Phosphorus and calcium release for ENCF 3 under oxic conditions. 83
Figure 67: Arsenic release from scorodite and ENCF 1, 3 and 3 repeat, 1g at pH 9 and 150 mV 84
Figure 68: Phosphorus and Calcium release under anoxic conditions (pH 9 150 mV) for fluoroapatite encapsulated scorodite. 84

Figure A- 1: Solubility of 0.1 mol of hydroxyapatite in 1 L of water. 93
Figure A- 2: Solubility of 0.1 mol of fluoroapatite in 1 L of water. 93
Figure A- 3: Amount of solids in solution following the introduction of hydroxyapatite in a solution containing the stoichiometric amount of fluoride ions. 94
Figure A- 4: Amount of solids in solution following the introduction of hydroxyapatite in a solution containing twice the stoichiometric amount of fluoride ion. 94
Figure A- 5: Amount of solids in solution following the introduction of hydroxyapatite in a solution containing 10 times the stoichiometric amount of fluoride ions. 95

Figure B - 1: TGA curve for reference hydroxyapatite powder showing a 7.25 % weight loss. ... 96
Figure B - 2: TGA curve for HAP 3 powder showing a 8 % weight loss. 96
Figure B - 3: TGA curve for HAP 8 powder showing a 4 % weight loss. 97
Figure B - 4: TGA curve for FAP 1 powder showing a 4.5 % weight loss. 97

Figure E - 1: pH values measured for the scorodite stability tests. With a four-point red star on the top right are marked the measurements for which the pH was adjusted so that it would be closer to the starting value. 112

Figure E - 2: pH values measured for the ENCH 10 stability tests. With a four-point red star on the top right are marked the measurements for which the pH was adjusted so that it would be closer to the starting value. 113
Figure E - 3: pH values measured for the ENCH 11 and 13 stability tests. With a four-point red star on the top right are marked the measurements for which the pH was adjusted so that it would be closer to the starting value. 114
Figure E - 4: pH values measured for the scorodite mixtures with HAP and HAP only stability tests. With a four-point red star on the top right are marked the measurements for which the pH was adjusted so that it would be closer to the starting value. 115
Figure E - 5: e_h values measured for the scorodite stability tests. 116
Figure E - 6: e_h values measured for the ENCH 10 stability tests. With a four-point red star on the top right are marked the measurements for which the pH was adjusted so that it would be closer to the starting value. 117
Figure E - 7: e_h values measured for the ENCH 11 and 13 stability tests. With a four-point red star on the top right are marked the measurements for which the pH was adjusted so that it would be closer to the starting value. 118
Figure E - 8: e_h values measured for the scorodite mixtures with HAP and HAP only stability tests. With a four-point red star on the top right are marked the measurements for which the pH was adjusted so that it would be closer to the starting value. 119

List of tables

Table 1: Solubility products of hydroxyapatite and fluoroapatite (adapted from [63], added values from [64]) 18
Table 2: List of chemicals and materials used for the experiments 26
Table 3: Experimental parameters for the homogeneous precipitation of hydroxyapatite powders and the Ca:P ratio in the resulting solids. 44

Table C - 1: Summary of the encapsulation experiments that were conducted. 98

Table D - 1: Oxic test results for naked scorodite. 99
Table D - 2: Oxic test results for ENCH 10. 100
Table D - 3: Oxic test results for ENCH 10 in gypsum saturated water. 101
Table D - 4: Anoxic test results for naked scorodite. 102
Table D - 5: Anoxic test results for ENCH 10 in gypsum saturated water. 103
Table D - 6: Anoxic test results for ENCH 10 and 11. 104
Table D - 7: Results for oxic and anoxic tests for ENCH 1. 105
Table D - 8: Anoxic test results for ENCH 13 and mixtures of naked scorodite and hydroxyapatite powders. 106
Table D - 9: Oxic and anoxic test results for hydroxyapatite prepared in the lab and hydroxyapatite purchased from Sigma Aldrich. 107
Table D - 10: Oxic and anoxic test results for scorodite 1. 108
Table D - 11: Oxic and anoxic test results for fluoroapatite encapsulated scorodite 109
Table D - 12: Oxic and anoxic test results for fluoroapatite encapsulated scorodite 110
Table D - 13: Oxic and anoxic test results for fluoroapatite encapsulated scorodite 111

Chapter 1. Introduction

The widely acknowledged hazardous properties of arsenic as a soil and natural water contaminant and its adverse health effects when present in drinking water, have led to very strict environmental regulations [1], aiming at the drastic reduction of the presence of arsenic in the effluents of the mining and metallurgical industries.

In Canada, the Metal Mining Effluent Regulations dictate that the maximum authorised monthly mean concentration in tailings for arsenic must be lower than 0.5 mg/L [2]. At the same time the new Environmental Protection Agency's (EPA) standard for drinking water foresees concentrations of arsenic less than 0.01 mg/L, which means that the leachability limit for the industrial waste is set at 1 mg/L arsenic [3, 4]. One of the preoccupations of the mining and metallurgical industries is directed to the elimination of arsenic presence in all its effluents, especially since arsenic is commonly found in many ores in the form of oxides and sulphides. After processing of arsenic-containing ores and concentrates, arsenic can be present either in solid residues and tailings, liquid effluents or in flue dusts. Several of these forms of arsenic waste materials are soluble and therefore may cause the contamination of ground water, if disposed of without further treatment.

The successful elimination of arsenic from the mining and metallurgical operations has to be combined with the production of a waste material, which can be disposed of in an environmentally safe way, i.e. in a stable form exhibiting low solubility/leachability in the long term. This has been the purpose of extensive research work in the last several years.

The prevailing technique for the removal of arsenic from process effluent solutions is lime neutralisation combined with coprecipitation with ferric iron [5, 6]. The arsenic (typically as arsenate) bearing solids formed are stable only if the Fe(III) to As(V) molar ratio is 3 or higher [7]. When processing arsenic-rich and iron-deficient materials or solutions it is advantageous to produce the crystalline ferric arsenate compound, scorodite ($FeAsO_4 \cdot 2H_2O$) [8]. As mentioned above, the limit for industrial wastewaters is 1mg/L As. When scorodite is subject to tests according to the Toxicity

Characterisation Leachability Procedure established by the Environmental Protection Agency (EPA) the results in general are within the acceptable limits, i.e. < 1 mg/L As after equilibration at pH 5 for 18-24 hours. It has been recently reported by Bluteau et al., though, that scorodite undergoes incongruent dissolution in pH values over 5 [9]. More specifically arsenic is released in the solution and ferrihydrite (FeOOH) is formed. The process is strongly influenced by pH meaning that for pH values in industrial tailings higher than 7 the dissolution of scorodite may produce high arsenic concentration in solution. Similarly scorodite is known to become unstable under reducing conditions [10, 11].

One way to improve the stability of the scorodite particles, over a wider pH and redox potential range, is to create some kind of a protective layer around the surface of said particles. The process is called encapsulation and previous research at McGill University has proved its feasibility in principle. The previous McGill encapsulation research included coating of scorodite particles with aluminium and calcium phosphates, as well as with aluminium hydroxy-gels [12, 13].

The work described in this thesis aims to improve the results of the previous research done with calcium phosphates. Namely, hydroxyapatite ($Ca_5(PO_4)_3OH$) and fluoroapatite ($Ca_5(PO_4)_3F$) are used for the encapsulation of scorodite particles using direct crystallisation of these phosphates on the surface of the particles. The main objectives are:

a) The elaboration of appropriate crystallisation procedures for the protection of scorodite via its encapsulation with hydroxyapatite (HAP) and fluoroapatite (FAP) coatings.
b) The evaluation of the effectiveness of said encapsulating calcium phosphates via appropriate characterisation and stability testing in oxic and anoxic waters.

Prior to embarking into the encapsulation and stability investigation, this work dealt with the homogeneous precipitation of hydroxyapatite and fluoroapatite powders, the determination of their metastable zones, and their characterisation.

This thesis is organised into chapters that include in addition to this Introduction chapter:

- Chapter 2: Literature review, which provides a coverage of aspects of arsenic disposal in the form of scorodite, theory of crystallisation, relevant papers on precipitation and stability of calcium phosphates and previous encapsulation attempts.
- Chapter 3: Description of experimental procedures and characterisation methods employed including the atmospheric crystallisation of scorodite.
- Chapter 4: Results & Discussion, consisting of (1) the homogeneous preparation of HAP and FAP as a function of temperature and concentration; (2) encapsualtion of scorodite by alternative nucleation-growth procedures for HAP and FAP; and (3) measurement of the stability of the encapsulated materials along characterisation and discussion of the above.
- Chapter 5: Conclusions.

Chapter 2. Literature Review

2.1 The arsenic problem

Arsenic is the 20th most abundant element in the earth's crust and it is found in more than 245 minerals, commonly associated with ores containing copper, nickel, lead, cobalt or other metals. It is also 14th in seawater and 12th in the human body. Albertus Magnus isolated the element in 1250 A.D. and since then, it has been used for various purposes in many different aspects of human life, but mostly as poison. As far as minerals are concerned, arsenic appears in forms of arsenates, sulphides, sulphosalts, arsenides, arsenites, oxides, silicates and elemental arsenic [1]. Arsenic and its compounds can be used in wood preservation, paints and varnishes, glass and glass products, alloys, electronic components and other applications [14]. However, the amount produced exceeds by far the amount needed in the above mentioned sectors [15]. Thus, the presence of arsenic in ores requires the metallurgical industry to deal with it either as a contaminant in the production of certain metals, or as an environmental problem in the disposal of tailings, effluents, flue dusts, etc.

As such, arsenic volatilises during roasting, smelting and conversion in pyrometallurgical plants in the form of As_2O_3 or As_2S_3 and they are removed in electrostatic precipitators or wet gas scrubbers [16]. Arsenic trioxide is a very soluble and toxic compound, therefore it has to be converted into a more stable form for the industry to be able to dispose of it [17].

In hydrometallurgical operations, arsenic can be found in spent copper electrorefining electrolyte, where it is necessary to have arsenic concentrations less than 20g/L. In order to achieve this, bleed streams from the process pass through liberator cells to remove copper and other impurities as an arsenide sludge [18]. In other instances arsenic reports to acidic process solutions as are those produced after the solvent extraction separation of uranium [19] Arsenic is removed from such solutions via coprecipitattion with ferric iron and lime neutralisation [5, 6]. Another occurrence of arsenic waste is in flotation tailings, where sulphides and other compounds (arsenopyrite, jarosite, scorodite, arsenical ferrihydrite) that contain arsenic can become

soluble due to pH variations caused by acid mine drainage [20, 21]. Finally, high temperature high pressure oxidation-leaching, as it is used for refractory gold ore processing, leads to the formation of various crystalline iron arsenate phases such as scorodite, ferric arsenate sub-hydrate (FAsH; $FeAsO_4 \cdot 0.68\text{-}0.77H_2O$) and basic ferric arsenate sulphate (BFAS; $Fe(AsO_4)_x(SO_4)_y(OH)_z \cdot wH_2O$, where $0.26 \leq x \leq 0.69$, $0.19 \leq y \leq 0.5$, $0.55 \leq z \leq 0.8$ and $0.2 \leq w \leq 0.45$) [22].

2.2 Arsenic removal and fixation

There are several different ways to approach the removal of arsenic from solutions. These include adsorption, ion exchange, cementation and precipitation processes [16], the latter being of most interest to this work. Arsenic can be precipitated into copper arsenates, calcium and manganese arsenates (svabite and tilasite [23]), arsenate-hydroxyapatite [24], sulphides and iron arsenates [7, 25].

The most common way of arsenic removal and fixation from mineral processing effluent solutions is by co-precipitation with trivalent iron in combination with lime neutralisation [19]. This process is described as the “Best Demonstrated Available Technology” according to the U.S. Environmental Protection Agency for the removal of arsenic from aqueous solutions [25]. For this procedure, the molar ratio of iron(III) to arsenic(V) has to be 4:1 or higher and the result is amorphous ferric arsenate and arsenate-bearing ferrihydrite with poor crystallinity and settling characteristics [7, 16, 26, 27].

In special cases, where the waste materials and effluents are rich in arsenic but have low iron content, like acid plant effluents or As_2O_3 flue dusts, co-precipitation is not suitable, because it requires large amounts of trivalent iron, leading to slow settling and voluminous solids and high cost. The precipitation of a crystalline ferric arsenate, scorodite ($FeAsO_4 \bullet 2H_2O$) is a better alternative, since the iron to arsenic ratio needed is 1:1. Scorodite solids can easily be dewatered in comparison to amorphous sludges formed by co-precipitation and the product is generally considered as sufficiently stable for disposal purposes, since it can pass the currently valid Environmental Protection

Agency's (EPA) Toxicity Characteristic Leaching Procedure (TCLP), < 1 mg/L of arsenic after 20 h extraction period at pH 5.0 [4, 28]

2.2.1 Scorodite Synthesis

Scorodite is a naturally forming mineral and it is the result of oxidation of ore deposits that contain arsenic. The formation of crystalline scorodite has been reported to occur during autoclave processing as is pressure oxidation of gold flotation concentrates treated at 190-200 °C [16]. Scorodite can be precipitated under hydrothermal conditions in an autoclave in nitrate, sulphate or chloride media [29-31]. The temperatures used are in the range of 140-180 °C. Below 150 °C the scorodite produced in nitrate solutions was reported to suffer from low crystallinity [29] and above 180 °C in sulphate solutions other ferric arsenate phases, namely FAsH ($FeAsO_4 \cdot 0.75H_2O$) and BFAS ($Fe(AsO_4)_x(SO_4)_y(OH)_z \cdot wH_2O$) form at the expense of scorodite [32]. However, crystalline scorodite can also be precipitated atmospherically, from chloride or sulphate solutions at temperatures below 100 °C. This is accomplished via supersaturation control to avoid homogeneous nucleation and promote growth on scorodite seed or other particles [33, 34]. Supersaturation control may be accomplished via pH regulation [17, 34, 35], oxidation [36, 37] or dissolution of a precursor poorly crystalline compound [28]. As a result of these advances the atmospheric scorodite process was developed [11, 38, 39].

2.2.2 Stability of Scorodite

2.2.2.1 Oxic environment

Observation shows that scorodite is a common mineral in nature and as such it is considered to be quite stable [32]. Scorodite passes the EPA Toxicity Characteristic Leaching Procedure (TCLP) as it has already been mentioned above but a more critical issue is its long term stability behaviour, in particular at pH environments higher than 5, which is typically the case in tailings disposal sites. This issue was addressed by Bluteau and Demopoulos in a recent study [9]. Thus, according to this long-term stability study, which was run for more than one year, scorodite undergoes incongruent

dissolution at pH>5 under oxic conditions leading to conversion to ferrihydrite and release of arsenic into solution (with part of it re-adsorbing on the freshly formed ferrihydrite):

$FeAsO_4 \cdot 2H_2O(s) \rightarrow FeOOH(s) + H_3AsO_4(aq)$	(2.1)

In the following figure the solubility results from the recent study by Bluteau and Demopoulos are plotted along with those from previous researches. Thus at pH 7 the equilibrium concentration of arsenic was found to be 5.8 mg/L As. At higher pH arsenic concentration increased to unacceptable higher levels (e.g. > 80 mg/L at pH 8) hence the need to enhance scorodite's stability via other means, as is encapsulation studied in this thesis.

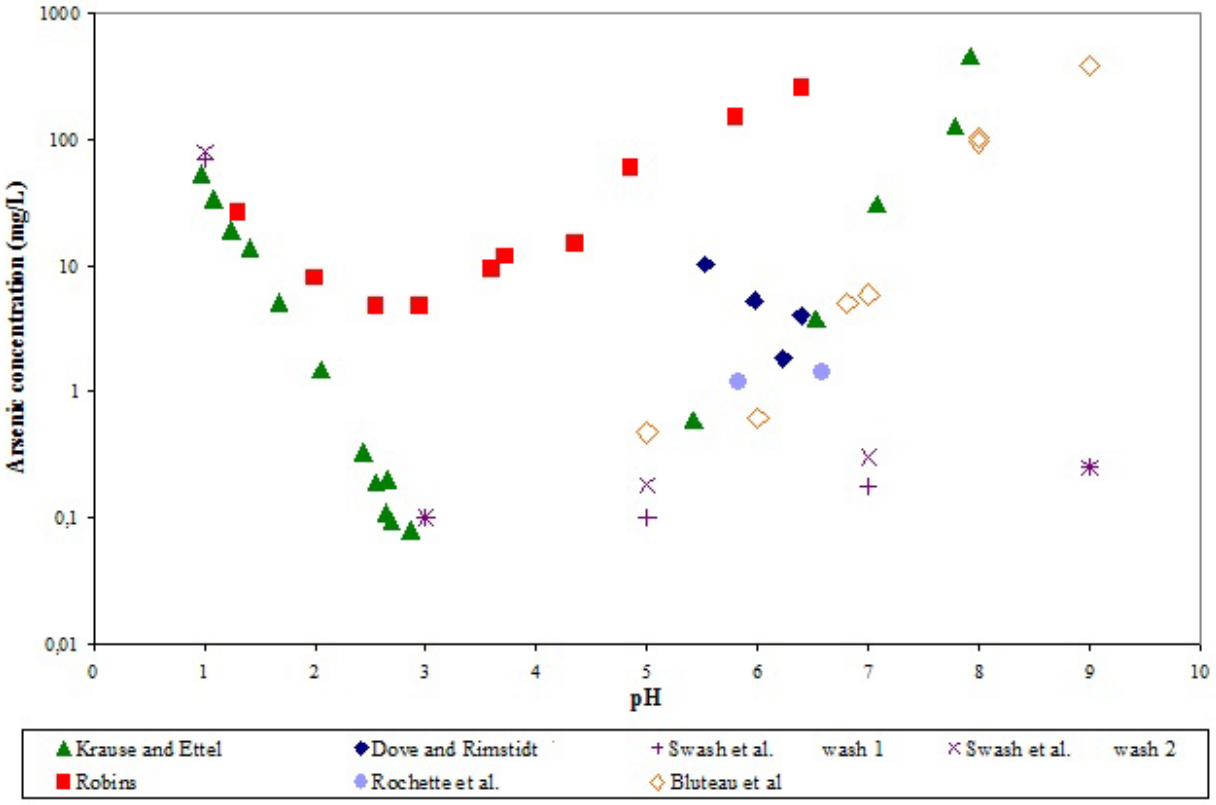

Figure 1: Comparison of the final arsenic concentrations from different studies [8-10, 40-42] of scorodite stability at 22-25 °C [9].

2.2.2.2 Anoxic environment

Under anoxic conditions, scorodite has been reported [9] to undergo reductive decomposition to Fe(II) and As(III), when E_h decreases near or below 100 mV. The reductive decomposition reaction of scorodite:

$FeAsO_4 \cdot 2H_2O(s) + H^+ + e^- \rightarrow Fe^{2+} + H_3AsO_3(aq) + H_2O$	(2.2)

Such reductive conditions may prevail in cases, where the deposition of tailings is sub-aqueous with the presence of soluble organic carbon or in depths about 2 m below the ground in anaerobic environment, where reactive metal sulphides may act as reducing agents [16].

2.3 Crystallisation theory

The separation of compounds by precipitation of crystals out of solution is widely used in industry, as a production technique of useful chemical, metallurgical, pharmaceutical, etc. products. Crystallisation is based on the principles of solubility and supersaturation: For example compounds (solutes), which are more soluble in hot solutions than they are in cold ones, are crystallised upon cooling. The same technique is also applied in environmental technology, in order to effectively separate and remove undesirable constituents from process effluent solutions. The products, which may subsequently be safely disposed of as waste, it is important that they are characterised with low solubility and adequate stability, to avoid the hazardous constituent's reintroduction to the environment.

Crystallisation is controlled by supersaturation, on which nucleation, growth and Ostwald's ripening depend. Supersaturation is expressed by the saturation ratio S, which in a simplified form is the ratio of the actual concentration of component ions in excess of the equilibrium concentration [33].

$S = \frac{C}{C_{eq}}$	(2.3)

Where C is the bulk solute concentration and C_{eq} the equilibrium concentration (solubility) of the solute at given temperature and pressure of the system. If S>1, the solution is supersaturated and precipitation of crystals takes place.

A solubility diagram for a soluble salt with inverse solubility is depicted in Figure 2. This is the typical salt behaviour in solution, where the equilibrium concentration decreases when the solution temperature is increasing. At the point A the solid salt is in equilibrium with the solute, this equilibrium might be upset by: increasing the solution concentration at constant temperature (line AB), increasing the temperature (line AC), or varying concentration and temperature (line AD).

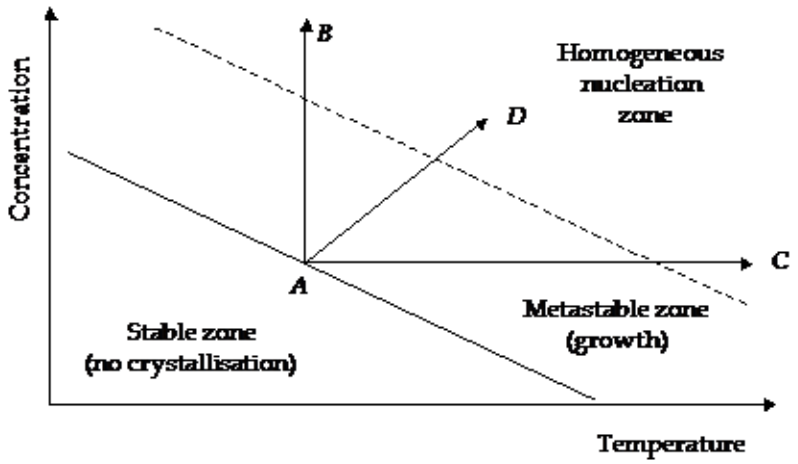

Figure 2: Solubility-supersaturation diagram explaining the stable metastable and labile zones for a salt with inverse solubility (adapted from [43]).

The continuous line is the solubility line, below which no crystal precipitation can occur. In the metastable zone, deviation from equilibrium is observed to a certain extent. Once the critical homogeneous nucleation line is reached (dashed line), spontaneous precipitation occurs. This range of supersaturation defines the homogeneous nucleation zone (also called labile zone).

In case formed crystals are present in undersaturated solutions, they start to dissolve. In industrial processes, crystallisers are designed to operate in the metastable zone under controlled conditions, to produce the desired crystal purity, size, shape, etc., which characterise the quality of the product [44].

Supersaturation in solutions may be induced via different parameter manipulation such as changing the solution temperature, dissociation of metal complexes, dissolution

of precursor solids, or pH change. The latter is most frequently used in hydrometallurgical processes, although all methods may be used to generate a particular solid phase.

2.3.1 Nucleation

The crystallisation is initialised in a crystal-free supersaturated solution, by the formation of nuclei. Nuclei may form directly out of solution (primary homogeneous nucleation mechanism) or via the use of seed crystals. If the seed crystals are from the same compound that is being crystallised, the mechanism is called secondary surface nucleation. If the seed crystals are foreign material particles, on which surface nucleation develops, the mechanism is called primary heterogeneous nucleation. Other secondary nucleation mechanisms involve nuclei formation caused by external forces, such as attrition and fragmentation ("apparent") or plastering on equipment surfaces ("contact"). The following figure shows the various nucleation mechanisms.

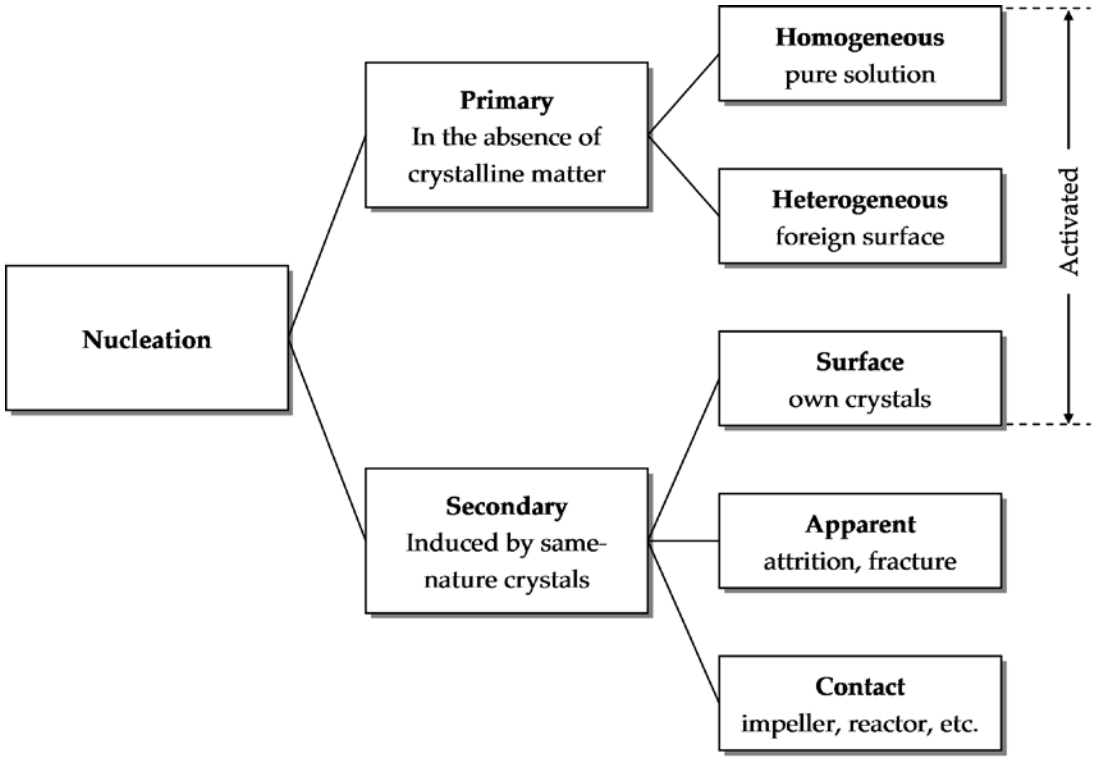

Figure 3: Classification of nucleation mechanisms (adapted from [45]).

2.3.1.1 Primary homogeneous nucleation

In a supersaturated solution, lacking any solid seed crystal, molecules or ion pairs combine to form tiny clusters of 10-1000 units, called embryos, which grow to form stable nuclei, as soon as they are above a minimum critical size, r_{cr} [46].

The rate of nuclei formation and the critical nuclei size depend on the solution's saturation ratio S. At high S, a large number of ultra fine colloidal particles will form at a very fast rate and crystallisation propagates quickly. The critical nuclei size is usually between 40 and 200 Å and it is a function of supersaturation. The higher the degree of supersaturation, the larger the number of ultra-fine particles formed [33].

Complex equations describe the nucleation rate, as a function of the embryo size; the work necessary to form an embryo of size *r* in a supersaturated solution, which is defined as the difference between the free energy of the system in its final and initial states [46]; the interfacial free energy γ_{sl} [47], and other parameters. The following diagram depicts the free energy variation during a primary homogeneous nucleation process.

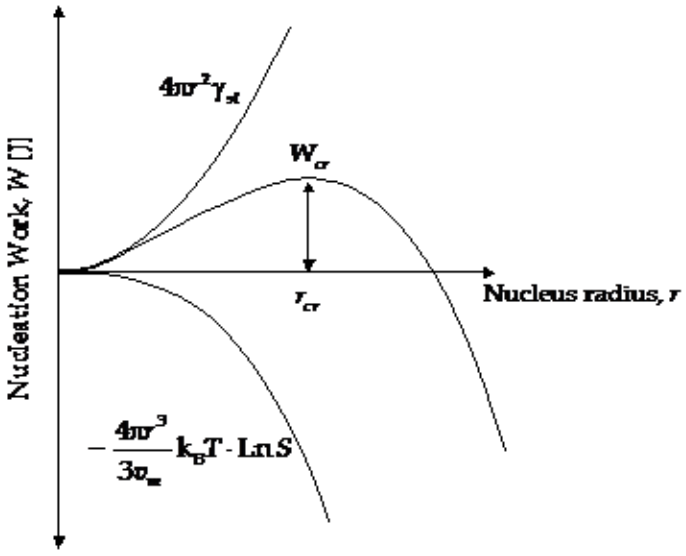

Figure 4: Overall free energy change resulting from an embryo nucleating homogeneously from solution, according to equation (2.4) (reproduced from [47]).

2.3.1.2 Primary heterogeneous nucleation

This type of nucleation takes place at supersaturation levels that are lower than the critical supersaturation for homogeneous nucleation, because of the lower surface energy of the foreign particles compared to the surface energy of the nuclei of the crystallised material. Therefore, the overall free energy change or nucleation work, necessary for the formation of a nucleus with the critical size in a heterogeneous nucleation mechanism, is lower than the free energy change corresponding to homogeneous nucleation [46].

2.3.1.3 Supersaturation control

As mentioned previously, the nucleation rate is dependent upon the saturation ratio S of the solution. For all types of nucleation mechanisms described above, nucleation initiates after a critical S value (S_{cr}) is reached. In the following diagram, nucleation rates are presented for each of the characteristic mechanisms, with the associated critical saturation ratios. Surface nucleation is associated with low supersaturation, heterogeneous nucleation with medium supersaturation and homogeneous nucleation with high supersaturation.

$S_{cr,surf} < S_{cr,het} < S_{cr,homo}$	(2.4)

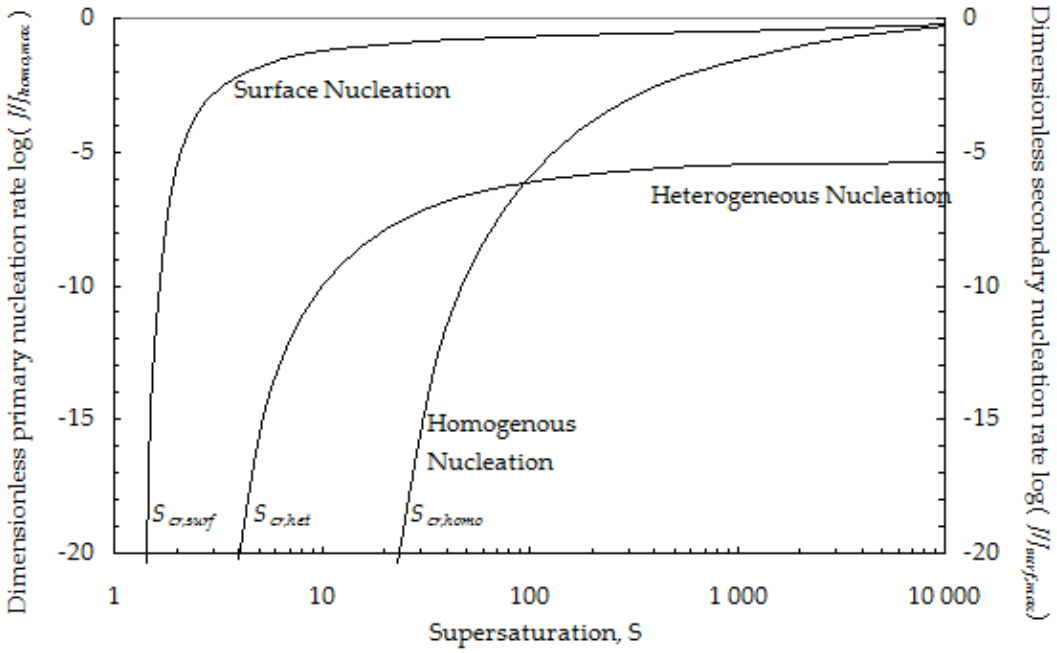

Figure 5: Generalised nucleation rate diagram showing the dominant areas for homogeneous, heterogeneous and surface nucleation (reproduced from [48]).

2.3.2 Crystal growth

Following nucleation, the nuclei grow to form crystals and this growth phase is very important for the product quality, in terms of purity, shape, final particle size distribution and crystal habit. In the case of the primary growth mechanism, the crystals are enlarged by continuous deposition of layers of material on each particle. By secondary growth mechanism, called also agglomeration, two or more particles are combined to form a bigger particle. The difference in the two mechanisms is that crystals of an irregular morphology are formed by secondary growth. These two mechanisms often occur simultaneously especially in batch reactors, where at lower supersaturation values primary growth dominates and at higher supersaturation values secondary becomes the dominant mechanism [12, 13, 33]

2.4 Encapsulation

As it has been discussed above, even though scorodite is a stable compound, there are occasions in which it is possible for arsenic to be leached in levels higher than the allowed limits for waste disposal. One way of enhancing the stability of scorodite is for the surface of the particles to be protected in such a way, so that arsenic release is minimal in alkaline (pH>7) environments and when the redox potential is lower than 200 mV. Such protection can be effected if the particles are encapsulated. Encapsulation entails the deposition on a substrate material a layer of another compound. Encapsulation methods are used for pharmaceutical preparations, cosmetics, pigment imparting materials, and other active agents aiming mainly to control the release of the encapsulated material [12, 49].

In this work the encapsulation minerals considered for coating the scorodite particles are hydroxyapatite and fluoroapatite, two calcium phosphate minerals that are known for their stability among the calcium phosphates. Aqueous precipitation is the method that will be described as the means for achieving the desired result of stabilising scorodite.

2.5 Calcium Phosphates-Apatites

Apatites belong to the wider mineral group of phosphates. In nature, phosphates can be found in a variety of environments, such as silicate melts, natural soils, and ocean floors [50]. Besides the interest expressed for the biomedical application of calcium phosphates, they are also very important in the removal of phosphorus from wastewaters and the formation of lake and ocean sediments [51]. Eutrophication, the increase in the rate of supply of organic matter to an ecosystem, is a serious environmental issue to which phosphate salts contribute when their supply to the recipient aquatic systems is increased, therefore the removal of said salts from wastewater by precipitation with calcium, iron or aluminium, has been investigated extensively [52, 53].

Calcium phosphates is a group of minerals that contain the orthophosphate anion (PO_4^{3-}) and calcium ions (Ca^{2+}). These compounds have been studied extensively, namely because of the dominant role calcium phosphates play in the formation of human bones and teeth [54, 55] and their use for biomaterials applications and implants [56], but also for wastewater treatment [53].

There are eleven well-known calcium phosphates in the ternary system $Ca(OH)_2$-H_3PO_4-H_2O with a range of 0.5 to 2 of the calcium to phosphate molar ratio. These are: monocalcium phosphate monohydrate (MCPM), monocalcium phosphate anhydrous (MCPA), dicalcium phosphate dehydrate (DCPD), dicalcium phosphate anhydrous (DCPA), octacalcium phosphate (OCP), β-tricalcium phosphate (β-TCP), two forms of α-tricalcium phosphate (α-TCP), amorphous calcium phosphate (ACP), hydroxyapatite (OHAp), and tetracalcium phosphate (TTCP). By substitution of the hydroxide ion for a halide anion, fluoroapatite (FAp) or chloroapatite (ClAp) is obtained [57]. Monocalcium phosphate monohydrate, amorphous calcium phosphate and calcium deficient hydroxyapatite are considered low-temperature calcium phosphates and monocalcium phosphate, α and β tricalcium phosphate, hydroxyapatite, oxyapatite and tetracalcium phosphate are considered high temperature calcium phosphates and the latter are the ones used in medicine, while the first group is used to produce the high temperature ones [58].

2.5.1 Solubility and stability

In order to achieve the protection needed with the encapsulation of scorodite, the materials selected for the coating have to be stable in a wide range of conditions and certainly in those that scorodite is the weakest. Therefore, these materials have to present low dissolution in pH environments higher than 6 and good behaviour in reductive conditions. As such calcium phosphates are considered to be good candidates, and since hydroxyapatite and fluoroapatite are considered to be the most stable of the group, they were selected for the encapsulation experiments.

In the following diagrams the solubility lines of the main (hydroxy) phosphate phases are depicted. Hydroxyapatite is the most stable phase of these phosphates in the pH range that we are interested in.

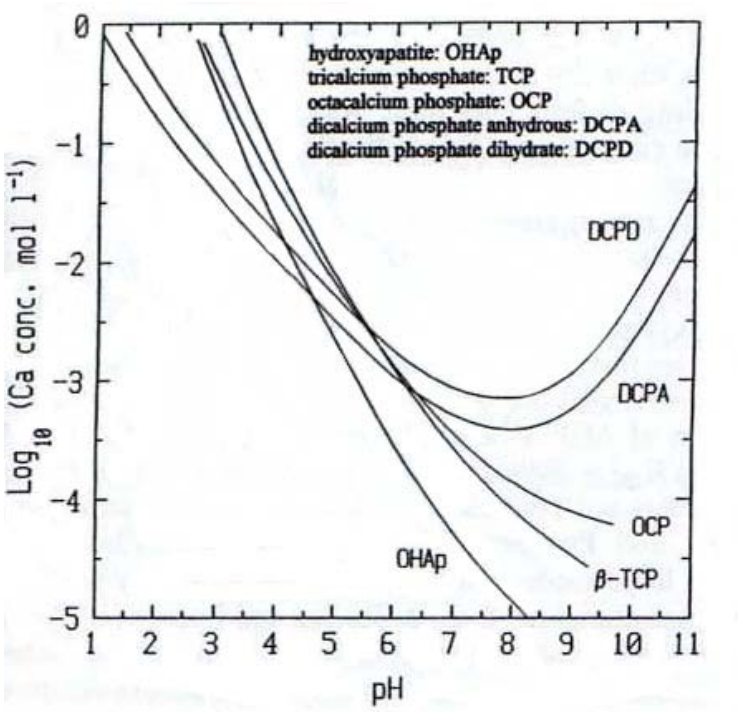

Figure 6: Solubility isotherms of calcium orthophosphate phases in the system $Ca(OH)_2$-H_3PO_4-H_2O at 37 °C (Taken from [59]).

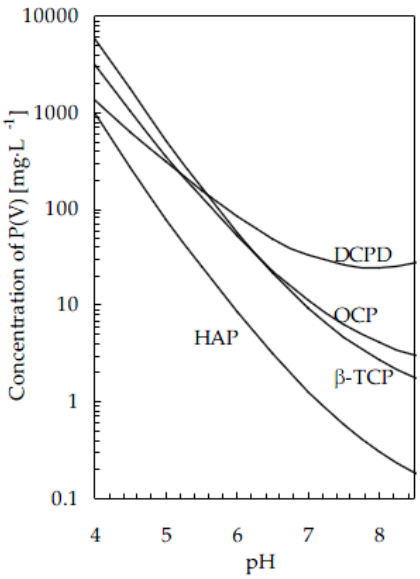

Figure 7: Solubility isotherms of calcium phosphate phases in the ternary system Ca^{2+}-PO_4^{3-}-H_2O at 25 °C (taken from [12]).

According to literature, hydroxyapatite is more soluble than fluoroapatite, with fluoroapatite having about one order of magnitude (12 times) lower solubility product than hydroxyapatite [60]. This is explained by the fact that H^+ ions have greater affinity for OH^- than for F^- ions, and this is especially more evident when the pH is low [59]. According to Chow et al. if the concentration of F^- is greater than 0.082 times the concentration of OH^- in a solution, then fluoroapatite is more stable than hydroxyapatite. Following this, it was calculated that a solution saturated with hydroxyapatite would be supersaturated for fluoroapatite if the concentration of the F^- ions is greater than 8.2×10^{-9} for pH 7 and 8.2×10^{-12} for pH 4, which will be exceeded with only a small amount of fluoride source and therefore fluoroapatite is less soluble than hydroxyapatite in almost all cases. In the same research paper it is also explained that fluoroapatite dissolves a bit less than hydroxyapatite when HCl is used to adjust the pH [61].

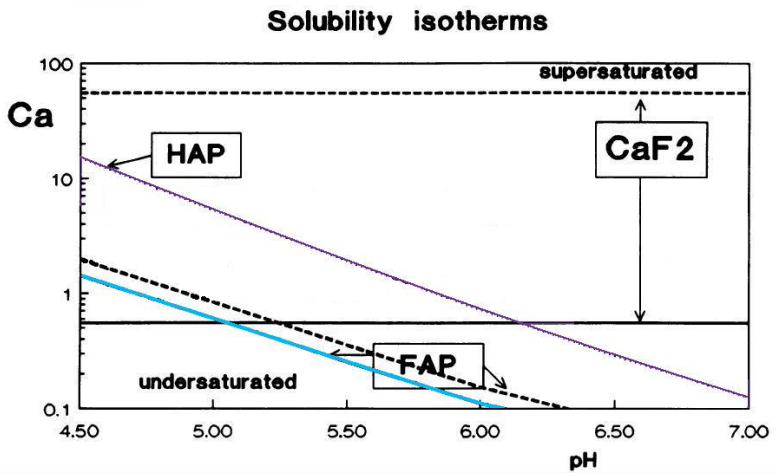

Figure 8: Solubility Isotherms for hydroxyapatite, fluoroapatite and calcium fluoride at fluoride concentrations in solution of 1 and 10 mg/L, respectively. For FAP and CaF_2 the solid lines represent the saturation calcium concentrations at 10 mg/L fluoride and the dashed lines are the corresponding calcium levels at 1 mg/L fluoride (adapted from [55]).

As studied by Dorozhkin there are eight dissolution models according to which apatites (including hydroxyapatite and fluoroapatite) dissolve. These models include: diffusion and kinetically controlled models, a polynuclear model, a self-inhibition (calcium-rich layer formation) model, stoichiometric/non-stoichiometric dissolution, a chemical model, etch pit formation, an ion exchange model and a hydrogen catalytic model. These models, cannot describe the dissolution of the apatites each on their own, but they are complementary to each other [62]. Therefore, following and controlling the dissolution of apatites is a complex matter.

However, calculating the solubility product (K_{sp}) of hydroxyapatite (HAP) and fluoroapatite (FAP) is feasible and different values have been reported. A list of some of them can be seen on Table 1.

Table 1: Solubility products of hydroxyapatite and fluoroapatite (adapted from [63], added values from [64])

Reference	Year	K_s	Phase	Temp (°C)
Zhu et al.	2009	$1x10^{-53.28}$	HAP	25
Zhu et al.	2009	$1x10^{-55.73}$	HAP	45
Jaynes et al.	1999	$1x10^{-56.02}$	HAP	20-25
Valsami-Jones et al.	1998	$1x10^{-58}$	HAP	25
Elliot	1994	$1x10^{-62.6}$	HAP	25
Chander & Fuerstenau	1984	$1x10^{-57.5}$	HAP	25
Nancollas	1982	$1x10^{-58.33}$	HAP	25
Stumm & Morgan	1981	$1x10^{-57}$	HAP	25
Snoeyink & Jenkins	1980	$1x10^{55.9}$	HAP	25
*Fawzi et al.	1978	$1x10^{-61}$	HAP	30
*McDowell et al.	1977	$1x10^{-88.5}$	HAP	25
*Brown et al.	1977	$1x10^{-57}$	HAP	?
*Wu et al.	1976	$1x10^{-62.5}$	HAP	30
*Smith et al.	1976	$1x10^{-58.5}$	HAP	20
*Avnimelech et al.	1973	$1x10^{-58.2}$	HAP	25
*Saleeb & deBruyn	1972	$1x10^{-57.5}$	HAP	?
*Chien	1972	$1x10^{-60.5}$	HAP	25
*Weir	1971	$1x10^{-58.5}$	HAP	25
Zhu et al.	2009	$1x10^{-55.71}$	FAP	25
Zhu et al.	2009	$1x10^{-55.89}$	FAP	45
Jaynes et al	1999	$1x10^{-58.13}$	FAP	20-25
Valsami-Jones et al.	1998	$1x10^{-70}$	FAP	?
Elliot	1994	$1x10^{-68.1}$	FAP	25
Chin-Nancollas	1991	$1x10^{-60.1}$	FAP	37
Driessens	1982	$1x10^{-60.6}$	FAP	25
Amjad et al.	1981	$1x10^{60.15}$	FAP	37
Stumm & Morgan	1981	$1x10^{-59}$	FAP	25
Lindsay	1979	$1x10^{-58.89}$	FAP	

***Taken from tabulated values in Chander & Feuersternau (1984).**

For this work, thermodynamic simulations were run using the OLI systems electrolyte simulation software, OLI analyzer 3.0, and the solubility product was calculated as well. On the presupposition that these compounds have very low solubilities, the activity coefficients of the ions in solution are considered to be nearly equal to one and the equations that were used for the calculation of the K_{sp} are:

$K_{sp}=[Ca^{2+}]^5\ [PO_4^{3-}]^3\ [OH^-]$ and $K_{sp}=[Ca^{2+}]^5\ [PO_4^{3-}]^3[F^-]$	(2.5)

The values that were calculated for 25 °C are $1x10^{-56.55}$ for hydroxyapatite and $1x10^{-59.54}$ for fluoroapatite. These values are within the range given by previous studies (as listed in Table 1) and they also agree with the statement that fluoroapatite is less soluble than hydroxyapatite.

These calculations with the OLI program also showed that 0.1 mol of hydroxyapatite in 1 L of water start to dissolve at pH 5.5 and by pH 4.48 it is completely in solution. Also for 0.1 mol of fluoroapatite in 1 L of water the pH values are 4 and 1.96 respectively.

2.5.2 Synthesis of hydroxyapatite and fluoroapatite

Many methods exist for the synthesis of hydroxyapatite and fluoroapatite. These include solid-state or glass ceramics synthesis [56, 65-68], mechanochemical synthesis [69, 70], precipitation in a heterogeneous system (microemulsion, emulsion liquid membrane system, polyol-mediated synthesis) [71-74], sol-gel synthesis [71, 75, 76] and aqueous precipitation [71, 77-81].

The solid-state synthesis of apatites consists of mixing powders containing phosphate, or phosphorus oxide, a calcium compound and a fluoride compound in the case of fluoroapatite and heating up the mixture so that solid state reactions occur. The temperature at which the mixture is heated up to depends on whether the material is prepared by itself (1000-1370 °C) [65, 67, 68] or in a glass matrix (1480 °C, 1600-1650 °C) [56, 66]. For the mechanochemical synthesis of apatites a strategy similar to that of solid-state synthesis is used, the powders containing phosphate, calcium (and fluoride for the synthesis of fluoroapatite) compounds are mixed and milled for different times and subsequently some of the products are heat treated at 1100 °C [69, 70].

For the precipitation in heterogeneous systems, such as microemulsion mediated synthesis, aqueous solutions of calcium or phosphate are titrated into oil (n-octane) and surfactant (Empilan KB6ZA, 1-butanol) mixtures, or polyols (diethylene glycol) under vigorous mixing conditions and then another aqueous solution with the second compound is added to the heterogeneous mixture. Reaction times differ according to conditions and media used, but once the reaction is over the solids are washed and centrifuged in order to separate the powders from the oil phases [71, 72, 74].

The synthesis in sol-gel is either water based, or organic solvent (anhydrous ethanol) based. The compounds used as precursors for calcium and phosphorus are mixed in stoichiometric amounts with the solvent in separate solutions and then one of the solutions is added to the other while the mixture is agitated. The resulting mix becomes a gel after certain ageing time, depending on the materials and the solvents. The product is dried and/or subjected to thermal treatment at different temperatures ranging from 80-800 °C [75, 76, 82].

A sol-gel technique used in bone tissue engineering for the synthesis of porous hydroxyapatite scaffolds, that are used to induce new tissue and bone formation, has been developed the last years. This technique involves the preparation of a hydroxyapatite slurry containing monomers and initiators and the immersion of a polyurethane foam of desired shape and size in this slurry under vacuum, so that the slurry is siphoned through the pores of the foam. The following step is the drying of the impregnated foam, and then it is heated so that the foam is burned away and the solid scaffold remains only, which is then sintered [83-85].

The aqueous precipitation of hydroxyapatite and fluoroapatite is based on the control of supersaturation of the water-based solutions used for the synthesis. Supersaturation, as was mentioned above, is controlled by the concentration of the ions, the pH and, the temperature of the solution. Due to the nature of the system investigated in this work, aqueous precipitation was selected for the production of hydroxyapatite and fluoroapatite powders, as well as for the encapsulation of scorodite.

Different precursor solutes have been used for the aqueous precipitation of HAP and FAP. Paschalis et al. precipitated hydroxyapatite adding a $(NH_4)_2HPO_4$ solution to

a solution of $Ca(NO_3)_2$ and using a NH_4OH solution for pH adjustment at pH 10 for 5 h [86]. Similarly Mobasherpour et al. using the same reagents but with more concentrated solutions and maintaining the pH at 11, while the temperature was kept constant at 25 °C, synthesised nanocrystalline hydroxyapatite [87]. Boskey & Posner formed hydroxyapatite by adding a solution of $CaCl_2$ to a solution of Na_2HPO_4, or vice versa, and adjusted the pH at 7.4 with NaOH. The Ca/P ratio varied between 1.0 and 1.7 [88]. Hydroxyapatite was also precipitated by Gomes et al. by the reaction of $Ca(OH)_2$ and H_3PO_4, using NH_4OH solution to control pH, in different temperatures and pH values [89].

The precipitation of fluoridated hydroxyapatites has been reported by Okazaki et al. More specifically $Ca(CH_3COO)_2$, $NH_2H_2PO_4$ and KF were supplied continuously into a 1.3 mol/L acetate buffer solution at 80 °C and pH 7.4 for 3 h [80, 81]. Willigeroth et al. produced fluoroapatite powders by slowly adding a solution of Na_2HPO_4 and KF in stoichiometric amounts to a solution of $CaCl_2$ under stirring, or vigorous stirring and at 25 or 90 °C [71]. Rodriguez-Lorenzo & Vallet-Regi precipitated calcium phosphate apatites with different stoichiometries and morphologies, hydroxyapatite among them, by introducing simultaneously in a reactor $Ca(NO_3)_2$ and $(NH_4)_2HPO_4$ at a flow rate of 22 mL/min at various temperatures, reaction times and pH values. Koutsoukos et al. report the precipitation of hydroxyapatite and fluoroapatite at 37 °C by preparation of a supersaturated metastable solution containing PO_4^{3-}, Ca^{2+} and F^- where applicable, and the addition of seed material (hydroxyapatite or fluoroapatite) in order to commence the precipitation reaction. Once the reaction had started and the pH dropped from 7.4 the addition of solutions containing $CaCl_2$, KH_2PO_4, KOH and NaF for fluoroapatite was triggered by a pH-stat [90].

Some of the powders produced in the above mentioned aqueous precipitation processes were thermally treated in high temperatures for better crystallinity results. In most cases it is noted that the best purity hydroxyapatite and fluoroapatite powders are obtained, when the calcium to phosphate ratio is kept at the stoichiometric ratio 1.67 during the reaction.

2.5.3 Substitution of OH^- with F^- and the effect on solubility

Since fluoroapatite is a more stable form than hydroxyapatite, theoretically when provided with fluoride ions, hydroxyapatite should transform to fluoroapatite. This in fact is possible, but it depends on the concentration of fluoride ions [55]. For the formation of fluoride substituted hydroxyapatite there are two mechanisms [59]. The first one consists of the adsorption of F^- to the surface of the hydroxyapatite particles, their slow diffusion inside the structure, their replacing the OH^- ions and the diffusion of the latter out of the particles. The other mechanism is the consumption of Ca^{2+} and PO_4^{3-} that already exist in the solution at the same time with the hydroxyapatite, for the precipitation of fluoroapatite, which can contain OH^- in the structure.

Chen et al. report the synthesis of fluoroapatite nanostructures by mixing hydroxyapatite powder with a sodium fluoride solution in near stoichiometric conditions and adjusting the pH between 6 and 11. The suspension was then kept in a water bath at 70 °C for 5 days. The resulting powders were nanoscale structures of fluoroapatite [79].

A thermodynamic simulation for the synthesis of fluoroapatite by substitution of the OH^- of hydroxyapatite with F^- was done as part of the present work making use of the thermodynamic software package OLI. The calculation involved placing solid hydroxyapatite in an aqueous solution of NaF, for which the concentration varied from stoichiometric to the hydroxyapatite content, and non-stoichiometric. The results showed that if the amount of fluoride ions is stoichiometric, then the substitution is completed for the total amount of hydroxyapatite, but when the fluoride ions concentration exceeds the stoichiometric amount, the substitution does not happen fully unless the pH reaches 8.5, and when the amount of fluoride ions is in great excess the substitution is hindered at low pH.

2.6 Previous use of calcium phosphates for coating purposes

Hydroxyapatite and fluoroapatite are two very important materials used in biomaterials applications [56, 91, 92]. Research for both dental and bone implants is investigating the possibilities of using these two materials as coatings, in order to avoid implant rejection by the human organism and to induce osteointegration. The methods used for this kind of coating include electron beam evaporation [93], laser cladding [94, 95], sputtering [96], plasma spraying [97, 98], glass ceramics [91], electrochemical deposition [99] and aqueous deposition processes [100-102]. Most of these techniques are used for coating large items, such as hip replacement implants primarily made of titanium and its alloys, except for the aqueous deposition techniques, which can be used for particle applications.

Aqueous deposition is the process that utilises the heterogeneous nucleation mechanism in a solution, which depends on the control of supersaturation of the solution. As it was explained previously in the crystallisation theory section, supersaturation is dependent on pH, temperature and concentration of the solute compounds. Heterogeneous nucleation requires medium supersaturation levels in the solution. Since aqueous deposition can be used for particle applications and the present study deals with the development of an environmental technology, it is of greater interest to this work, since scorodite particles are relatively small and cannot be dealt with in macro scale in terms of encapsulation. Therefore, aqueous deposition was examined more closely than the other techniques that used hydroxyapatite and fluoroapatite for coating materials.

More specifically Wu et al. used a constant composition technique for the aqueous deposition of hydroxyapatite and fluoroapatite on titanium dioxide particles. Following this method a supersaturated solution containing NaCl to adjust the ionic strength, $CaCl_2$ and NaH_2PO_4 was prepared, the pH was adjusted by adding KOH and then the solution was left to equilibrate for approximately an hour. Subsequently, TiO_2 slurry was introduced in the solution, which initiated the reaction and caused the pH to decrease, which in turn triggered the addition of two solutions that provided adjustment of the pH, the ionic strength and the concentrations of calcium and phosphate. The

concentrations of these solutions were calculated in such a way so that the reaction was self sustained. Temperature was kept at 37 °C and the pH level was set at 7.4 [100]. By using this method it is easier to ensure that supersaturation is kept at the required level so that the homogeneous precipitation line is not exceeded and heterogeneous precipitation is favoured.

2.6.1 Scorodite encapsulation studies

Previous research at McGill University has studied the stabilisation of scorodite with aluminium hydroxy-gels [13]. In this case aluminium hydroxy-gels were prepared by base hydrolysing of aqueous aluminium solutions with sodium hydroxide. Once the gels were prepared, the scorodite particles were mixed with them and the mixture was left to age from 1 to 58 days. After the ageing step the solids were washed in order to remove excess soluble gel and they were then characterised and subjected to long term stability testing to verify the quality of the protection offered by the stabilisation process. The characterisation showed that the particles were coated but not uniformly and the long term stability results showed that the partial coverage of the surface of the scorodite particles reduced the arsenic release [13].

Research at McGill University also investigated the encapsulation of scorodite with phosphate coatings by aqueous precipitation. The experiments included the use of aluminium phosphate and hydroxyapatite as encapsulation materials [12]. For the encapsulation experiments using aluminium phosphate, an acidic phosphate solution of 0.16 mol/L of P and an Al/P ratio of 1:1 was introduced in the reactor, the temperature was raised to 95 °C and the solution pH was increased by addition of 1 mol/L NaOH solution until the pH reached 1.7, within the metastable zone of aluminium phosphate. Scorodite particles were added to the solution after it was left to equilibrate for 30 minutes. The pH was kept at 1.7 by addition of NaOH. The resulting solids were characterised and tested for long term stability. The coating produced was uniform and considerably thick, but the long term stability results showed that it was slowly dissolving over time and therefore after a certain period of time it would not offer protection any more [12].

Due to these results, another material was considered for the encapsulation of the scorodite particles. Lagno conducted experiments with calcium deficient hydroxyapatite where a metastable solution containing NaH_2PO_4 and $CaCl_2$ (0.9 and 1.5 mmol/L respectively) was prepared and left to equilibrate for 30 min, then the scorodite particles were introduced into the solution in order to start the precipitation and it was allowed to proceed for 30 min, and after that two solutions of Ca and P (100 and 60 mmol/L respectively) were simultaneously added to the metastable solution. The Ca/P ratios for all the solutions were kept at 1.67 and the pH of the solution was adjusted by addition of a 100 mmol/L NaOH solution. The characterisation of the solids demonstrated that a very thin layer of hydroxyapatite had been created and the long term stability results were not as good as the results for the aluminium phosphate coatings [12].

This work intended to repeat the hydroxyapatite experiments conducted by Lagno in order to improve the nature of the hydroxyapatite coating, since the earlier experiments had very thin hence not adequately protective coating. In addition the present work was undertaken to examine the possibility of forming coatings of fluoroapatite around the scorodite particles, taking advantage of the enhanced stability (lower solubility) of fluoroapatite compared to hydroxyapatite.

Chapter 3. Experimental

The experiments conducted for this work consisted of: 1) the homogeneous precipitation of hydroxyapatite and fluoroapatite separately, 2) the encapsulation experiments, or more specifically the heterogeneous deposition of hydroxyapatite or fluoroapatite on atmospherically precipitated scorodite particles and 3) the long term stability testing of the resulting solids from the encapsulation experiments. As part of this work scorodite was prepared under atmospheric pressure on scorodite seed particles prepared in an autoclave, in this section the common experimental setup and analytical methods are described, as well as the preparation of scorodite by atmospheric precipitation.

3.1 Chemicals

A list of all chemicals used is provided in Table 2.

Table 2: List of chemicals and materials used for the experiments

Name	Formula	Supplier	Grade
Arsenic(V) Oxide Hydrate (s)	$As_2O_5 \cdot xH_2O$	Sigma Aldrich	Analytical
Calcium Chloride (s)	$CaCl_2 \cdot 2H_2O$	Fisher Scientific	Reagent
Calcium Oxide (s)	CaO	Fisher	Reagent
Calcium Sulphate dihydrate (s)	$CaSO_4 \cdot 2H_2O$	Sigma Aldrich	Reagent
Hydrochloric Acid (sol)	HCl		
Hydroxyapatite (HAP ref.) (s)	$Ca_5(PO_4)_3OH$	Sigma Aldrich	Reagent
Iron (III) Sulphate Hydrate (s)	$Fe_2(SO_4)_3 \cdot xH_2O$	Sigma Aldrich	Reagent
Nitric Acid (sol)	HNO_3		
Sodium Chloride (s)	NaCl	Fisher Scientific	Reagent
Sodium Fluoride (s)	NaF	Anachemia	Reagent
Sodium Hydroxide (sol)	NaOH	Fisher Scientific	
Sodium Phosphate Monobasic Anhydrous (s)	NaH_2PO_4	Fisher Scientific	Reagent
Sodium Sulphite Anhydrous (s)	Na_2SO_3	Fisher Scientific	Reagent
Sulphuric Acid (sol)	H_2SO_4		

.

3.2 Experimental Setup

The experimental setup used for the precipitation experiments consisted of a 2 L Applikon Bioreactor adapted for inorganic precipitation, an ADI 1010 Bio Controller, which was connected to an ADI 1025 Bio Console with the ability to record data with the help of the BioXpert software by connection to a computer: pH, temperature and agitation speed. Agitation speed and pH were also controlled by the system. As the pH changed, the controller added either a base (typically 0.1 or 0.01 M NaOH) or an acid (typically 5 % HCl) to the solution in the reactor through two peristaltic pumps attached to the console. The bioreactor was a double walled glass cylindrical vessel with a stainless steel lid and agitator. Through the glass double walls oil, supplied from a ThermoHaake B3 bath was circulated by a Haake DC 30 bath temperature controller and pump for the temperature adjustment.

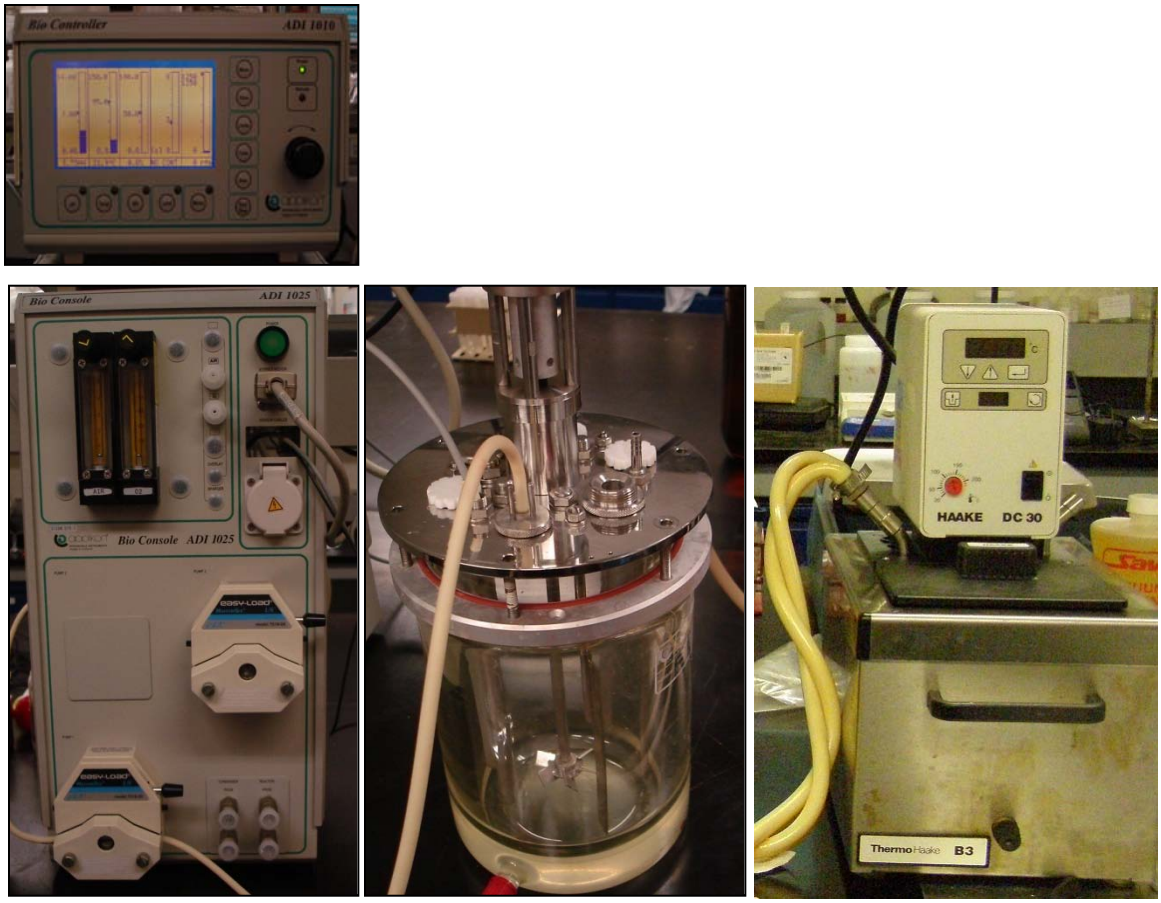

Figure 9: Left: ADI 1010 Bio Controller, Lower left: ADI 1025 Bio Console, middle: Applikon Bioreactor, right: Haake oil bath and temperature controller.

For the majority of the experiments only the base pump was equipped with a basic solution and a separate external pump drive with two pump heads was used for the addition of the feed solutions to the reactor. For some of the experiments two pump heads were mounted on the console on the same pump drive, to simultaneously add two different solutions automatically by the controller.

The external pump system, a pump drive that was used with two pump heads mounted on it, was calibrated to verify that the two pump heads were providing the reactor with the same flow rate of feed solutions. The following diagrams in Figure 10 give the results of this calibration.

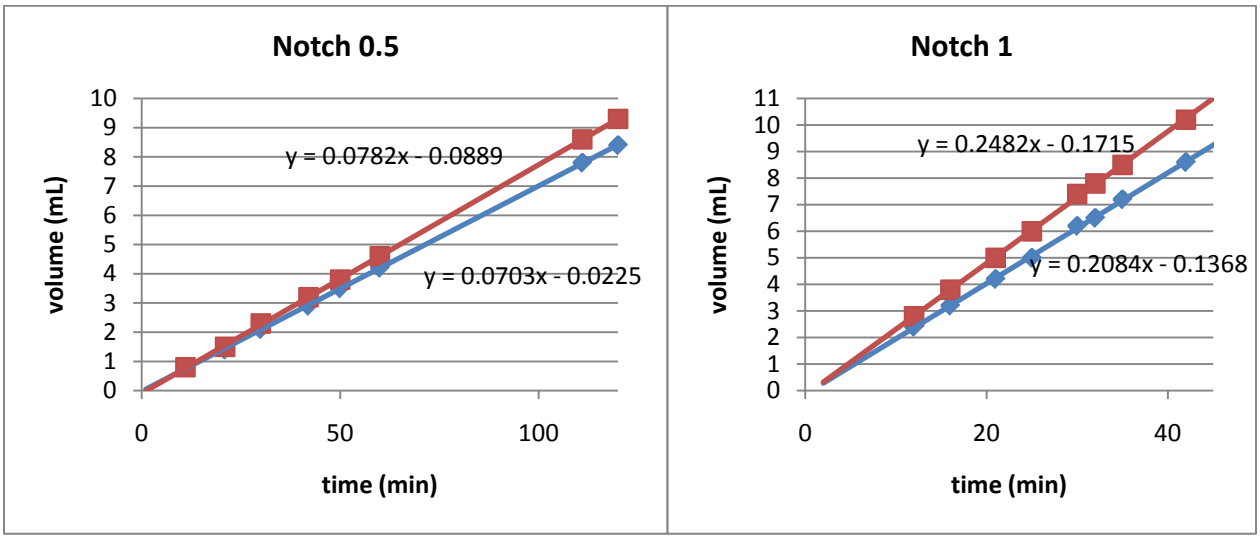

Figure 10: Volume of addition over time for two pump drive rotation speeds. ◆ for pump 1 and ■ for pump 2

The calibration shows that the two pump heads have a slightly different flow rate over time. Notches 0.5 and 1 represent the values given on the controller of the pump drive. The resulting flow rates for these two pump drive indications and for L/S 13 tubing were: Notch 0.5) 4.218 mL/h for pump 1 and 4.692 mL/h for pump 2, Notch 1) 12.504 mL/h for pump 1 and 14.892 mL/h for pump 2. The resulting difference in the supply of the feed solutions is considered negligible.

In Figure 11 a schematic diagram of the experimental setup that was used is shown. It should be noted that the entrance of the reagents to the reactor was separate for each of them. The tubing was placed in such way so that the solutions were introduced to the reactor through holes situated diametrically opposite to each other on

the reactor lid. This was done in order to ensure that the solutions were mixing well and supersaturation was kept at the desired level topically. The hole through which the base was added was also a different one, except for the case that the base and one of the reagents were in the same solution.

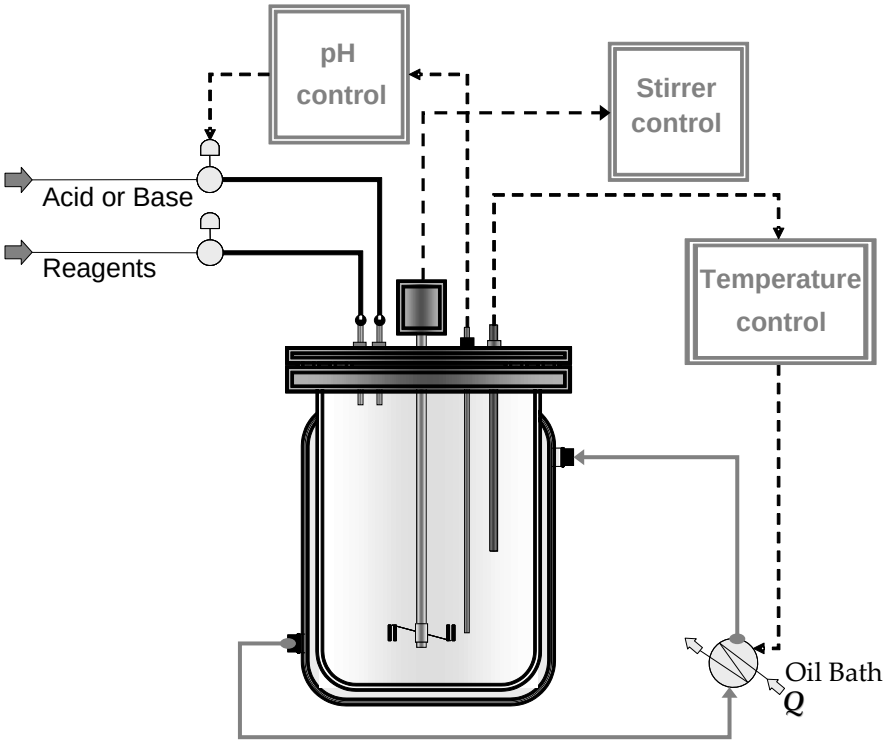

Figure 11: Schematic diagram of experimental setup.

For the recovery of scorodite powders following its atmospheric precipitation synthesis a stainless steel pressure filter of 1 L volume, whose surfaces that come in contact with the solutions are covered with a Teflon layer, was used. The pressure inside the airtight chamber was created by injecting pressurised air from a cylinder. However, for any solids containing hydroxyapatite or fluoroapatite, the suspension was left to settle in a glass beaker for a period of time and the liquid was decanted. This was done to avoid heavy agglomeration of the calcium phosphate particles, since it was discovered during the precipitation experiments of hydroxyapatite, that the particles have a sticky behaviour and tend to agglomerate into big bulky pieces.

The AppliSens pH^+ sensors used for pH measurements consisted of a non-toxic solid gel in a glass body with a fixed sleeve diaphragm. These probes were particularly accurate and stable in their measurements. When used for the experiments and the stability testing they were calibrated using buffer solutions from Fisher Scientific of pH 4, 7, 10.

3.3 Chemical analysis

For the determination of solute concentrations of samples taken either from the solutions used in the precipitation experiments, or those taken from the suspensions under long term stability testing and also the digested solids, the method Inductively Coupled Plasma - Optical Emission Spectroscopy (ICP-OES) was used. The elements analysed with this technique were arsenic, iron, calcium and phosphorus. The digestion of the solids was done in concentrated hydrochloric acid (100 mg powder in 50 mL 36.5 % HCl, that were manually shaken until no solids were visible and then left for 30 minutes to homogenise, and subsequently samples were diluted within the detection limits of the ICP-OES) at room temperature. The samples taken from the solutions used for the precipitation experiments, or during an experiment, were filtered with 0.22 µm pore size syringe filters and diluted in 4 % nitric acid to avoid further precipitation and to have a common matrix with the standards. The multi point calibration for the ICP-OES was done with standards depending on the concentration of the samples: a) standards of 0.5, 5, 50 mg/L Ca, P for the samples from the homogeneous precipitation experiments, b) standards of 0.5, 5, 50 mg/L As, Fe for the scorodite precipitation samples, c) standards of 0.5, 5, 50 mg/L Ca, P and 0.1, 1, 10 mg/L As, Fe for the encapsulation experiment samples, and d) standards of 0.5, 5, 50 mg/L Ca, P and 0.1, 1, 10 mg/L or 0.5, 5, 50 mg/L As, Fe for the long term stability samples depending on the expected concentration of the sample. In the case of fluorine, Ion Chromatography (IC) was used to determine its concentration using standards of 1, 5, 10 mg/L. All standards were prepared from 1000 mg/L ICP standards.

To verify the validity of the ICP-OES results and when an on-the-spot analysis of the phosphorus levels was required in order to control supersaturation and avoid

homogeneous precipitation during the encapsulation tests, a UV colorimetric method was used [103]. The method involved preparing samples with an ammonium vanadate – ammonium molybdate colour reagent and scanning them with a Perkin Elmer Lambda 20 UV-Vis Spectrometer. For the preparation of the colour reagent 25 g of ammonium molybdate ($(NH_4)_6\ Mo_7O_{24}.4H_2O$) were dissolved in 300 mL of deionised water and 1.25 g of ammonium metavanadate (NH_4VO_3) were dissolved in 300 mL of boiling deionised water. Once the second solution had cooled down, 330 mL of concentrated HCl were added and once it had reached room temperature, the first solution was added to it. The final solution was mixed well and completed up to 1 L. The multi point calibration for the Spectrometer was done with standards of 5, 10, 15 and 20 mg/L, which were all prepared from a phosphorus ICP standard. The samples were mixed with the colour reagent depending on the expected concentration of the sample. Mostly they were prepared in the following fashion: 7 mL or less of the sample with a phosphorus amount of 0.05 to 1.0 mg were mixed with 2 mL of colour reagent, and the container was filled up to 10 mL. The samples were read using the Spectrometer after 10 minutes had passed, so that all of the phosphorus in the sample had been complexed with the colour reagent, at a wavelength of 470 nm (for phosphorus concentrations of 4 to 18 mg/L). The software translated the absorbance to concentration.

For the characterisation of the solids various techniques were employed.

- X-Ray Diffraction Analysis (XRD): The solids were ground and then analysed with a Philips PW 1710 X-Ray Diffractometer with a copper target (Cu $K\alpha_1$ radiation, λ=1.5405Å), a crystal graphite monochromator and a scintillation detector. The diffractometer operated at 40 kV and 20 mA. The samples were scanned from 2 to 100 °2θ at a step size of 0.1 °2θ and at a scan step time of 3 s. The crystal phases were identified using the X'Pert Highscore software, version 2.1b.
- Scanning electron microscopy – Energy dispersive X-ray spectroscopy (SEM-EDX): All sample powders were characterised morphologically by SEM analysis.

Two methods were used: first, particles were placed on double sided carbon tape and examined with a JEOL JSM-840a, Hitachi S-4700 Field Emission Scanning Electron Microscope (FE-SEM) or a Hitachi S3000N Variable Pressure Scanning Electron Microscope (VP-SEM), and second, particles were mounted in cold setting epoxy resin, which once it had solidified it was ground and polished to uncover the particles from the resin and create cross-sections of the particles which were then examined under low pressure, to avoid charging of the sample, in the Hitachi S3000N VP-SEM. Cross-section samples were also analysed by EDX and elemental mapping in order to verify the composition of the layers. The software used for EDX was INCA Energy Software.

- Fourier Transform Infrared Spectroscopy (FTIR): Sample spectra over the 4000-650 cm^{-1} range were obtained using a Perkin Elmer FTIR (Spectrum BX model) spectrometer with a Miracle single bounce diamond ATR cell from PIKE Technologies. The Spectrum software (version 5.02) was used to perform spectral manipulation, such as baseline adjustment and normalisation.
- Thermogravimetric analysis (TGA): Samples were analysed using a TA Instruments Q500 TGA. The temperature range was from 25 and 1000 °C at a heating rate of 20 °C/min. The purge gas used was nitrogen.
- Particle size analysis (PSA): Particle size distribution of the scorodite particles in an aqueous suspension was obtained with a HORIBA LA-920 Laser Scattering Particle Size Analyzer.
- Raman Vibrational Spectroscopy: Scorodite particles were analysed with a Renishaw In Via microscope with 20x short distance objective and a polarised argon laser at 514 nm operating at 10 % power at the microscope exit.
- BET Surface Area Characterisation: A Micromeritics TriStar 3000 was used to measure the BET surface area of the scorodite particles. The conditions were nitrogen controlled atmosphere at 80 °C.

3.4 Preparation of scorodite

The preparation of scorodite was completed in two steps following procedures previously described elsewhere [13]. Firstly, scorodite seed was produced hydrothermally in sulphate media, and secondly the hydrothermal scorodite seed was used for the precipitation of scorodite under atmospheric pressure conditions. Below the procedures for both steps are described followed each by the characterisation of the corresponding solids.

3.4.1 Preparation of Scorodite Seed

The scorodite seed that was used for the atmospheric precipitation of scorodite was produced according to a modified procedure originally described by Dutrizac and Jambor [29]. The difference from the original procedure is that sulphate rather than nitrate media were used [22, 104]. A solution containing 0.3 mol/L of arsenic pentoxide and 0.3 mol/L hydrated ferric sulphate was prepared and introduced in the autoclave, where it was heated up to 160 °C under continuous stirring. The experiment had a duration of 24 h. It was then cooled down and the suspension was filtered, washed 2 times and repulped, and the cycle was repeated 3 times using a 0.2 μm pore size microcellulose membrane with the pressure filter that is described in 3.2. The solids were dried at 50 °C for several hours.

3.4.1.1 Characterisation

The precipitated scorodite had very good crystallinity as the following X-ray diffraction pattern shows. It also verifies that the precipitate was scorodite when compared to a reference pattern of scorodite.

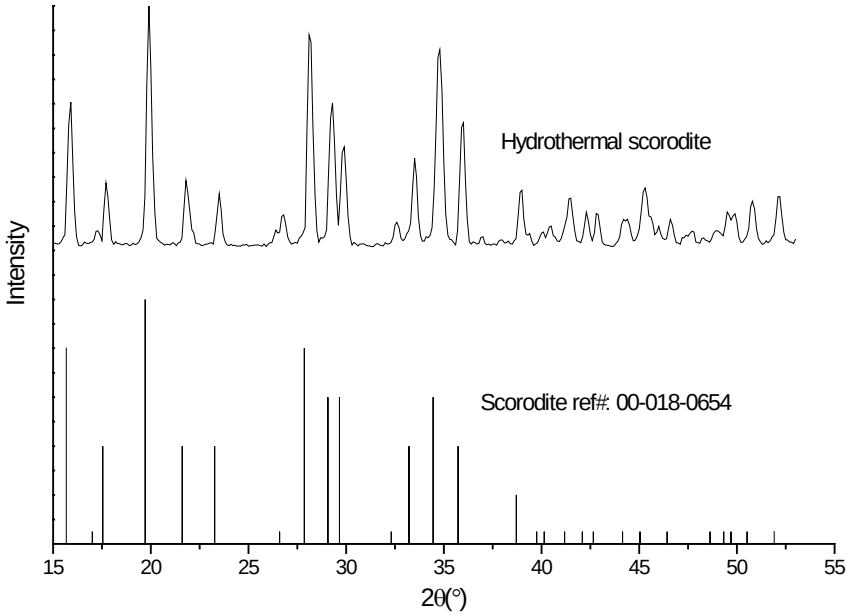

Figure 12: XRD spectrum of hydrothermally precipitated scorodite.

The SEM images taken of the scorodite particles are shown below.

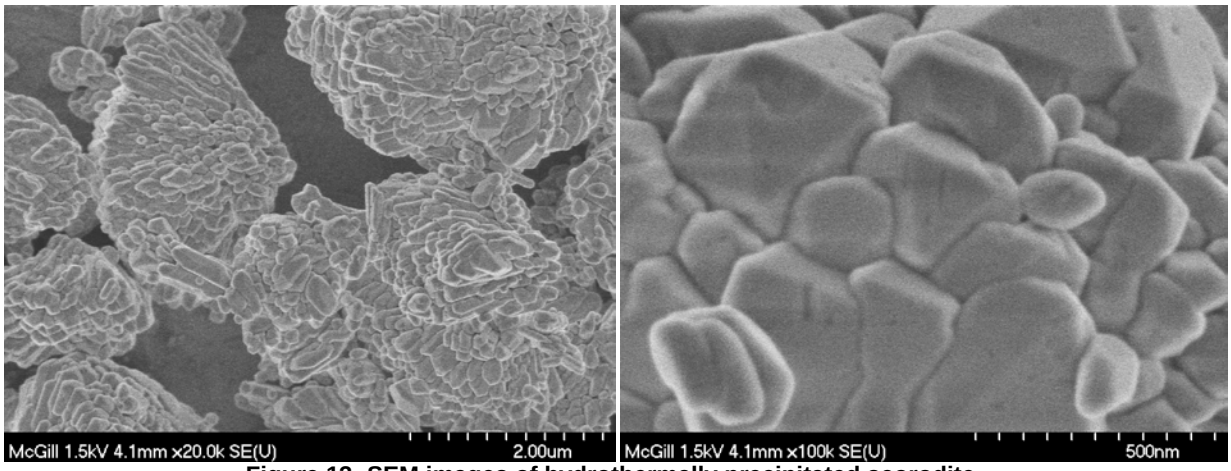

Figure 13: SEM images of hydrothermally precipitated scorodite.

The particle size distribution is presented in the following diagram. The mean value of the particle size was 2.15 μm and the median 1.48 μm. This shows that homogeneous nucleation was the main precipitation mechanism, although there was significant heterogeneous growth mostly via agglomeration.

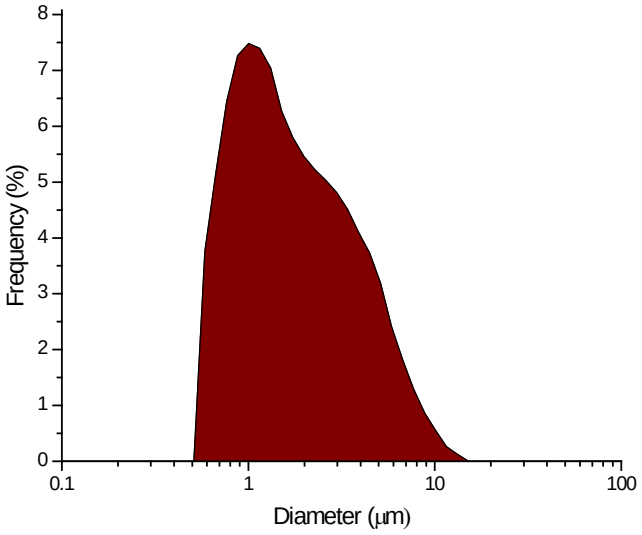

Figure 14: Particle size analysis of hydrothermally precipitated scorodite.

The Raman spectrum of the hydrothermal scorodite particles depicts the Raman shifts that are expected for this material. Peaks and bands at 3517, 3079, 891, 800, 424, 337 and 180 cm^{-1} all belong to AsO_4^{3-}. The next spectrum is that of FTIR where the AsO_4^{3-} peak is clear at 792 cm^{-1}, a small band at 1070 for SO_4^{2-} cm^{-1}, the water broad bands at 1588 and 2971 cm^{-1} and the OH^- vibrations at 3517 cm^{-1}[104].

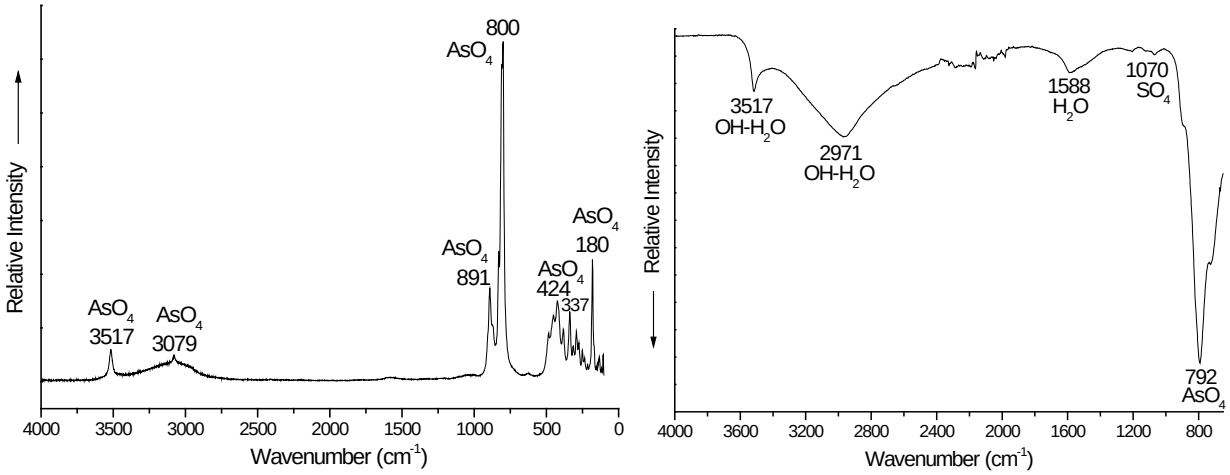

Figure 15: On the left Raman spectrum and on the right FTIR spectrum of hydrothermally precipitated scorodite.

The thermogravimetric analysis (Figure 16) of the hydrothermal scorodite shows that the water that was part of the crystal lattice of the scorodite was 15.4 % of the whole mass, which is a bit less than the 15.6 %, which is the theoretical amount.

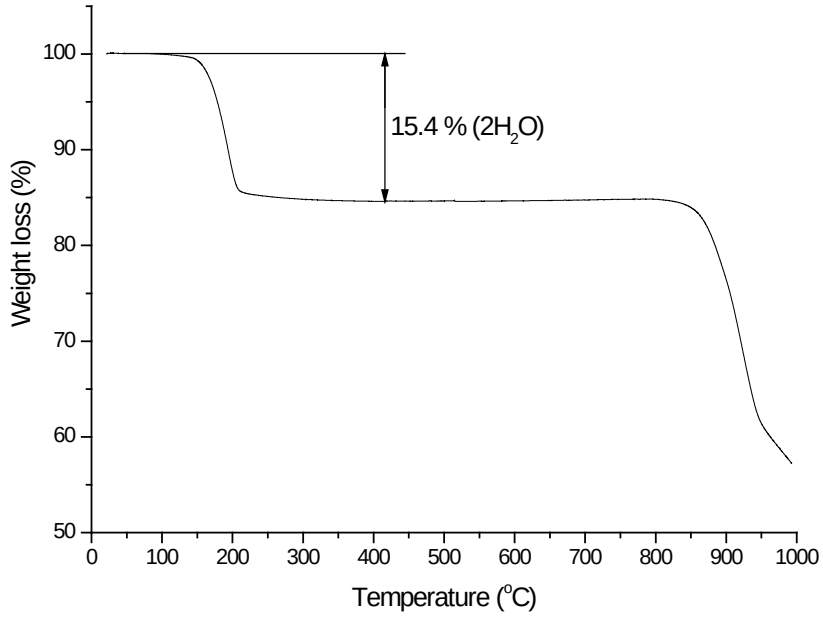

Figure 16: Thermogravimetric analysis of hydrothermally precipitated scorodite.

The measurement of the BET surface area of the hydrothermally precipitated scorodite was 7.5726 m^2/g. Using this value we can calculate the equivalent primary crystallite size (0.24 µm-see equation 3.1) of which the bigger agglomerated particles consist.

$d = \frac{6 \times 10^4}{\rho \times S} = \frac{6 \times 10^4}{(3.27 g/cm^3) \times (7.5726 \times 10^4 cm^2/g)} = 0.24 \mu m$	3.1

Where d = Equivalent particle size (µm)

ρ = Density (g/cm^3)

S = Specific surface area (cm^2/g)

3.4.2 Production of Scorodite under Atmospheric Pressure Conditions

For the atmospheric precipitation of scorodite on hydrothermally produced seed, a variation of the procedure described by Leetmaa [13] was followed. It consists of the

preparation of a solution of arsenic pentoxide of 40 g/L arsenic concentration, and ferric sulphate with a ratio of 1. The solution is prepared by adding the arsenic pentoxide to deionised water and heating it up (no more than 50 °C), so that dissolution happens faster. Then, once all of the arsenic pentoxide has been dissolved the heating is stopped, the ferric sulphate is added and the solution is magnetically stirred until all of it is dissolved. The colour of the solution is a deep green-brown, yet transparent and the pH is about 0.38. It is then filtered to remove any impurities or any amorphous material that might have formed during the preparation of the solution and it is subsequently introduced to the reactor, where it is heated up to 85 °C, where a small cloud of precipitate is formed and sulphuric acid is added to the solution in order to dissolve it (pH drops to 0.34). Once the solution is clear, the hydrothermal scorodite seed (5 g/L) is introduced to the solution and the temperature is kept stable at 85 °C, until after 2 hours have passed and then the temperature is brought up to 95° in order to speed up the kinetics of the precipitation. The solution is left at that temperature for 9 hours. The temperature and pH profiles of a typical precipitation test are shown in Figure 17. At the end of the experiment the solution is left to cool down and it is then filtered and washed.

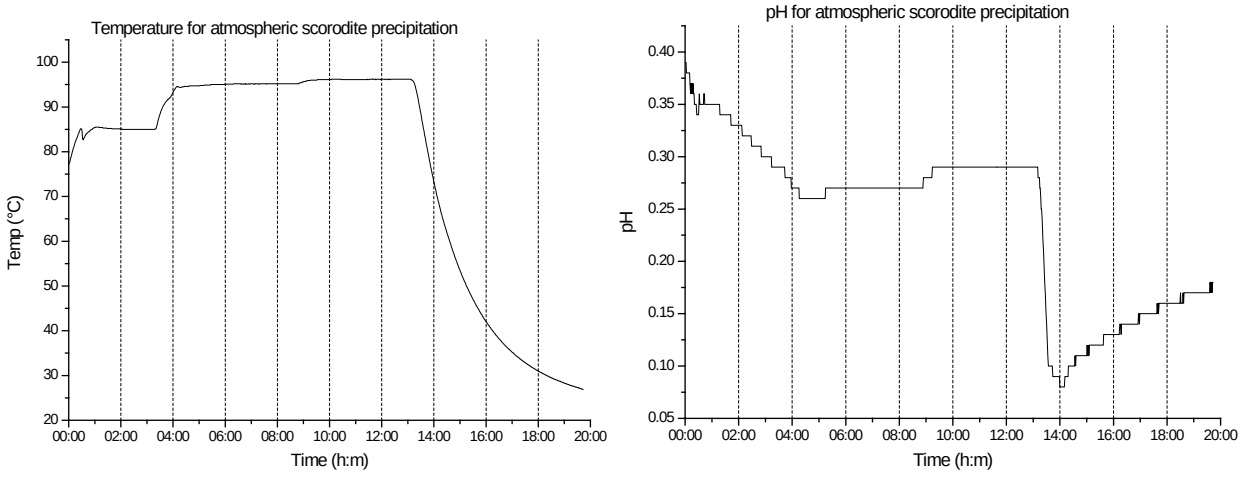

Figure 17: Temperature and pH during atmospheric scorodite precipitation.

The filtering and washing procedure consists of a pressure filtration step, two washing steps by adding 1 L of deionised water in the filter each time and filtering it through the solids, and a re-pulping step, where the solids are placed in 1 L of deionised water and the suspension is left for 3 hours, or overnight under stirring with a

mechanical impeller. This procedure was employed in order to remove any amorphous, and therefore soluble, material that would affect the stability results and possibly the encapsulation process. In Figure 18 the concentration of arsenic in the various filtration, washing and repulping stages is reported.

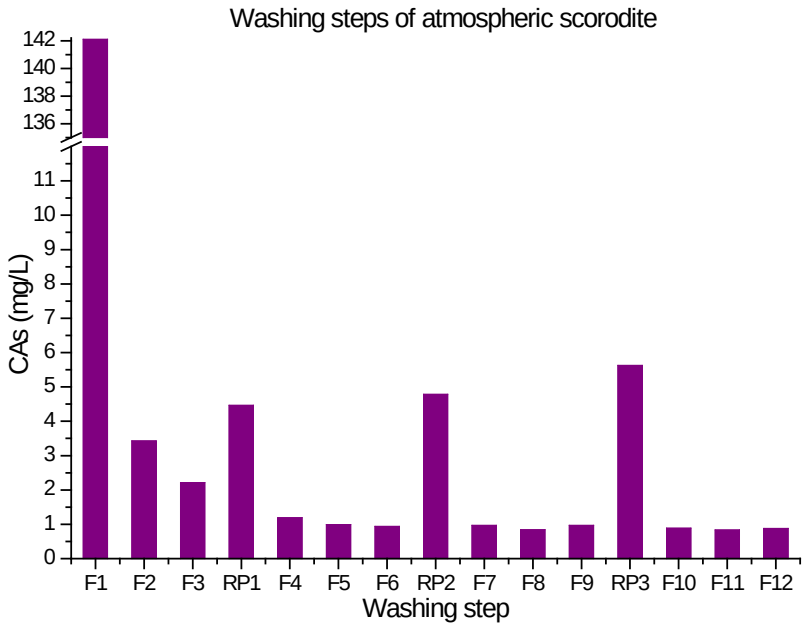

Figure 18: Arsenic concentration for the filtering washing and repulping steps for atmospherically precipitated scorodite. F1 is the filtration right after the synthesis, and steps RP1, RP2 and RP3 give higher concentrations due to the repulping step before the filtration.

The chemical analysis of the initial solution before the precipitation showed that the solution contained 40.94 g/L of arsenic and the final solution concentration, once the experiment was stopped, was 5.785 g/L of arsenic. This means that there was a total of 85.9 % arsenic removal during the precipitation.

The solids were stored wet in glass jars that were air tightly closed, to avoid drying and therefore any change in the surface properties of the particles, such as cracking that may interfere with the subsequent encapsulation tests. The scorodite that was used for characterisation was dried at 50 °C, while the scorodite used for scanning electron microscopy was dried at lower temperature using ethyl alcohol to disperse the particles.

3.4.2.1 Characterisation

The atmospherically precipitated scorodite was subjected to XRD analysis and the following spectrum is the result. When compared to a reference spectrum it has all the characteristic peaks of the scorodite and it also has very good crystallinity.

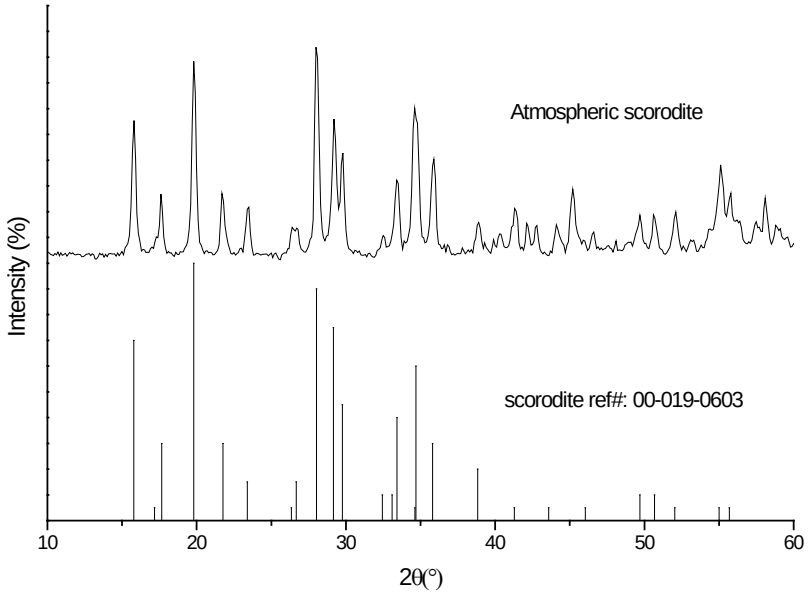

Figure 19: XRD spectrum of the atmospherically precipitated scorodite.

The Scanning Electron Microscopy images that follow represent scorodite particles that were precipitated. It is possible to see here that surface deposition, as it is described in 2.3.2 the deposition of layers of material on the particles, was the main growth mechanism (epitaxial growth).

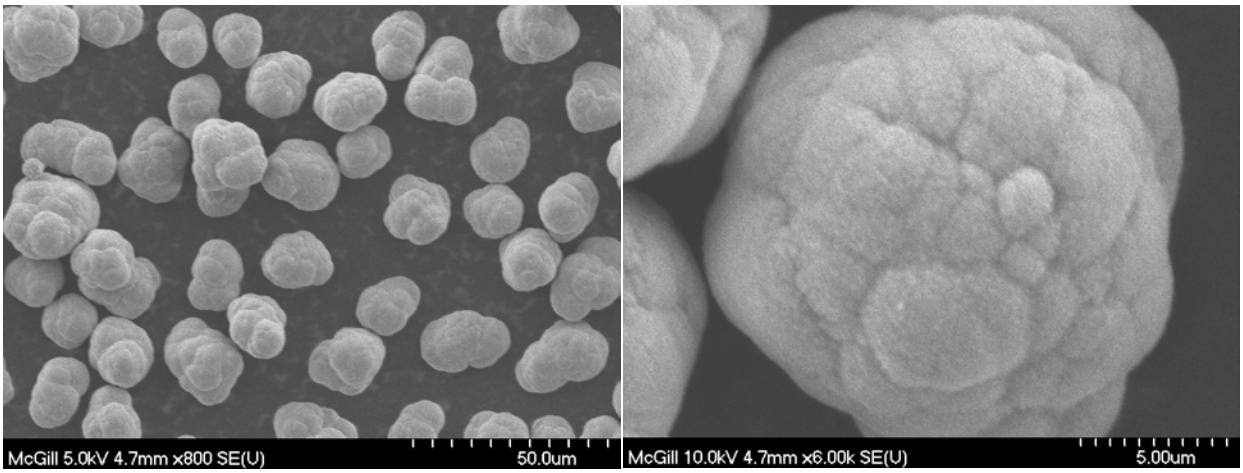

Figure 20: SEM images of the atmospherically precipitated scorodite particles.

The particle size analysis results demonstrate (Figure 21) that the average size of the particles is 19.84 μm and the median is 19.70 μm.

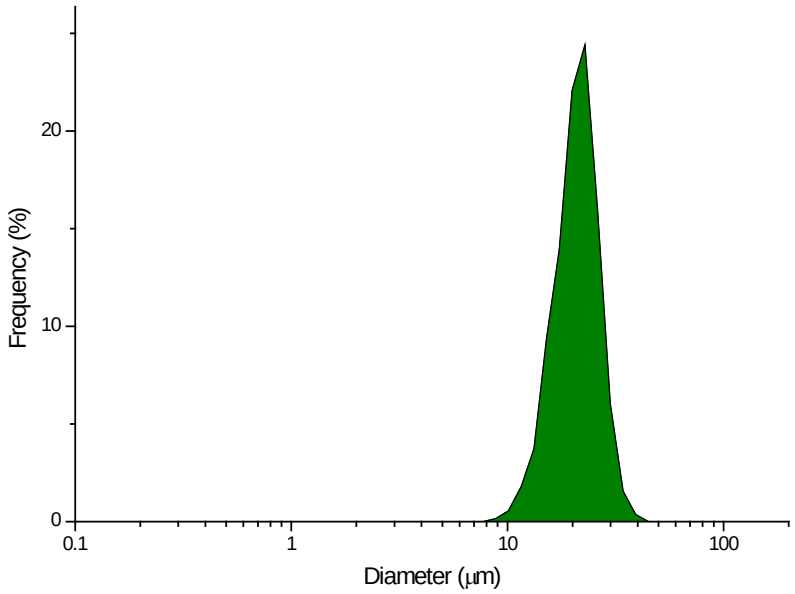

Figure 21: Particle size distribution of atmospherically precipitated scorodite.

As seen from the above graph the precipitation of scorodite on the hydrothermally produced seed happened in its entirety heterogeneously, as in there was no homogeneous precipitation of scorodite particles that would be present in the particle size analysis as sizes between 1 and 5 μm. This means that during the experiment supersaturation was well controlled within the metastable zone.

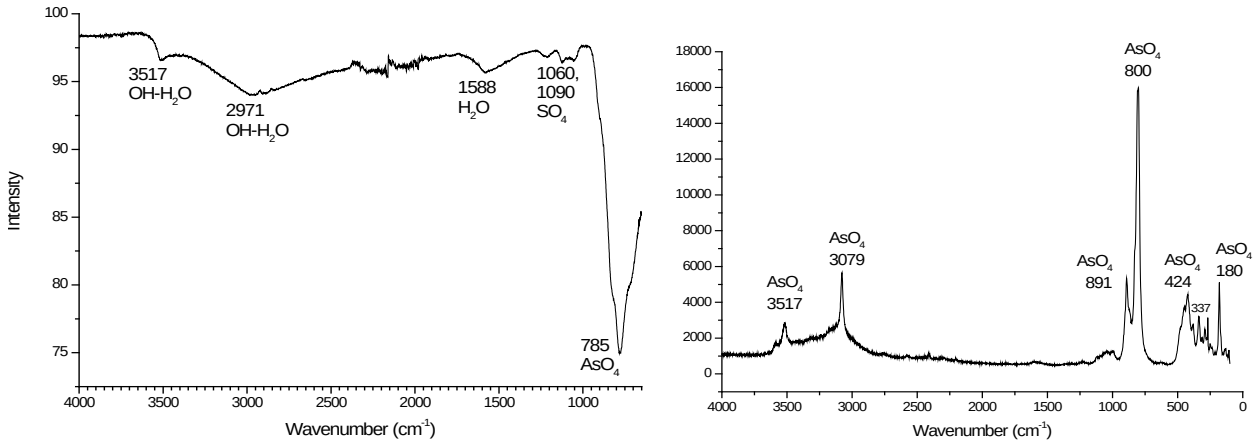

Figure 22: On the left FTIR spectrum and on the right Raman spectrum of the atmospherically precipitated scorodite.

Once again spectroscopic analysis (Figure 22) confirmed on the basis of previous work the scorodite identity of the produced material [104]. Thus in the FTIR spectrum the AsO_4^{3-} peak is sharp at 785 cm^{-1}, sulphate bands at 1060 and 1090 cm^{-1}, and water and hydroxyl bands at 3517, 2971 and 1588 cm^{-1}. In the Raman pattern the AsO_4^{3-} are all visible at 3517, 3079, 891, 800, 424, 337 and 180 cm^{-1}[104].

The thermogravimetric analysis (Figure 23) of the scorodite powder shows that 15.6 % of the weight is lost between 100 and 200 °C, which is the theoretical amount of crystallisation water present in scorodite.

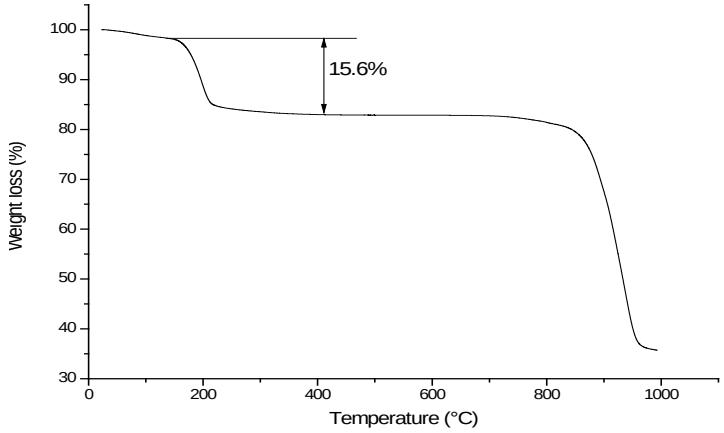

Figure 23: Thermogravimetric analysis for the atmospherically precipitated scorodite.

The BET surface area measurement was 0.7550 m^2/g. This translates into 2.43 µm of equivalent primary crystallite size. This is 10 times larger than the corresponding crystallite size of the hydrothermally produced seed.

$$d_p = \frac{6\times10^4}{\rho\times S} = \frac{6\times10^4}{(3.27 g/cm^3)\times(7.55\times10^3 cm^2/g)} = 2.43\mu m \qquad (3.2)$$

Where d_p = Equivalent particle size (µm)

ρ = Density (g/cm^3)

S = Specific surface area (cm^2/g)

3.5 Stability Testing

In this section the procedure for the evaluation of the stability (resistance to arsenic release) of selected encapsulated scorodite products from the hydroxyapatite and the fluoroapatite encapsulation experiments is described, as well as for reference scorodite and hydroxyapatite. These tests included in general evaluation of leachability under oxic and/or anoxic (~150 mV against SHE) conditions at pH 8 and sometimes pH 7 & 9 over several weeks. Also, two stability tests were done at pH 8 and 150 mV where the solids consisted of a physical mixture of scorodite and hydroxyapatite, to verify that simply the presence of the hydroxyapatite powder in the suspension does not cause the reduced arsenic release from the scorodite. For these mixtures, the encapsulation solids percentage that is taken up by hydroxyapatite was calculated from their chemical analysis after digestion. This percentage was found to be 17 % for ENCH 10 and 13 % for ENCH 13, thus a 15 % of the mixture was decided to be hydroxyapatite and the rest scorodite. Of the two samples prepared, the first was a mixture of scorodite and the reference hydroxyapatite powder (acquired from Sigma Aldrich) and the second of scorodite and HAP 3-one of the homogeneously precipitated HAP products during the course of this work.

The stability tests were conducted using a 40:1 liquid to solid ratio, $Ca(OH)_2$ saturated deionised water slurry (14.76 g in 500 mL) and a 5 % H_2SO_4 solution to adjust the pH, Na_2SO_3 powder or a 1.4M solution to adjust the e_h for the anoxic tests and for some tests $CaSO_4 \cdot 2H_2O$ (4 g per sample of 200 mL), to see the effect of gypsum saturated water on stability [105]. The pH was adjusted regularly if it were measured to be at least 0.2 units lower or higher than the desired value and the e_h was adjusted when it was measured to be at least 20 mV lower or higher than the target (150 mV) value. This was done in order to avoid the frequent adjustment of the suspensions, which would cause them to get destabilised and shift away from equilibrium, resulting in higher release of the compounds' constituents, as already observed and discussed by Leetmaa [13]. The samples taken from the stability tests were chemically analysed by ICP-AES for As, Fe, Ca and P.

Chapter 4. Results and Discussion

In this chapter the homogeneous precipitation of HAP and FAP study is described first, followed by the encapsulation and stability testing results.

4.1 Homogeneous precipitation of hydroxyapatite and fluoroapatite

4.1.1 Hydroxyapatite precipitation

Hydroxyapatite was precipitated under different conditions of concentration and temperature. The procedure employed was similar to the method described by Rodriguez-Lorenzo et al.[78] as it was modified by Lagno [12]. Using the experimental setup described previously (3.2), a metastable solution of Ca and P was prepared, by introducing a 500 mL solution of NaH_2PO_4 in the reactor and then slowly adding 500 mL solution of $CaCl_2$. The pH of the metastable solution was initially around 5 and it was adjusted to 7.6 before the experiment was started. After about 30 min of equilibration, the feed solutions of NaH_2PO_4 and $CaCl_2$, 200 mL of each, were added at a rate of 20 mL/h. The pH was kept at 7.6 by addition of 0.1 M NaOH by the reactor controller, which activated a peristaltic pump when the pH meter measured a decrease in pH. The Ca:P ratio was kept at 1.67 (the stoichiometric ratio of HAP) for all experiments but one, which had a Ca:P=2.0 (HAP 2).

In Table 3 below, the different concentrations and temperatures of the experiments are provided along with the molar ratio Ca:P in the produced solids (determined via chemical analysis following digestion). With the exception of the first two experiments the produced hydroxyapatite has an average 1.575 Ca:P molar ratio hence qualifies as Ca-deficient HAP [12, 106]. It is interesting to note that hydroxyapatite powder of high purity and crystallinity obtained from Sigma Aldrich Chemical Co, that is frequently used as reference for the characterisation of the produced powders in this work, was also chemically analysed after digestion and the Ca:P ratio was 1.48.

Table 3: Experimental parameters for the homogeneous precipitation of hydroxyapatite powders and the Ca:P ratio in the resulting solids.

Experiment No	P concentration (mmol/L) metastable/feed	Ca concentration (mmol/L) metastable/feed	Temperature (°C)	Ca:P in the solids
HAP 1	1.8/30	3/50	22±1	1.31
HAP 2	1.8/30	3.6/60	22±1	1.25
HAP 3	19.8/330	33.06/561	22±1	1.58
HAP 4	10.02/167	17.04/284	22±1	1.65
HAP 5	15/250	25.5/425	22±1	1.49
HAP 6	25.02/417	42.54/709	22±1	1.53
HAP 7	19.8/330	33.06/561	50±1	1.58
HAP 8	19.8/330	33.06/561	80±1	1.62
AVERAGE (3-8)				1.575±0.058

4.1.1.1 Characterisation

From the XRD spectra of the precipitated powders (Figure 24 and Figure 25), it is shown that they are indeed hydroxyapatite. Judging from the breadth of the peaks it may be concluded that surprisingly the crystallinity increased with increasing concentration, i.e. with increasing supersaturation, which is the opposite expected from crystallisation theory-refer to Chapter 2. This apparent contradiction could not be explained at this point. Clearly the product obtained at low concentration (HAP-1 at 30 mmol/L P) was rather poorly crystalline and this might explain the somewhat lower ratio in it, i.e. 1.3. For the other room temperature HAP products crystallinity is reasonably good, but it is obvious that by conducting the experiments in higher temperature leads to enhanced crystallinity.

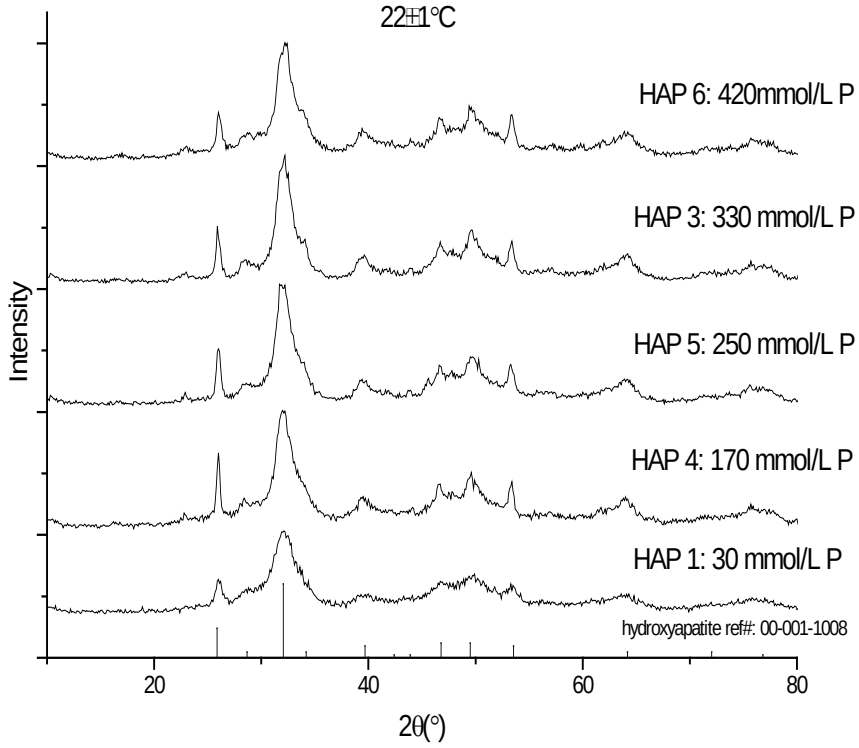

Figure 24: XRD patterns of the homogeneously precipitated hydroxyapatite powders for different concentrations at 22 °C.

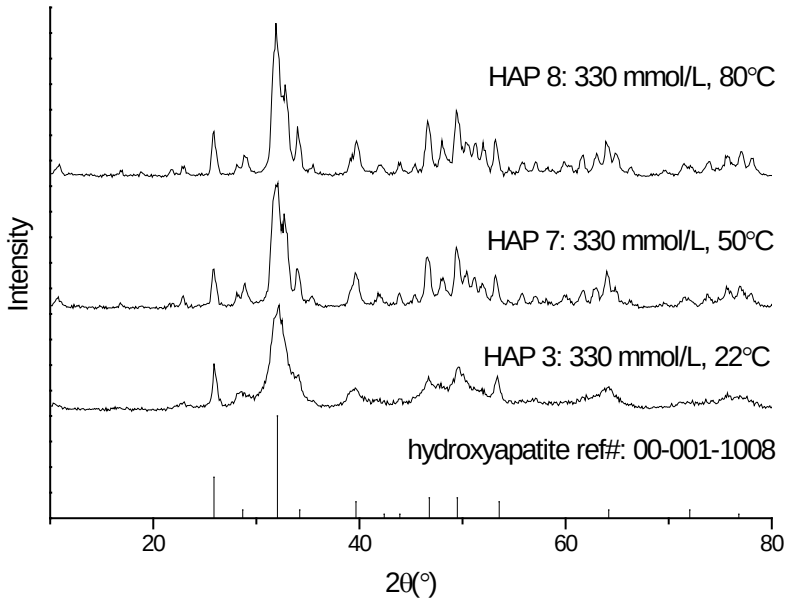

Figure 25: XRD patterns of homogeneously precipitated hydroxyapatite powders at different temperatures.

The scanning electron microscopy images (Figure 26-Figure 29) of the hydroxyapatite products show that they consist of heavily agglomerated particles. The extensive agglomeration may be however largely due to the drying of the powders prior to their examination.

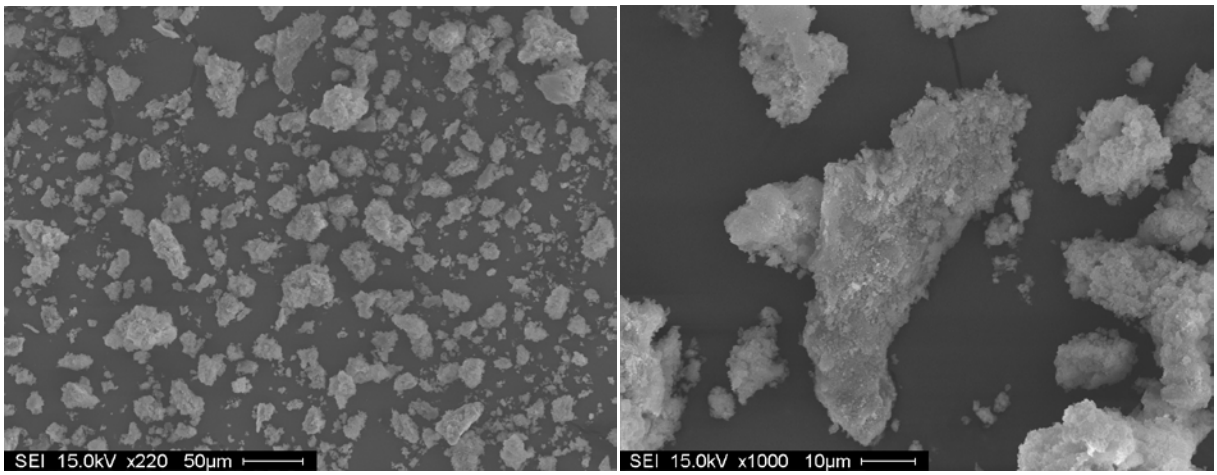

Figure 26: SEM images of hydroxyapatite product HAP 4: 170 mmol/L P.

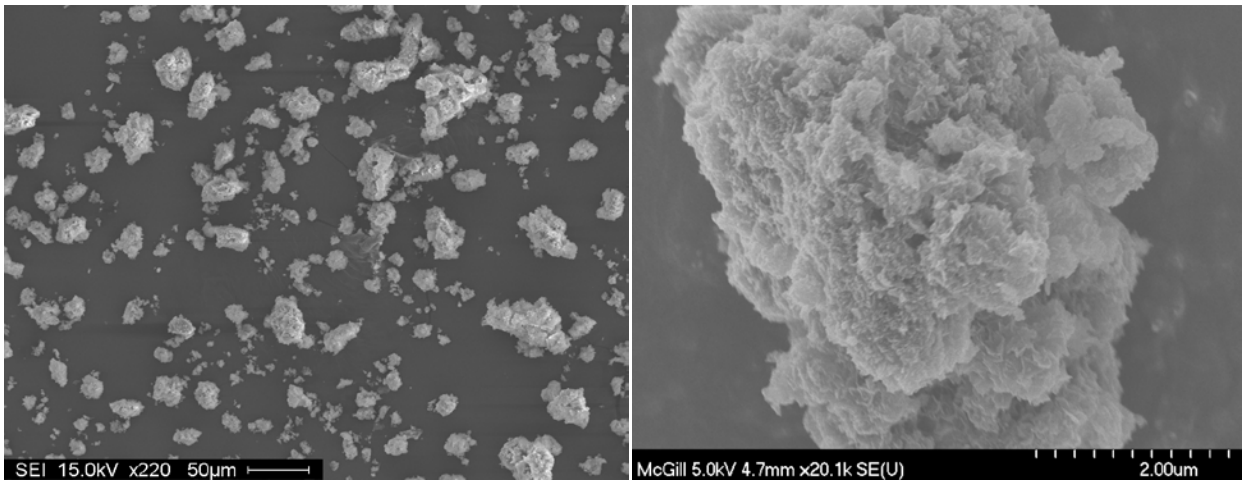

Figure 27: SEM images of hydroxyapatite product HAP 3: 330 mmol/L P.

In agreement with the previously made XRD observations about an enhancement in crystallinity with temperature elevation, this was also clearly visible from the SEM images (compare Figure 27, Figure 28 and Figure 29). As the temperature of the experiments increases, so does the length of the nanocrystals that are rod-like.

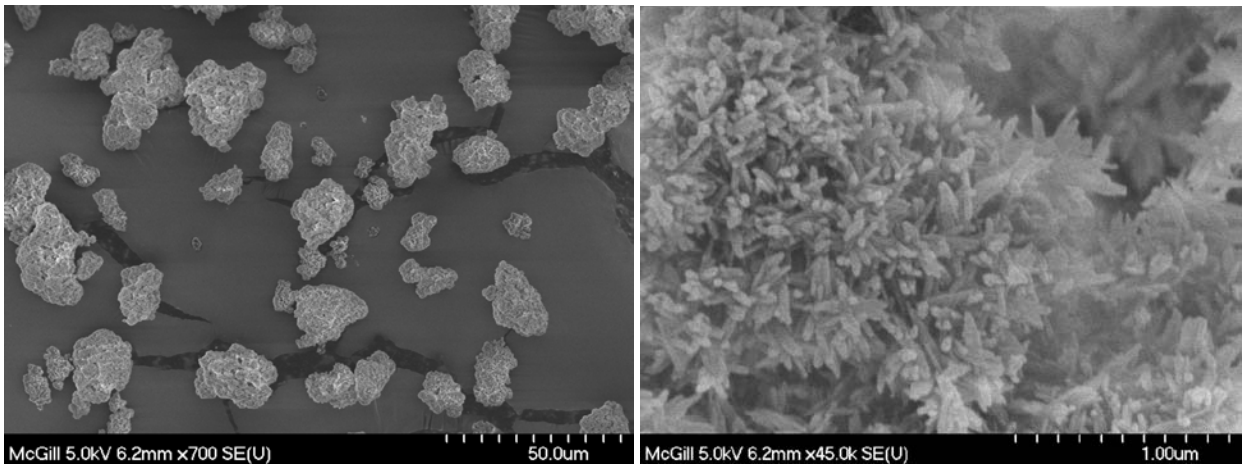

Figure 28: SEM images of hydroxyapatite product HAP 7: 330 mmol/L P, 50 °C.

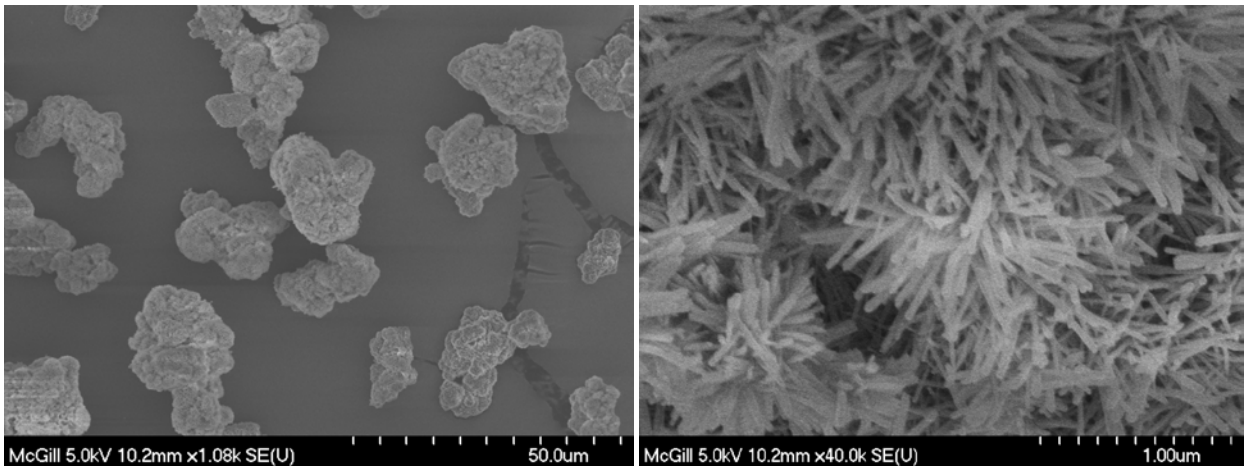

Figure 29: SEM images of hydroxyapatite product HAP 8: 330 mmol/L, 80 °C.

The hydroxyapatite powders were subjected to FTIR spectroscopy and the results are shown in Figure 30. For sample HAP 6 it seems that the powder had not been dried thoroughly as the spectrum shows a large amount of water.

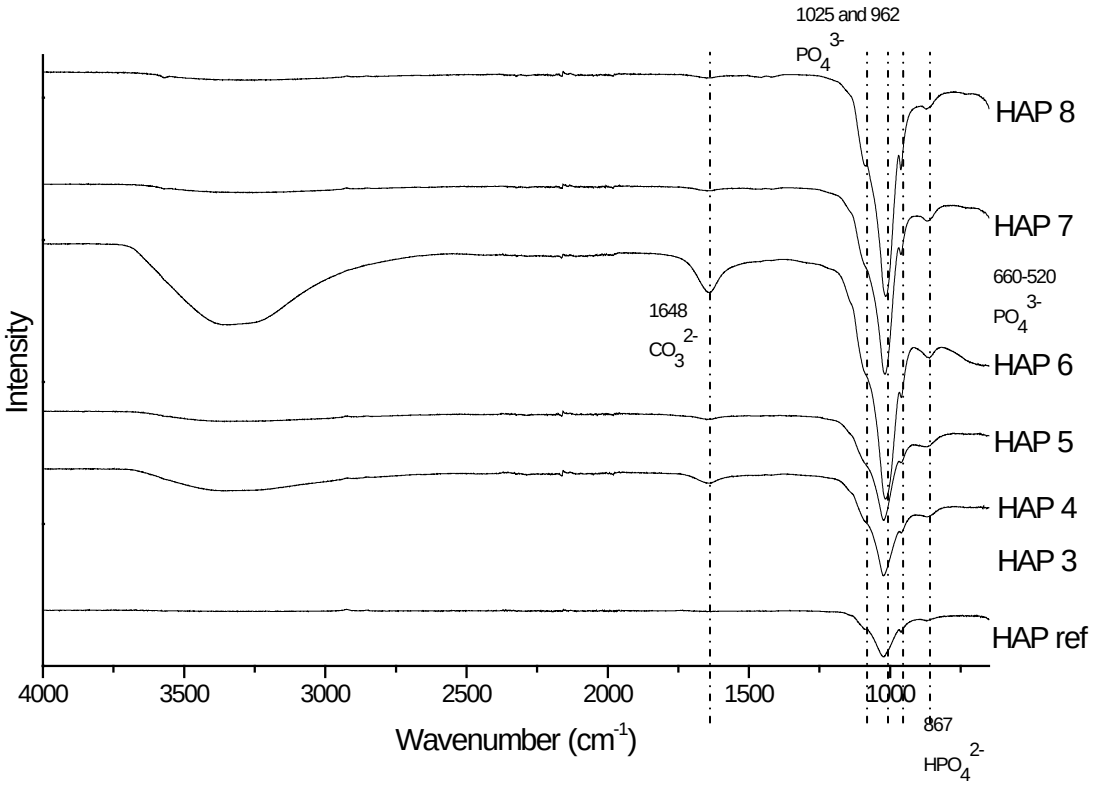

Figure 30: FTIR spectra of homogeneously precipitated hydroxyapatite powders.

The spectra show typical vibration modes of apatites. HPO_4^{2-} vibrations were observed at 867 cm^{-1} and PO_4^{3-} peaks at 962 cm^{-1} and 1027 until 1015 cm^{-1} as part of the 1080-967 cm^{-1} band. The bands that normally are observed for PO_4^{3-} between 660 and 520 cm^{-1} are unfortunately not included in the above patterns, since the measurement was executed for the range of 4000-650 cm^{-1}, but it is possible to observe the decrease in intensity starting at around 660 cm^{-1} [107, 108]. The OH-H_2O broad band is also present in all the spectra, but the hydroxyl band at 3567 is visible only if the spectra are viewed at a close range (Figure 30).

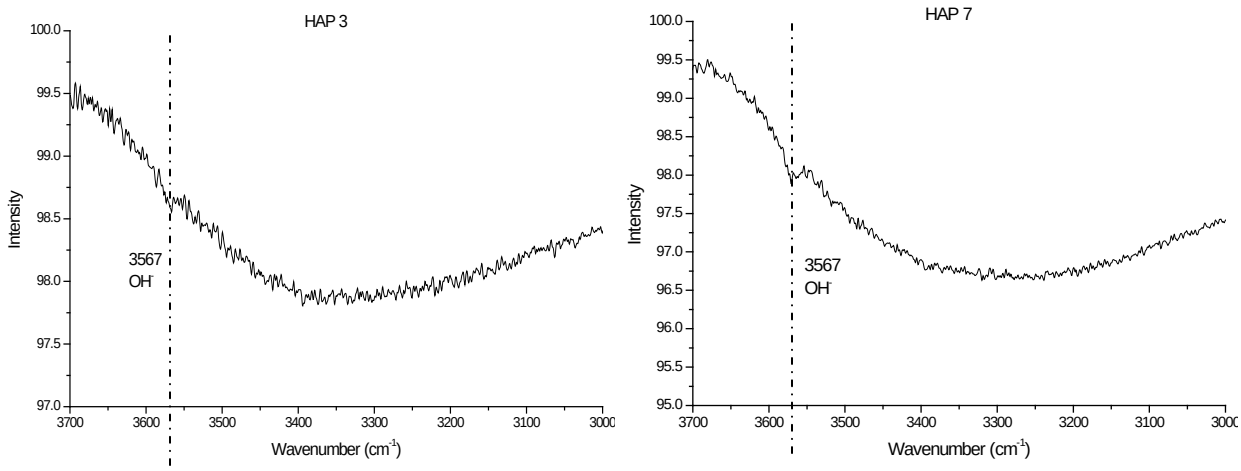

Figure 31: A closer look at the FTIR spectra of two hydroxyapatite powders where the OH^- vibrations are noticeable. On the left HAP 3 and on the right HAP 7.

For some of the FTIR patterns of the hydroxyapatite it is almost impossible to tell apart the hydroxyl band, as it seems that the H_2O broad band covers it completely.

4.1.2 Determination of the metastable zone of hydroxyapatite

In order to define at what conditions the encapsulation experiments would be executed a series of homogeneous precipitation experiments of hydroxyapatite were conducted, so that the metastable zone and the heterogeneous precipitation zone of the mineral are determined.

For these experiments, a solution was prepared containing Ca and P of known concentrations and the pH was increased gradually 0.1 pH points per 5 minutes. As soon as a cloud had started to form, the pH increase was stopped and the solution was left to equilibrate for 24 h. The diagrams resulting from these experiments consist of two curves, one for the pH and concentration at which precipitation (cloud formation) was first observed and one for the pH and concentration at pseudoequilibrium (end of 24-hour equilibration period). The experiments were conducted at 25 and 40 °C.

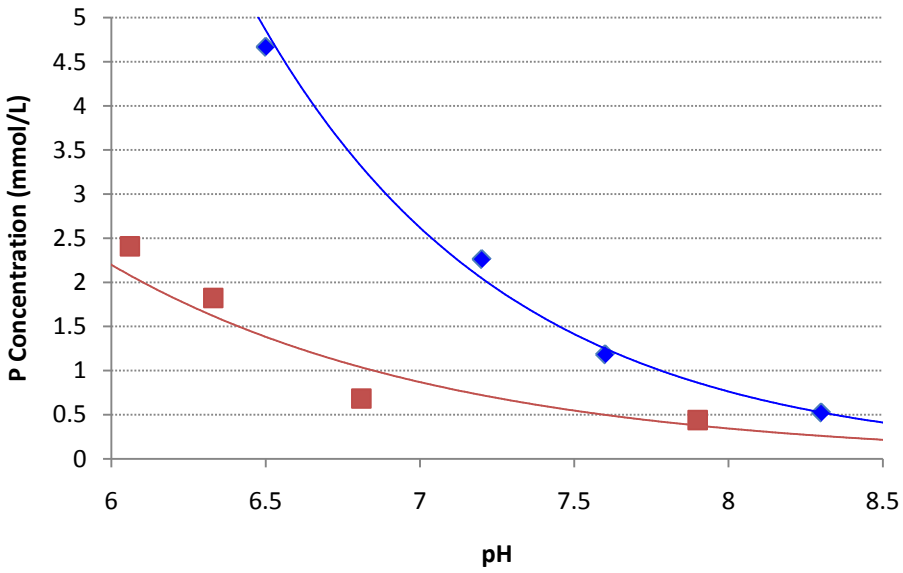

Figure 32: Metastable zone width for the $CaCl_2$-NaH_2PO_4-NaOH system at 22±1 °C.[1]

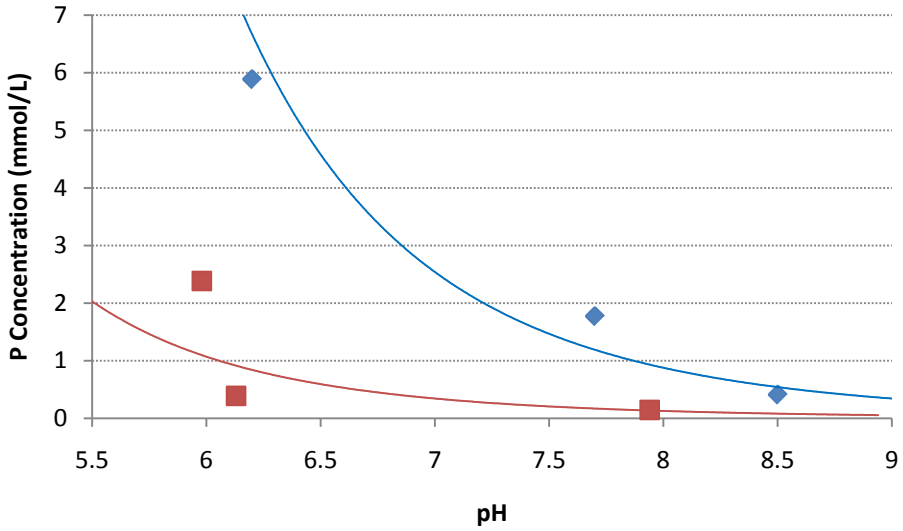

Figure 33: Metastable zone width for the $CaCl_2$-NaH_2PO_4-NaOH system at 40±1 °C.

[1] All the curves that have been prepared for this work were built out of data points produced from different analyses.

The results of these experiments for room temperature (Figure 32) agree with results from previous research [12] concerning the critical homogeneous precipitation line for hydroxyapatite. According to the above results the conditions of the experiments for the encapsulation of scorodite were selected: pH 7.6 and starting P concentration of 0.9 mmol/L, not exceeding 1.2 mmol/L during the experiments, or pH 7 and starting P concentration of 2 mmol/L, not exceeding 2.5 mmol/L during the experiments. Calcium concentrations were calculated stoichiometrically according to the 1:67 ratio.

4.1.3 Fluoroapatite precipitation

For the precipitation of fluoroapatite the setup described in 3.2 accompanied by a second external pump for the addition of NaF was employed. A solution of 500 mL of NaH_2PO_4 and NaF was added to another of 500 mL of $CaCl_2$ to prepare the metastable solution, and after 30 min of equilibration time the feed solutions were added at a rate of 20 mL/h. The feed solutions were 3 different solutions each containing NaH_2PO_4 30 mmol/L, $CaCl_2$ 50 mmol/L and NaF 10 mmol/L respectively. This experiment follows the conditions for the precipitation of hydroxyapatite as described in 4.1.1, with the modification of adding the stoichiometrical amount of fluoride ions.

4.1.4 Characterisation

The XRD spectrum of the precipitated fluoroapatite powder shows that the solids consist most likely of a solid solution (or mixture) of fluoroapatite and hydroxyapatite. The powder shows relatively good crystallinity.

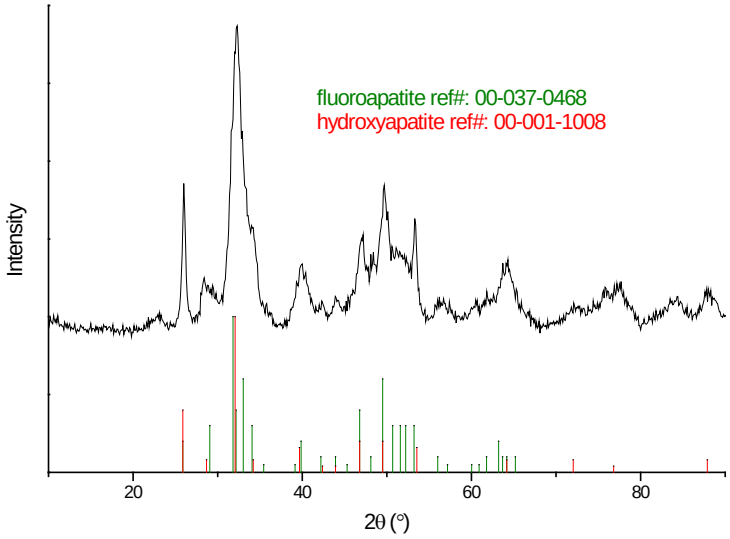

Figure 34: XRD spectrum of fluoroapatite precipitated powder.

When examining the powder with scanning electron microscopy (Figure 42), it can be observed that there is a wide distribution of the size of the particles. Some of the bigger particles have evident growth on certain crystallographic faces, while hydroxyapatite produced particles seemed to grow on all sides equally.

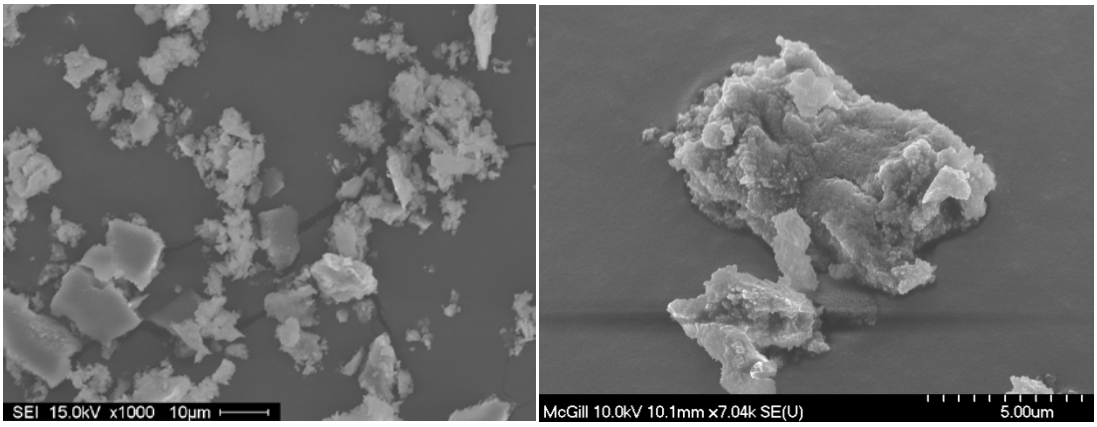

Figure 35: SEM images of fluoroapatite precipitated powder.

In the following FTIR spectrum (Figure 36) the characteristic vibrations for phosphates are visible, such as the ones at 1092, 1025, 962 cm^{-1} for PO_4^{3-} and at 867 cm^{-1} for HPO_4^{2-}. There is also the water broad band, whereas there are noticeable peaks for CO_3^{2-} at 1650, 1450 and 1427 cm^{-1}, which are probably a result of carbonate precipitation, due to presence of CO_2 from the atmosphere, since the reactor was not sparged/blanketed with an inert gas [107, 108].

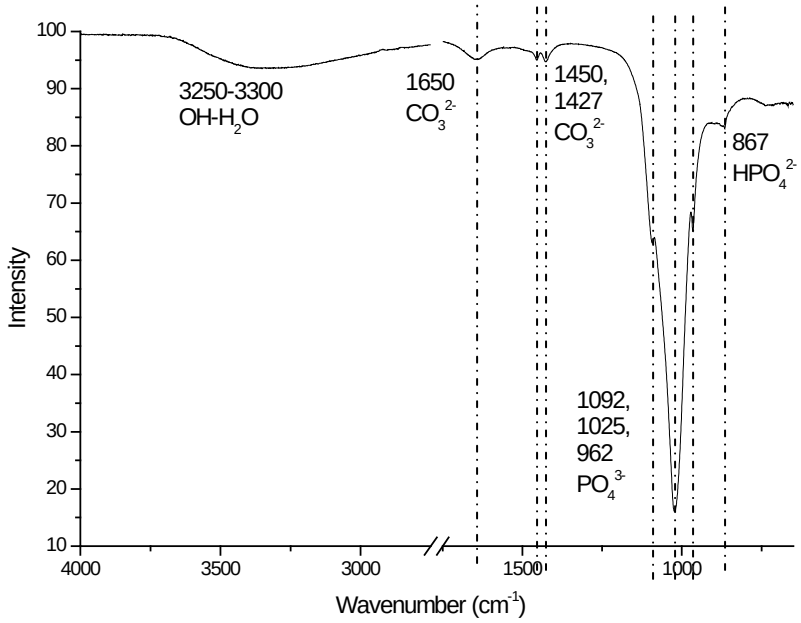

Figure 36: FTIR spectrum of fluoroapatite precipitated powder.

4.1.5 Determination of the metastable zone of fluoroapatite

The same procedure that was followed for hydroxyapatite was also followed for fluoroapatite, the only difference being that F^- was also present in the solutions.

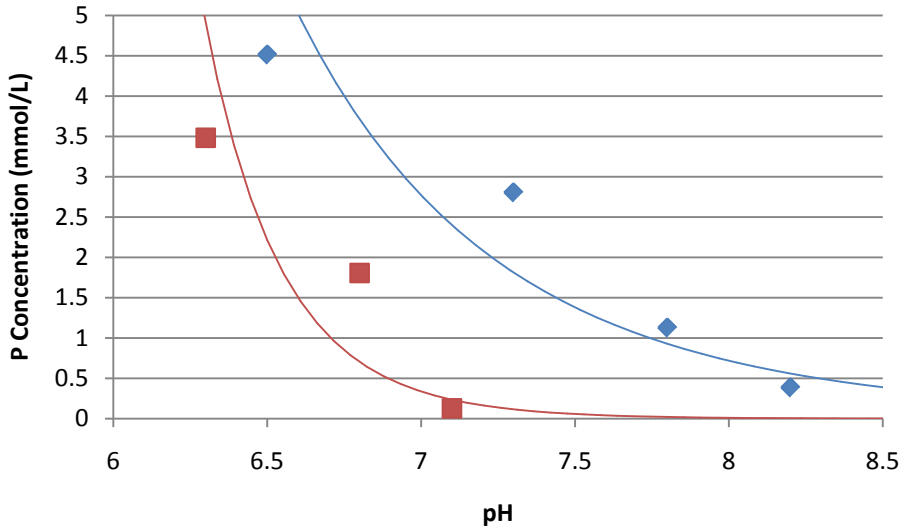

Figure 37: Metastable zone width for the $CaCl_2$-NaH_2PO_4-NaF system at 22±1 °C.

Comparing the homogeneous precipitation line of fluoroapatite with the one for hydroxyapatite, they are similar and it can be said that maybe fluoroapatite tends to precipitate at a lower pH value for the same phosphorus concentration.

Considering the above data the conditions chosen for the encapsulation experiments with fluoroapatite were decided to be the same as those for hydroxyapatite, i.e. pH 7.6 and starting P concentration of 0.9 mmol/L, not exceeding 1.2 mmol/L during the experiments, or pH 7 and starting P concentration of 2 mmol/L, not exceeding 2.5 mmol/L during the experiments. Calcium concentrations were calculated stoichiometrically according to the 1:67 Ca:P ratio with the additional stoichiometrical concentrations for fluoride ions .

4.1.6 Substitution of OH^- with F^-

In an Erlenmeyer flask containing 200 mL deionised water 1 g of hydroxyapatite powder, supplied by Sigma Aldrich, and 83.67 mg of NaF were added. The suspension was magnetically stirred for 24 hours. It was then filtered and washed and the solids were dried for characterisation. X-ray diffraction data (Figure 38) show that substitution has occurred and hydroxyapatite transformed (partially) into fluoroapatite, but the percentage of the transformation is not possible to be calculated. Furthermore, if the duration of the experiment was longer it is possible that a greater amount of fluoride would have substituted the hydroxyl ions in hydroxyapatite.

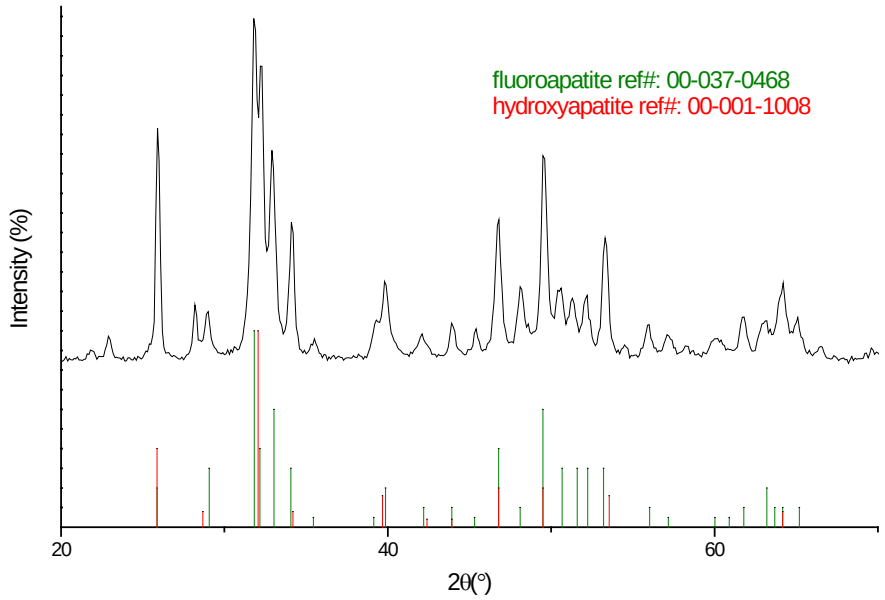

Figure 38: XRD spectrum of fluoride substituted hydroxyapatite.

This experiment was done to see if the information provided by literature considering the substitution of OH- with F- would be reproducible. The fact that hydroxyapatite can be transformed into fluoroapatite by supplying it with fluoride ions, could prove useful in the further stabilisation of hydroxyapatite coated scorodite particles.

4.2 Encapsulation

In this series of tests HAP or FAP were deposited under controlled supersaturation conditions on scorodite particles for the purpose of their protection via encapsulation. A summary of all encapsulation tests along with the key conditions applied is given in Table C - 1. The reactor (section 3.2) operating conditions were chosen so that the precipitation took place within the heterogeneous (metastable) zone as described in sections 4.1.2 and 4.1.5. The encapsulation process involved separate nucleation and growth steps. Due to difficulties experienced with the initiation of nucleation on the surface of scorodite various procedures were tried.

To roughly determine the number of experiments needed for the encapsulation of each scorodite sample, the amount of hydroxyapatite (or fluoroapatite) needed for the encapsulation of 5 g scorodite was calculated. For this calculation the shape of the scorodite particles was assumed to be spherical and their size was assumed to be uniform for the total of the particles at 20 μm, something that does not differ much from reality given the particle size analysis results of the atmospherically precipitated scorodite (data shown in Figure 21 of Chapter 3 (section 3.4)). For this calculation the thickness of the required layer was taken to be 2 μm of hydroxyapatite. Therefore:

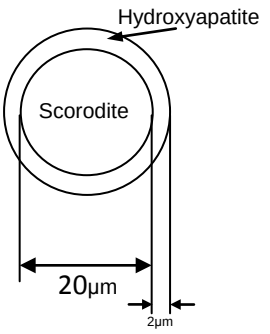

Figure 39: Schematic representation of particle and coating cross-section as per the calculation

Scorodite + layer volume: $v_{tot} = \frac{4}{3}\pi r^3 = \frac{4}{3}\pi 11^3 = 5575.28\ \mu m^3$

Scorodite: $v_{scor} = \frac{4}{3}\pi r^3 = \frac{4}{3}\pi 10^3 = 4188.79\ \mu m^3$

HAP volume needed: $v_{hap} = v_{tot} - v_{scor} = 1386.49\ \mu m^3$

HAP mass: $m_{hap} = \rho_{hap} \cdot v_{hap} = 3.08 \frac{g}{cm^3} \cdot 1386.49 \cdot 10^{-12} cm^3 = 4.27 \cdot 10^{-9} g$

Scorodite mass: $m_{scor} = \rho_{scor} \cdot v_{scor} = 3.2 \frac{g}{cm^3} \cdot 33510.32 \cdot 10^{-12} cm^3 = 10.34 \cdot 10^{-9} g$

Under the previous assumptions and according to the calculations, for every 5 g (2.166 mmol) of scorodite that are to be encapsulated, 1.59 g (0.317 mmol) of hydroxyapatite should be precipitated, so that we have a layer of 2 μm thickness. Using the density of fluoroapatite, 3.18 g/cm^3, the amount calculated for 5 g of scorodite is

1.65 g (0.327 mmol) of fluoroapatite. The amount of 5 g of scorodite was chosen for this calculation, because the majority of the encapsulation experiments used 5 g/L of scorodite as seed.

4.2.1 Procedures

4.2.1.1 Conditioning of scorodite

In order to prepare the surface of the scorodite particles for the deposition of a "foreign" material on them a pre-equilibration (conditioning) procedure was applied. The first type of conditioning that was used included introducing the scorodite particles into a de-ionised water solution, whose pH had been adjusted to 7.6 using NaOH, and leaving the suspension for 15-30 minutes under mild stirring on an orbital shaker. The solids were then separated from the solution and they were added to the solution in the reactor for the encapsulation test.

Another type of conditioning step that was used consisted of adding the scorodite particles into a solution containing Ca^{2+} ions (introduced as $CaCl_2 \cdot 2H_2O$). According to literature, and as it was also confirmed by the stability tests conducted for this work, scorodite demonstrates higher stability in gypsum saturated water, which can be attributed to the transformation of scorodite to yukonite ($Ca_2Fe_3(AsO_4)_4OH$), while thermodynamics simulations pointed to the formation of johnbaumite ($Ca_5(AsO_4)_3OH$) [105]. In either case this kind of pre-treatment of the scorodite could be beneficial for the encapsulation experiments, in terms of surface modification. Johnbaumite especially is called the hydroxyapatite analog for arsenates and crystallises in the hexagonal crystal system, in which case the transformation of the scorodite surface to this mineral would theoretically make it more receptive to the deposition of a hydroxyapatite layer.

4.2.1.2 Nucleation step

As nucleation step is considered the contact of the scorodite particles with a metastable solution for several hours. The purpose of this step (induction) and its repetition for the same substrate more than one time was the creation of a primal layer around the scorodite particles. This layer would make the surface of the scorodite less

foreign for the encapsulating compound and therefore facilitate the growth so that the deposition time is minimised.

4.2.1.3 Growth step

A growth step usually followed a nucleation step, and it is a semi batch experiment where the scorodite particles were added to a metastable solution in the reactor and after 30 minutes of equilibration time, feed solutions were added at a predetermined fixed rate. This step was meant to grow at an accelerated speed the initial layer that had been formed around the particles during the nucleation step(s).

4.2.1.4 "Nancollas" step

This step is very similar to a growth step, but it is necessary to be described separately. It has been inspired from Wu and Nancollas [100]. Once again, the scorodite particles are introduced to the reactor where a metastable solution has already been prepared. After the usual equilibration time of 30 minutes, two feed solutions are added, but the addition rate is not predetermined, only it is decided by the development of the reaction. As the precipitation reaction happens and the pH drops, the reactor controller adds the two solutions in an effort to bring the pH up to a pre-set value. One of the two solutions contains a calculated concentration of NaOH, so that when they are added the pH increases, but does not overcome the set pH value, which could cause homogeneous precipitation. This pH increase and simultaneous addition of reactants, increases the supersaturation and fuels the reaction, which by itself triggers the addition of reactants and base, and so on and so forth until the feed solutions are consumed.

The concentrations of the feed solutions were calculated according to the equations given by Wu and Nancollas. These are 10.8 mmol/L P, 18 mmol/L NaOH in one solution and 18 mmol/L Ca, 270 mmol/L NaCl in the other solution. For the fluoroapatite experiments 3.5 mmol/L F were added to the first solution. The experimental conditions included pH 7.4, temperature 37 °C, stirring speed 500 rpm and variable experimental time depending on the kinetics of the reaction.

4.2.2 Encapsulation of scorodite with hydroxyapatite

4.2.2.1 Nucleation

Some preliminary experiments (ENCH 2-refer to Table C - 1) were conducted to verify that the setup is functioning appropriately following the procedure initially described by Lagno [12]. For these experiments a metastable solution of NaH_2PO_4 and $CaCl_2$ was prepared and the scorodite particles (5 g/L wet) were added. After 30 min of equilibration time feed solutions were added, similarly to a growth step. The feed solutions contained 60 mmol/L P and 100 mmol/L Ca respectively and the addition rate was 20 mL/h for 7 h, pH was kept constant at 7.6 using NaOH (0.1 mol/L) and agitation speed was 750 rpm. This semi-batch step was repeated 5 times for the same scorodite sample and at the end samples were prepared for characterisation. This characterisation showed that the rate of addition of the reagents was too fast for the reaction, which caused the supersaturation to exceed the phosphorus critical concentration value and therefore homogeneous precipitation of hydroxyapatite occurred [12].

Following the preliminary experiments a new cycle of experiments (ENCH 3) was prepared, but this time the addition rate used was 6 mL/h for a total of 24 h for the first experiment (ENCH 3.1) and then for the 3 subsequent experiments 20 mL/h was again used. The scorodite particles were pre-equilibrated prior to the first deposition experiment in a 7.6 pH solution as described in 4.2.1.1. The intention was to have an initial deposition on the surface of the particles during the slow addition rate first step and the following steps to work as growth steps. Agitation speed was set at 800 rpm.

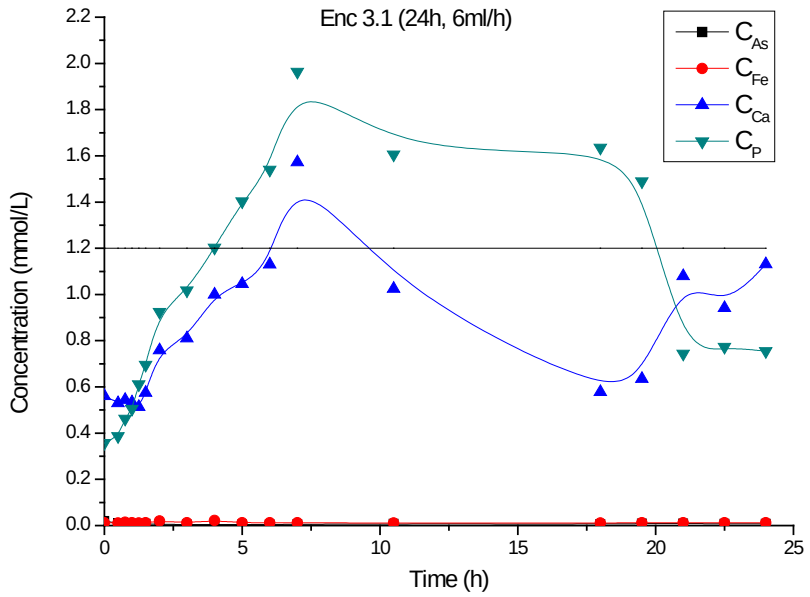

Figure 40: Concentrations of P, Ca, As, Fe during the first (nucleation) step of deposition of ENCH 3.

The plot in Figure 40 shows the concentration profiles during the first step previously described. Due to slow kinetics, the induction time of the heterogeneous precipitation of hydroxyapatite on the scorodite particles was longer than the time needed for the concentration of phosphorus to be raised more than the phosphorus critical homogeneous point for these conditions, which was 1.2 mmol/L, as it is visible in the graph, and therefore homogeneous precipitation prevailed. This resulted in the creation of hydroxyapatite nuclei on which growth was promoted away from the scorodite particles during the subsequent steps (refer to SEM images in Figure 41).

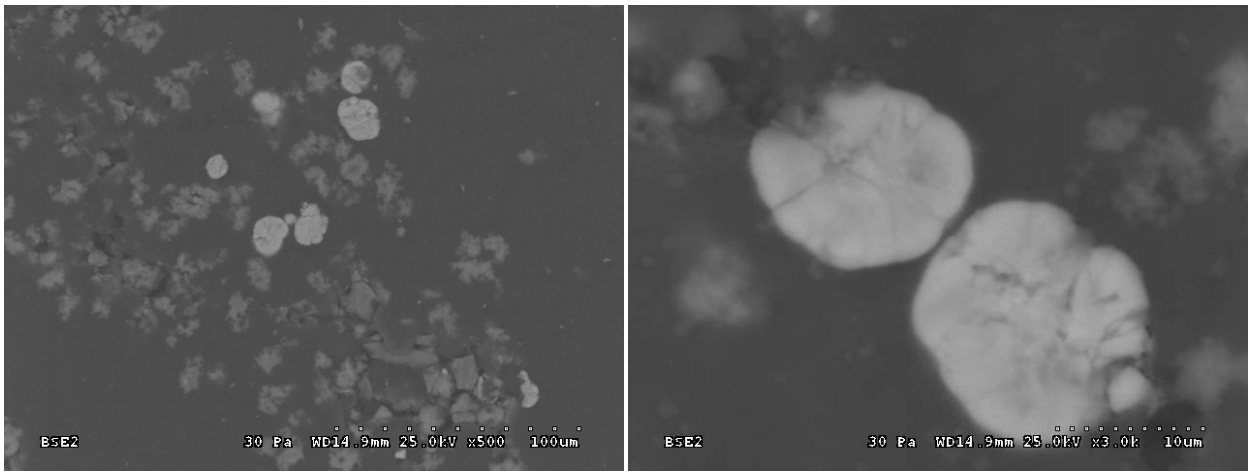

Figure 41: SEM cross-section images of resulting solids after ENCH 3 encapsulation steps.

Due to the results of the previous set of experiments another approach was designed, aiming to overcome the long induction time problem. Thus, the scorodite was brought into contact with a series of 5 identically prepared metastable solutions (ENCH 4), for one hour at a time. The metastable solutions contained 0.9 mmol/L P and 1.5 mmol/L Ca, pH was kept at 7.6 and the scorodite was conditioned once in a 7.6 pH solution (adjusted with 0.01 mol/L NaOH) prior to its addition to the first metastable solution. The solids were not washed between steps and the impeller stirring speed was set at 850 rpm.

The obtained concentration profiles from the first step of the ENCH 4 experiment series are shown in Figure 42. Within the duration of the experiment a very small decrease in the concentration of P and Ca can be noticed, which means that the heterogeneous precipitation of hydroxyapatite is happening very slowly if at all. The same applies for the other experiments of this series. Indicatively step 4 is plotted next to step 1.

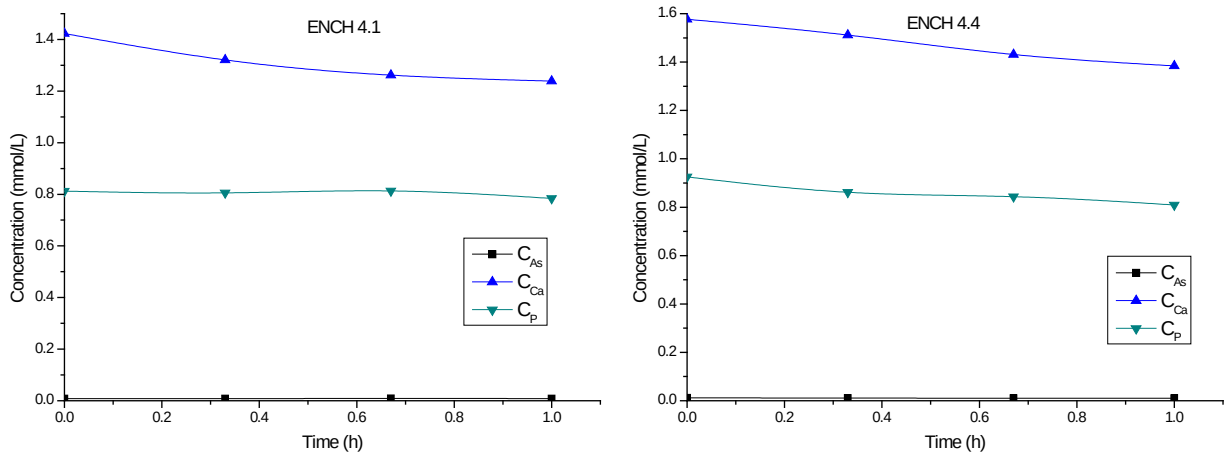

Figure 42: Concentrations of P, Ca, As during the first and fourth nucleation steps of ENCH 4.

When the particles were examined with scanning electron microscopy imaging, as is demonstrated in Figure 43, it was noticed that the precipitation had happened away from the scorodite particles and not on their surface. The reason for the homogeneous precipitation of the hydroxyapatite particles was not obvious at first but later it was assumed that the agitation speed was too high and that it deterred the heterogeneous precipitation. Since there were homogeneously precipitated

hydroxyapatite particles, it would have been unwise to continue with a growth step, for the precipitation would mostly happen on the surface of the hydroxyapatite.

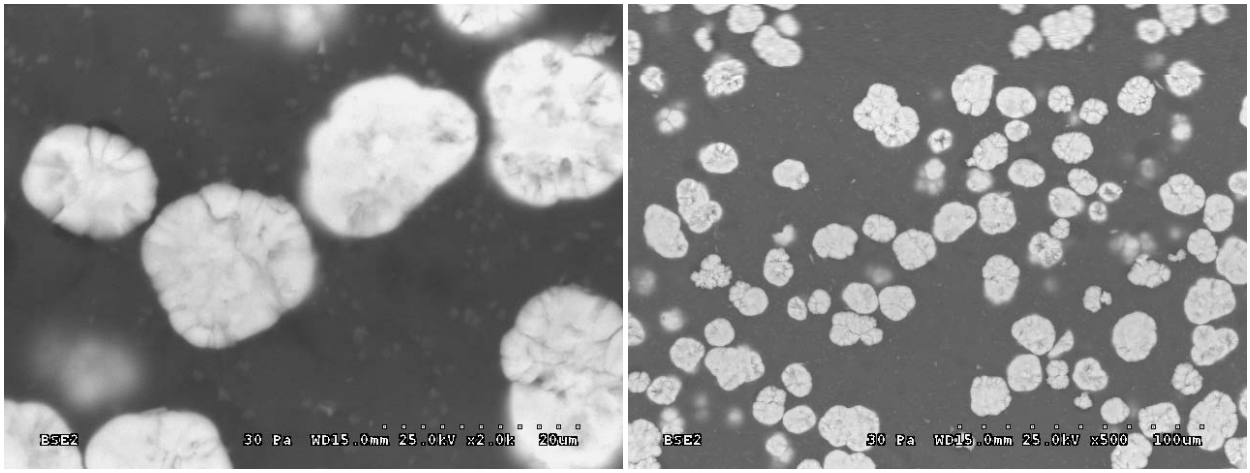

Figure 43 : SEM cross-section images of resulting solids after ENCH 4 encapsulation experiments.

Repetition of the previous test but this time using two contacts of 48 h each of scorodite and a metastable solution of 0.9 mmol/L P and 1.5 mmol/L Ca (Test ENCH 5) did not prove successful either. Hence it was decided next to evaluate the effect of agitation speed (lowering of it from 850 to 350 rpm) or elevation of temperature (from 22 to 40 °C). Again the pH was kept at 7.6 using a 0.01 mol/L NaOH solution. The concentration profiles from these tests are shown in Figure 44.

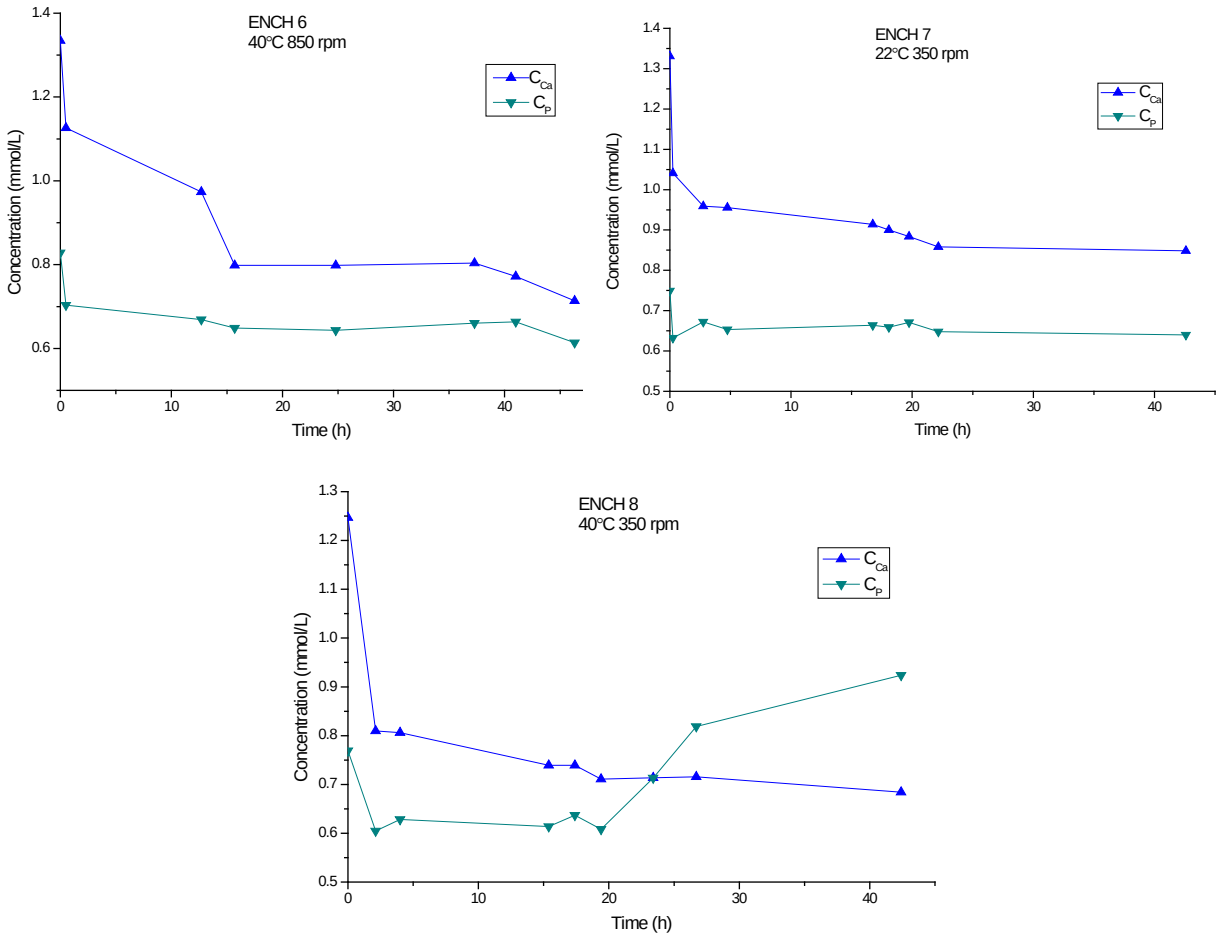

Figure 44: Concentrations of P and Ca during three nucleation experiments at different temperatures and agitation speeds, ENCH 6, 7 and 8.

As it can be seen removal of phosphorus and calcium from the solution seems to happen as soon as the scorodite is introduced to the solution, regardless of temperature, or agitation speed. But the amount that is removed differs for each experiment. It seems that compared to the previous data, that both low agitation speed and higher temperature promote the precipitation of hydroxyapatite. The ENCH 8 experimental data show an increase in phosphorus concentration after 20 hours have passed, where it appears to be higher than the initial phosphorus concentration. For this reason and since there was no addition of phosphorus for this experiment, the data after the 20 h mark is considered to be erroneous, and it is not taken into account.

When the solids from ENCH experiments 5, 6, 7 and 8 were examined by scanning electron microscopy it was very hard to notice any layer or any

homogeneously precipitated hydroxyapatite particles. The reason for this is that the total concentrations used for each experiment were relevantly low and in the case that it all had precipitated as a coating, this was too thin to be able to distinguish it.

4.2.2.2 Combined Nucleation & Growth

Deposition Procedure 1: The following experiments combined nucleation and growth steps. The scorodite was brought into contact with 9 metastable solutions (each contact lasted 24 h) before a growth experiment was done. This multiple metastable solution contacting was done in order to ensure that the scorodite particles would be covered by a thin layer of HAP heterogeneous nuclei, which would get thick during the subsequent growth step. In addition to using multiple contacting it was decided to lower the pH from 7.6 to 7 to allow for higher concentration solutions (2 mmol/L P, 3.34 mmol/L Ca) to be used (hence increase the available Ca and P) but always staying within the metastable zone-refer to Figure 32 in section 4.1. For the growth step the scorodite was introduced in a metastable solution with the same concentrations as the nucleation steps, and after an equilibration time of 30 min feed solutions of 60 mmol/L P and 100 mmol/L Ca were added to the solution. The addition rate was 20 mL/h and the growth time starting from the moment feed solution addition was initialised was 7 hours. During the experiment, the pumping of the feed solutions was paused and samples were taken and analysed by the colorimetric method described in section 3.3. This was done to verify that the phosphorus levels in the solution were kept below the critical homogeneous precipitation line. This was indeed accomplished. The concentration profile results are shown in Figure 45. As it can be seen in Figure 45, the concentration of P during the growth step of this experiment was kept below 2.5 mmol/L. The solids from this series of experiments were retained for subsequent stability testing-described in section 4.3.

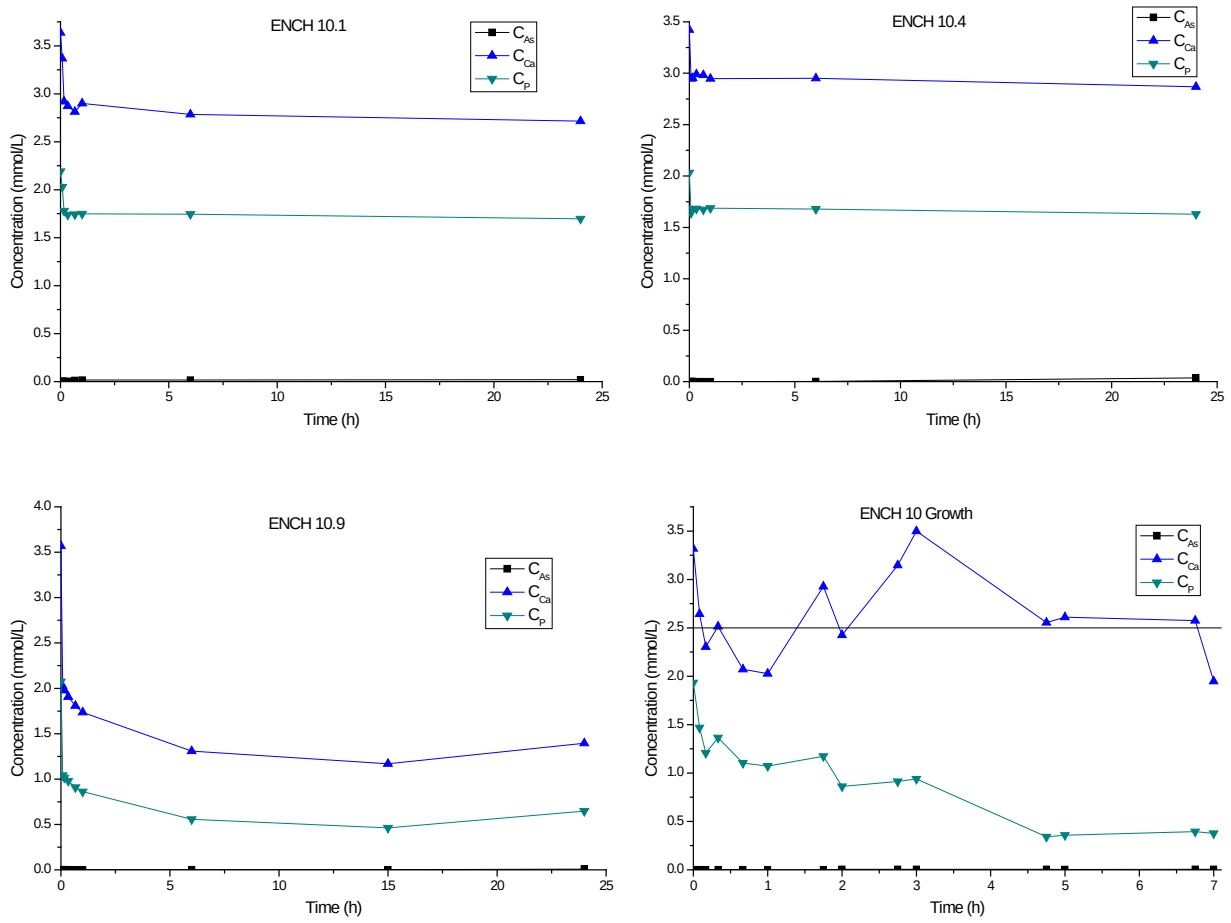

Figure 45: Concentration profiles for nucleation steps 1, 4 and 9 and the growth step of the ENCH 10 series.

The scanning electron microscopy images from the resulting solids (Figure 46) show that scorodite particles were partially covered by hydroxyapatite. There is obviously a large amount of hydroxyapatite that precipitated homogeneously, but there is also hydroxyapatite that is attached to the scorodite particles. The reasons for this preferential deposition are not clear. It may be tentatively assumed that during the course of the test, despite the best efforts in controlling supersaturation below the critical homogeneous nucleation level, this was not necessarily 100 % successful.

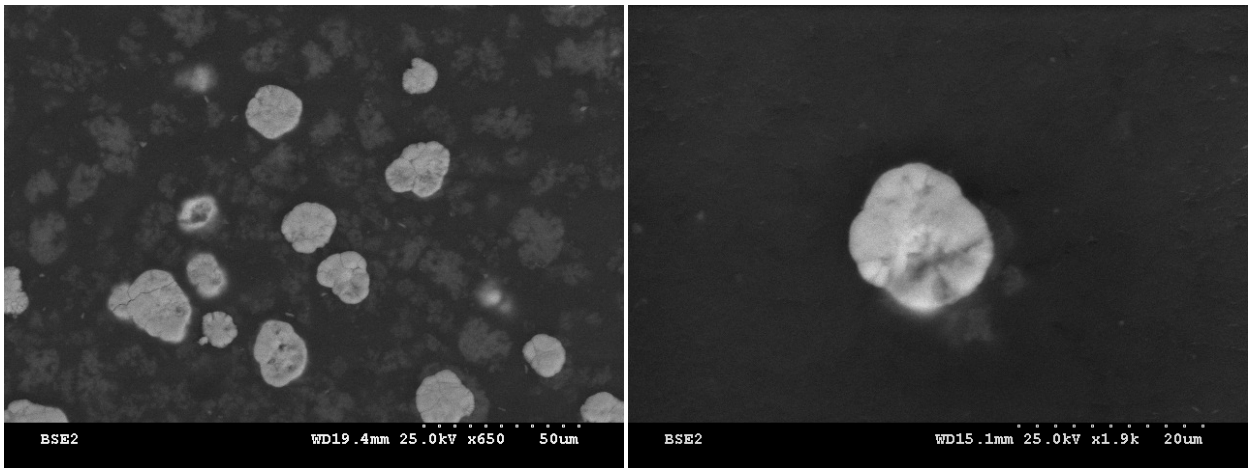

Figure 46: SEM cross-section images of resulting solids from ENCH 10 encapsulation experiments.

FTIR analysis done on the generated encapsulated solids from Test ENCH 10 produced the spectra shown in Figure 47. It is very characteristic from this data that the ENCH 10 solids exhibit the characteristic features of hydroxyapatite and scorodite. This analysis, however, cannot clarify the different precipitated types of HAP, namely homogeneously and heterogeneously (on the surface of scorodite) nucleated HAP.

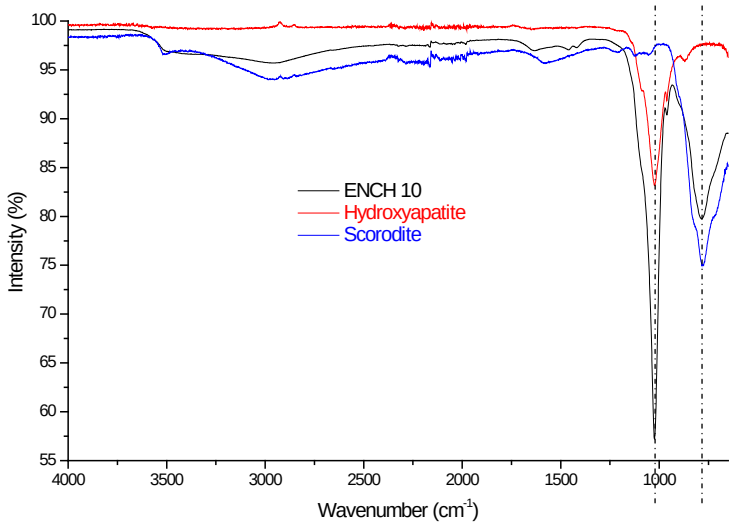

Figure 47: FTIR spectra of ENCH 10 solids and hydroxyapatite and scorodite reference patterns.

Deposition Procedure 2: For the next set of experiments (ENCH 11), nine sequential nucleation steps were performed in the same way as for ENCH 10, but the growth step this time was conducted following the Nancollas procedure (4.2.1.4) [100].

The initial metastable solution was prepared by adding a 500 mL solution of $CaCl_2$ and NaCl to a 500 mL solution of NaH_2PO_4, and acquiring final concentrations of 0.9 mmol/L P, 1.5 mmol/L Ca and 0.15 mmol/L NaCl. The metastable solution pH was adjusted to 7.4 by adding NaOH (0.1 mol/L) before adding the scorodite. The first feed solution contained 10.8 mmol/L NaH_2PO_4 and 18 mmol/L NaOH, and the second 18 mmol/L $CaCl_2$ and 270 mmol/L NaCl. The NaCl was added to adjust the ionic strength. The pH was set at 7.4 and temperature was kept at 37 °C. The relevant concentration profiles are shown in Figure 48. The nucleation concentration profiles to great extent resemble those of ENCH 10. However, this time the Nancollas procedure employed during the growth step clearly shows iso-composition (constant supersaturation) environment, i.e. better control of supersaturation. The resulting solids were tested for their long term stability properties and the results are reported in section 4.3.

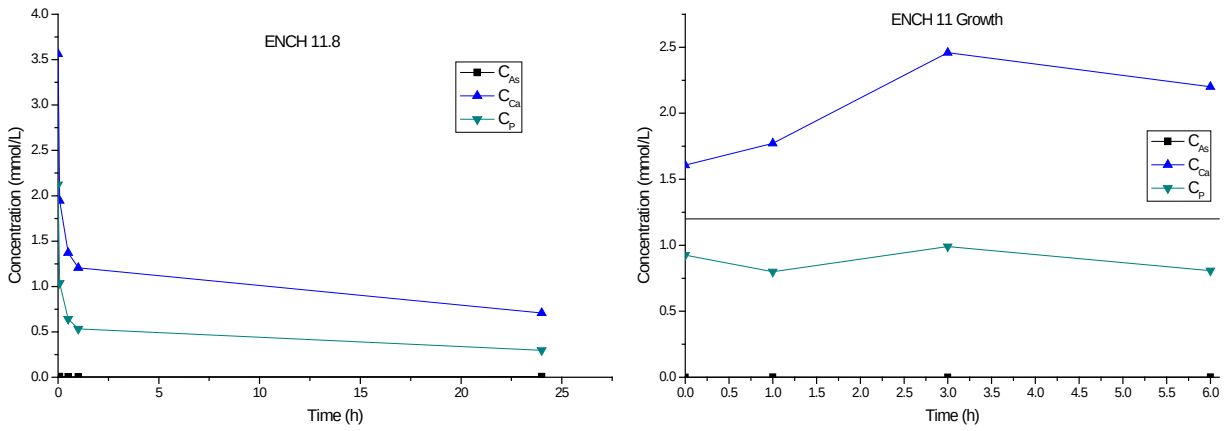

Figure 48 : Concentration profiles during a typical nucleation step and the Nancollas growth step of Test ENCH 11.

The cross-section scanning electron microscopy images for ENCH 11 (Figure 49) looked very similar to the ones from ENCH 10. Images of the particles placed on carbon tape were also taken to see how they look externally. The majority of the scorodite particles seemed to have been partially covered with hydroxyapatite, and there were also cases where the scorodite appeared to be part of a big agglomerate of hydroxyapatite and scorodite particles; clearly a much better encapsulated product than the previous one (Figure 46).

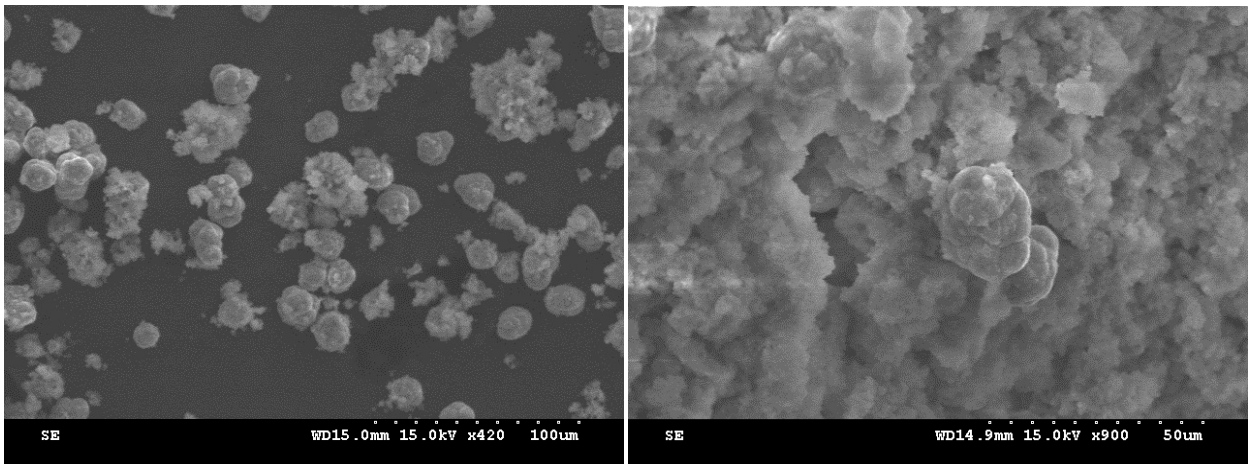

Figure 49: SEM images of resulting solids from ENCH 11 encapsulation tests.

Efficiency of Sequential Nucleation Steps: As mentioned at the beginning of this section one of the challenges encountered during the course of this work was the initiation of HAP deposition on the scorodite particle surface. Hence it is considered important to evaluate the efficiency of the multiple contacting nucleation procedure employed in the previous two nucleation-growth tests (ENCH 10 and 11). This is done by comparing the two series in terms of % P removal from the metastable solution. The results are shown in Figure 50. As it can be seen, there is a trend of increase of the phosphorus removal with each step of nucleation. This means that in the initial steps where P removal was low, heterogeneous nucleation on scorodite was happening slowly (induction period) but upon generation of the first heterogeneous nuclei hydroxyapatite deposition accelerated, because of favourable (lower activation energy) hydroxyapatite sites on scorodite surface.

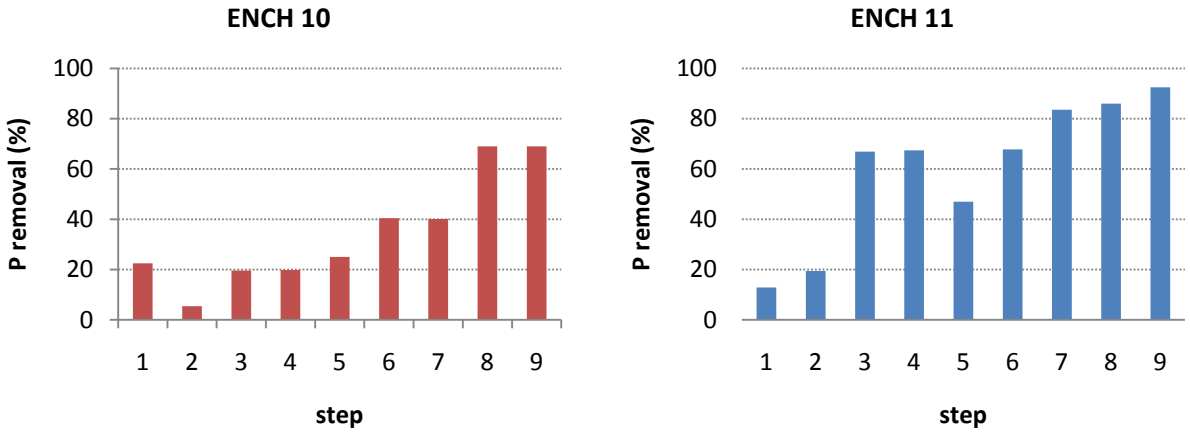

Figure 50: P removal (%) at the end of each nucleation step for ENCH 10 and ENCH 11 series.

Deposition Procedure 3: For the last experiment the Nancollas heterogeneous deposition step was used again, but this time the scorodite particles were conditioned in a calcium solution before the deposition experiment. For this conditioning step 15 g of wet scorodite powder were introduced in 1 L of 6 M $CaCl_2$ solution and were stirred for approximately 15 h. The actual concentration of the initial solution was found to be 4.25 M Ca, and at the end of the experiment it had dropped to 3.77 M Ca. This decrease in concentration of calcium can be attributed to adsorption of the ions on the surface of the scorodite particles. The Nancollas step had a short induction time of a few hours in comparison to naked scorodite not previously conditioned with other than immersion in pH 7.6 water[2] and it took approximately 32 hours for the feed solutions to be consumed. This means that the conditioning with the calcium solution had effectively changed the surface, most likely due the calcium adsorption, and thus it was easier for hydroxyapatite to nucleate on it.

SEM images of encapsulated particles via this procedure are shown in Figure 52. It is clear that (at least partially) heterogeneous deposition of HAP on scorodite took place. No evidence of homogeneously nucleated HAP was found. The partial coverage

[2] In this case the induction time was in the order of a few days.

of scorodite particles by HAP is further revealed by the cross sections presented in Figure 51.

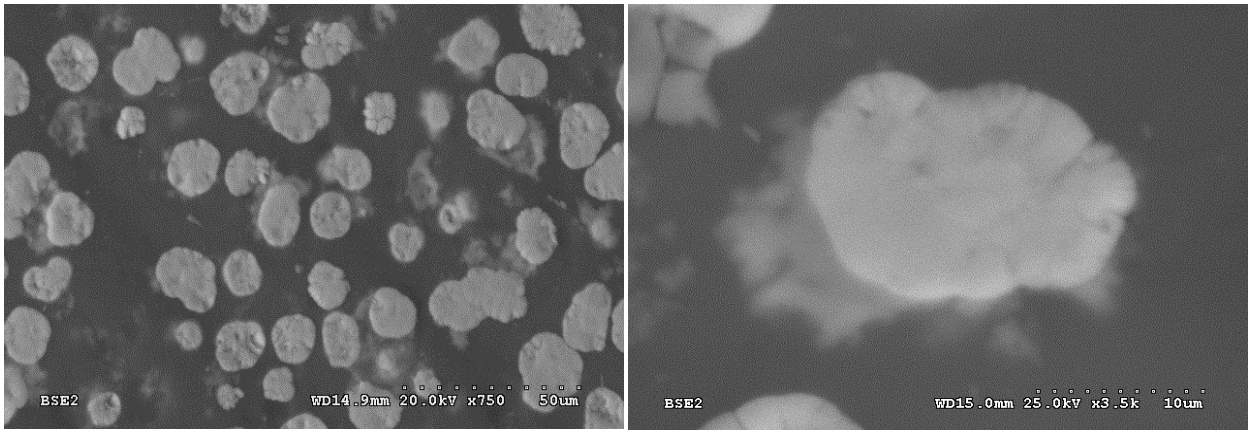

Figure 51: SEM cross-section images of resulting solids from ENCH 13 encapsulation test.

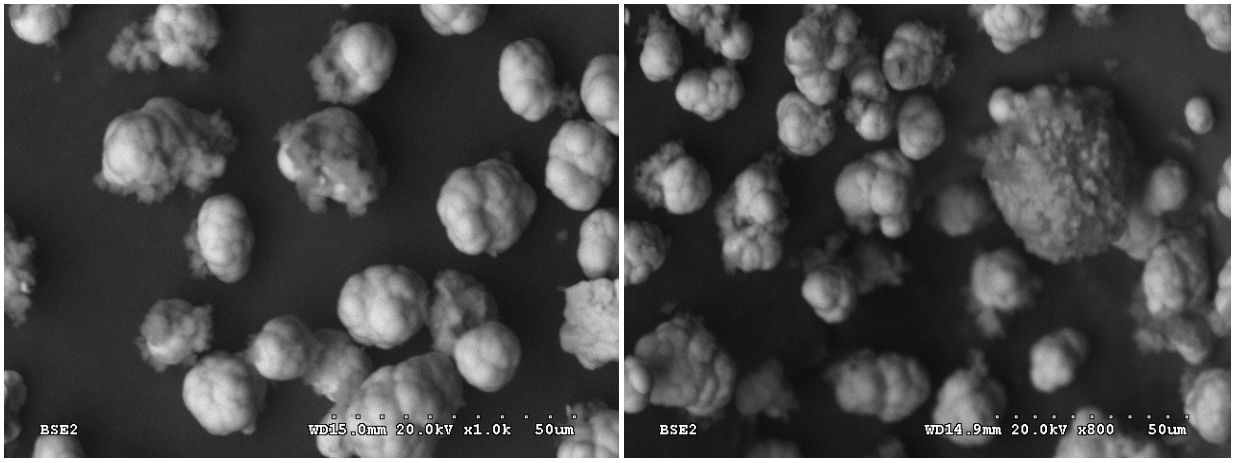

Figure 52: SEM images of resulting solids from ENCH 13 encapsulation experiment.

Elemental X-ray mapping of one of the cross sections (Figure 53) shows that the layer covering the scorodite particle is indeed a phosphate compound. It also confirms that for some reason the deposition only happened around half the particle, and the rest of the particle appears not to have a Ca-P layer. This was the case for several other particles that were examined by X-ray mapping. The reasons for this partial deposition are not clear and require further study.

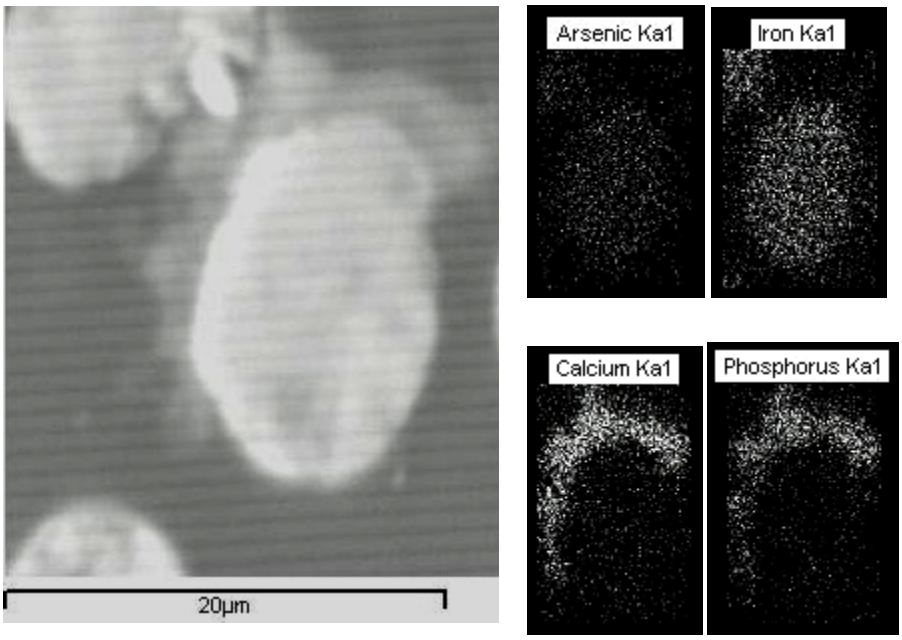

Figure 53: Backscattered electron image of a partially coated particle's cross-section and elemental mapping of the particle and the coating.

4.2.3 Encapsulation of scorodite with fluoroapatite

For the encapsulation of scorodite with fluoroapatite nucleation experiments were also tried first and growth steps followed.

4.2.3.1 Nucleation

For the first procedure (ENCF 1-see Table C-1 in Appendix) scorodite particles were subjected to two nucleation steps. In the first step 5 g/L wet scorodite were introduced in 500 mL of 2 mmol/L phosphate solution at pH 6.0, which was adjusted using 0.1 mol/L NaOH solution, and were left to condition for 30 minutes before 500 mL of 3.34 mmol/L calcium solution were added and the pH was raised to 6.5. After 22 h the pH was raised to 7.0, to encourage the precipitation of the remaining phosphate and calcium from solution, whose concentrations had dropped during the first hours of the experiment and were too low to continue precipitating, as it is done in the supersaturation-controlled precipitation strategy described by Demopoulos [33].

Subsequently the scorodite was separated from the liquid and was introduced to a metastable solution with the same concentrations as in the first step but the pH was set to 7.0 from the beginning. The concentration profiles for both steps can be seen in Figure 54.

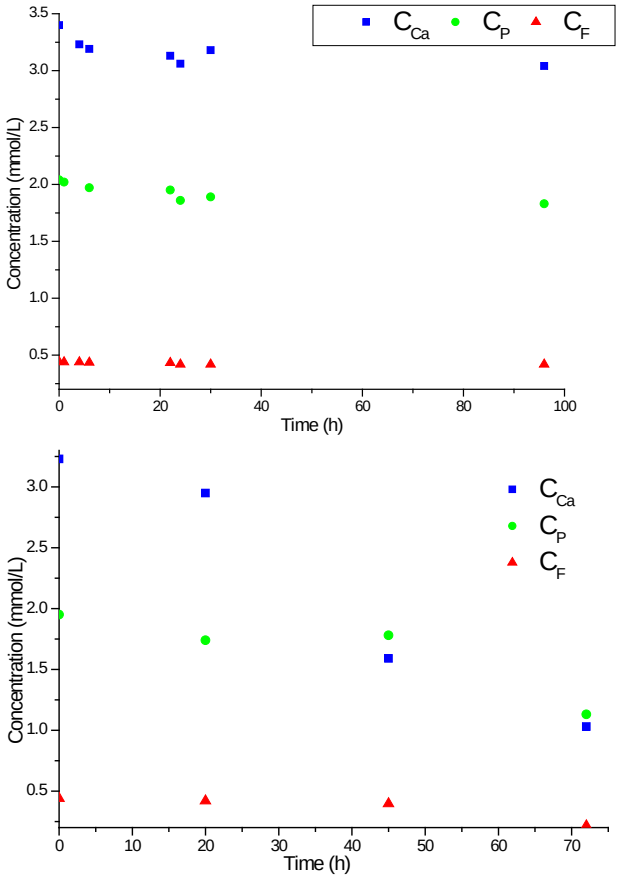

Figure 54: Concentration profiles during nucleation steps 1 and 2 of ENCF 1.

The scanning electron microscopy images seen in Figure 55 show that for some of the particles a very thin film (most likely FAP) has been deposited on the surface of the particles.

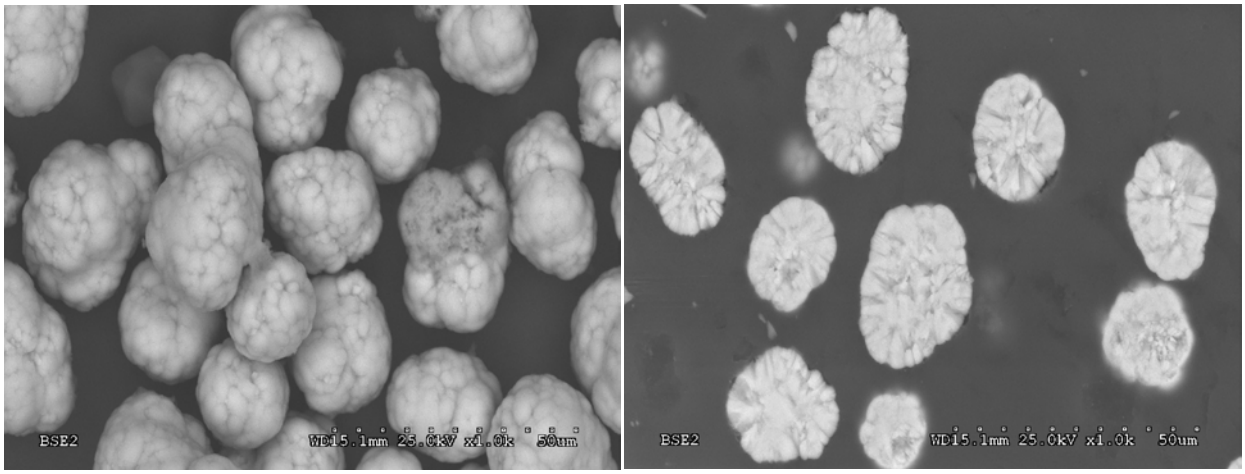

Figure 55: SEM images after nucleation step 1 of ENCF 1. On the left particles "as-is" and on the right cross-section of the particles.

4.2.3.2 Growth

Deposition Procedure 1 (ENCF 3): Scorodite (5 g) was conditioned in a 1 L of 10 mmol/L $CaCl_2$ solution for 24 h, after which the concentration of the solution for Ca had dropped to 8.85 mmol/L. Similarly with the HAP tests conditioning is believed to lead to calcium adsorption onto the surface of the scorodite particles (evident indirectly by a decrease in the concentration of Ca) thus creating a favourable local interfacial environment for nucleation of FAP. The solids were then used in a Nancollas type deposition step. Two steps of 500 mL of feed solutions were carried out. For the first step the induction time was two to three hours and the feed solutions were consumed after 40 hours and the second step lasted 29 hours.

In Figure 56 a backscattered electron image and the corresponding elemental mapping of encapsulated particles that resulted from ENCF 3 show variable degree of coating (with a calcium phosphate compound presumably) of some of the scorodite particles.

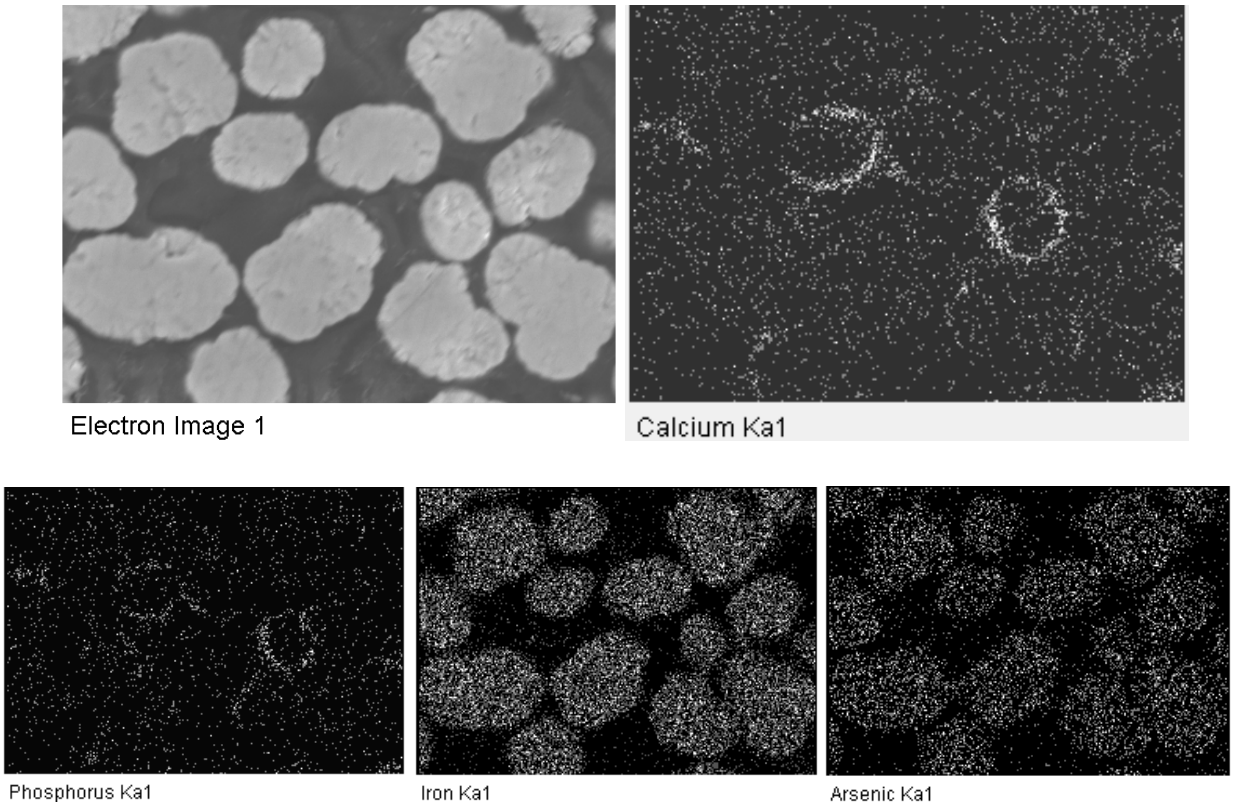

Figure 56: Backscattered electron image of particles coated with fluoroapatite from ENCF 3 and elemental mapping of the particles and their coating.

4.3 Stability testing

The procedure for the stability evaluation of the encapsulated products is described in section 3.5 (Chapter 3). These tests included stability under oxic and anoxic (150 mV) conditions at pH 8 (and sometimes 7 & 9). In addition to the encapsulated products (ENCH 10, 11 and 13 series for hydroxyapatite and ENCF 1 and 3) reference scorodite and hydroxyapatite alone or in mixture were tested for comparison purposes. Of the two scorodite-HAP mixtures (15 % HAP-85 % SCOR) tested, the first was a mixture of scorodite and purchased hydroxyapatite powder from Sigma Aldrich and the second of scorodite and HAP 3. The effect of gypsum on HAP stability was also evaluated [105]. Selected solids from the fluoroapatite encapsulation tests were also tested for their long term stability.

4.3.1 Stability of HAP

The hydroxyapatite powders that were subjected to the stability tests were the hydroxyapatite that was purchased from Sigma Aldrich and hydroxyapatite that was

prepared in the lab, specifically HAP 3 (see 4.1.1). Both powders were tested under oxic and anoxic conditions at pH 8. The leachability data is plotted in Figure 57 and Figure 58.

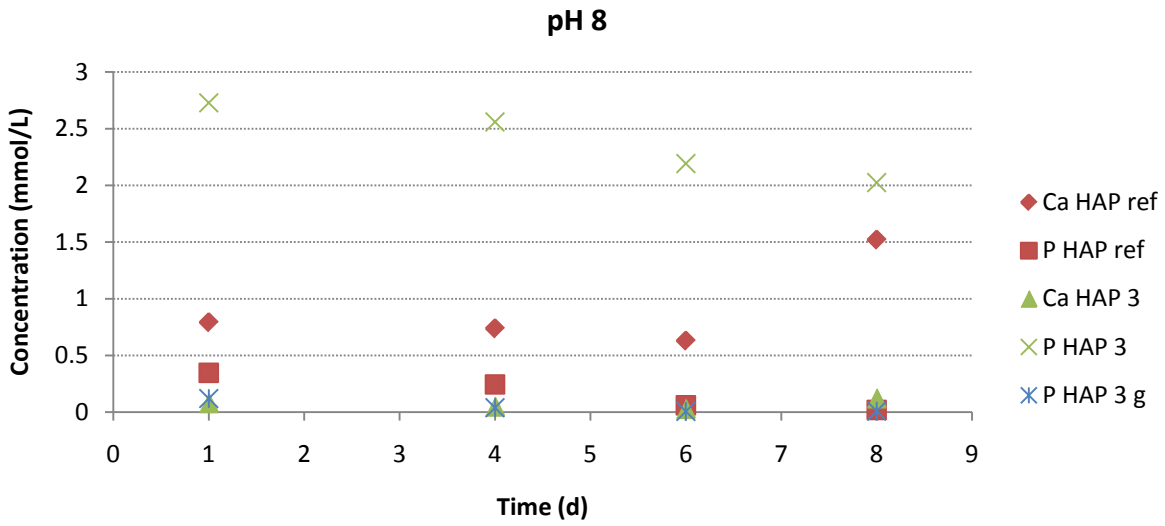

Figure 57: Ca and P release from reference HAP, HAP 3 and HAP 3/gypsum in pH 8 oxic environment.

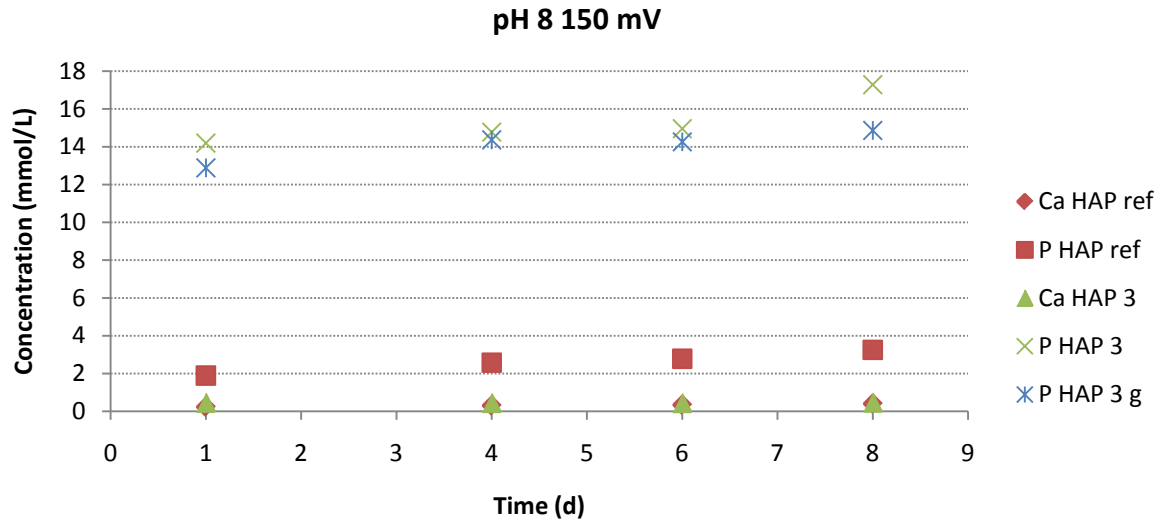

Figure 58: Ca and P release from reference HAP, HAP 3 and HAP 3/gypsum in pH 8 anoxic (150 mV) environment

The phosphorus release[3] is seen to be much higher from the HAP produced in this work (HAP 3) than the reference material purchased from Sigma Aldrich. This apparently reflects the nanocrystalline nature of the McGill product and the fact that it was not calcined (refer to XRD data in section 4.1). The difference in leachability between the two HAP materials is significant (~3-5 times higher). Preliminary thermodynamic calculations using the OLI software confirmed indeed that the produced HAP in this work is not fully crystalline exhibiting significantly higher solubility than the theoretically expected one. For example the OLI calculated concentrations for a pH solution were: for P $1.48 \cdot 10^{-6}$ mmol/L and for Ca 0.0021 mmol/L. By contrast the experimental values at pH 8 were: P 2.37 mmol/L and Ca 0.07 mmol/L for HAP 3; P 0.17 mmol/L and Ca 0.92 mmol/L for the reference HAP and 0.04 mmol/L of P for HAP 3 in gypsum saturated water.

Another interesting observation (totally unexpected) was the higher release of P in the anoxic tests that requires further investigation. One possible explanation is the involvement of sulphite (SO_3^{2-}) ions as complexing or ion exchange agents causing release of PO_4^{3-} from the HAP structure/surface. Use of other reducing agents like S^{2-} [12] would have to be tested to verify this hypothesis.

The presence of gypsum seems to suppress the phosphorus release in the oxic tests, but this effect is not so obvious for the anoxic ones. This means that the presence of gypsum, i.e. the excess of calcium ions, enhances the stability of the compound[4], but only for non-reducing conditions. In the latter case apparently the presence of sulphite ions may have interfered in an as yet unclear way.

[3] Calcium release on the other hand is rather negligible, i.e. the solids exhibited incongruent dissolution behaviour perhaps because of the atmospheric dissolved carbon dioxide/carbonate content of water.

[4] An apparent manifestation of common ion effect.

4.3.2 Stability of HAP-encapsulated scorodite

4.3.2.1 Oxic Environment

Arsenic release data under oxic environment is presented in Figure 59 for the case of ENCH 10 encapsulated solids. From the results it is obvious that the release of arsenic is reduced when comparing the naked scorodite samples and the encapsulated ones. It is clear therefore that the presence of a hydroxyapatite layer has a positive effect on the stability of scorodite, in the alkaline (pH>7) region, where scorodite is the least stable - refer to Figure 1 in the Literature Review Chapter.

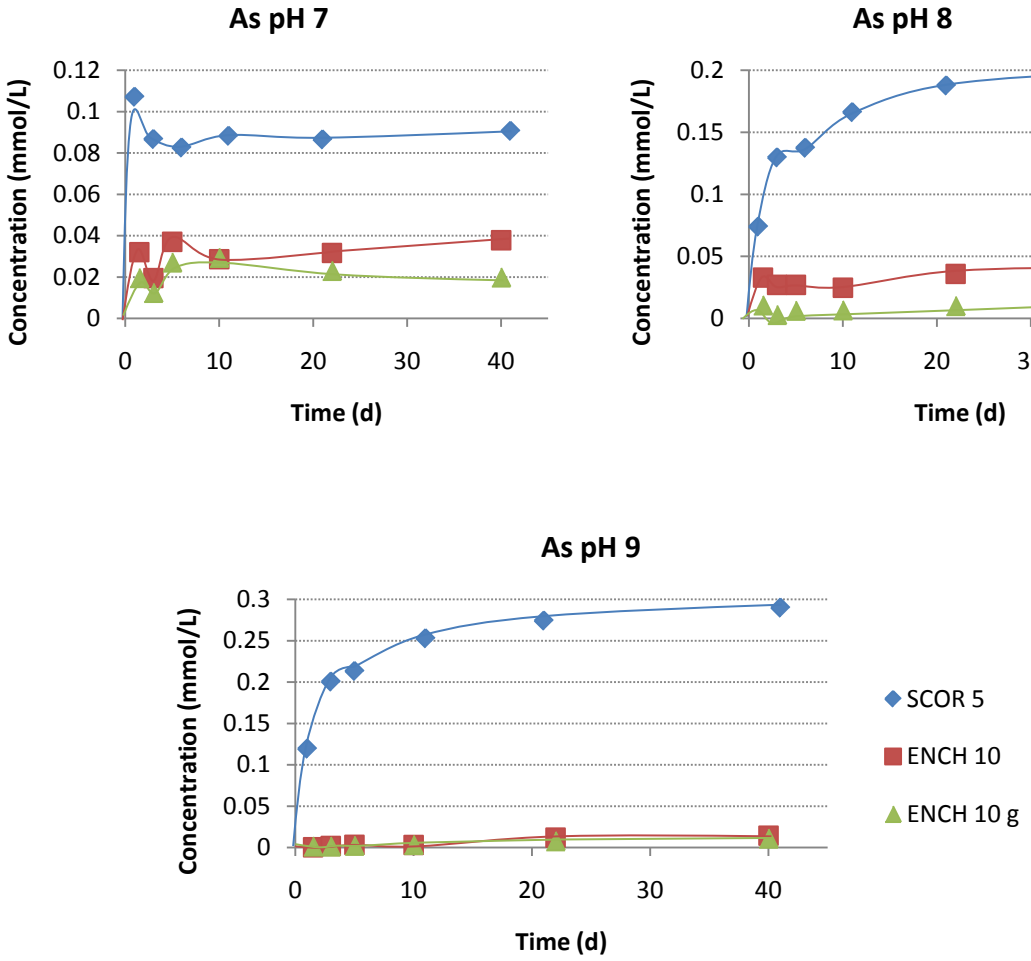

Figure 59: Oxic tests at pH 7, 8 and 9 for reference scorodite and ENCH 10 solids with and without gypsum saturated water.

Especially for pH 9 where scorodite releases 0.29 mmol/L (22 mg/L) As, the coated material releases 0.014 mmol/L (1.08 mg/L) As, which is improved a little bit in

the presence of gypsum, 0.011 mmol/L (0.82 mg/L) As, after a total of 40 days for all samples.

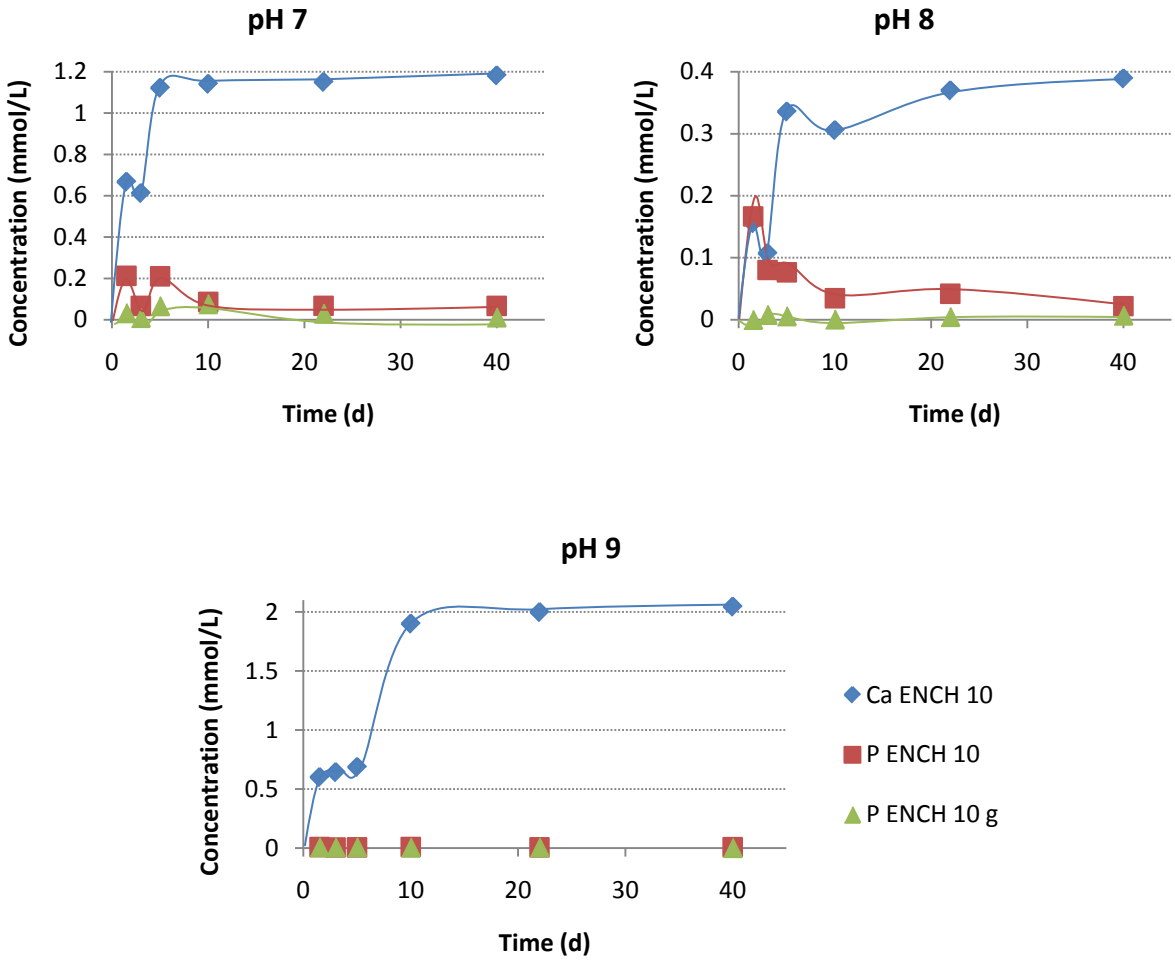

Figure 60: Release of Ca and P from ENCH 10 solids at pH 7, 8 and 9 with and without gypsum.

In addition to arsenic the release of P was monitored and the relevant results are plotted in Figure 60. The release of P was low varying from 0.28 mg/L (0.0098 mmol/L) at pH 9 to 6.5 mg/L (0.21 mmol/L) at pH 7. This was further suppressed in the presence of gypsum: 6.5 mg/L (0.21 mmol/L) vs. 2.3 mg/L (0.076 mmol/L) at pH 7.

The Fe concentration was found to be very low for all samples, which was expected, since at these pH values iron precipitates as ferrihydrite, and thus it cannot be measured by chemical analysis of the sample solutions.

4.3.2.2 Anoxic Environment

Arsenic release data from ENCH 10 encapsulated solids and reference scorodite under anoxic conditions (e_h target= 150 mV) is plotted in Figure 61 and Figure 62. The variation of e_h during the course of the stability test is shown in Figure E - 5 in Appendix E.

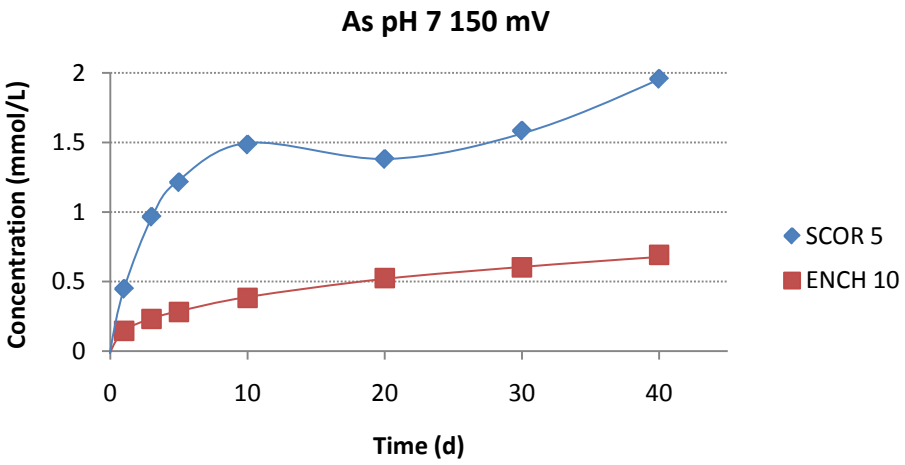

Figure 61: Arsenic release from scorodite and ENCH 10 solids at pH 7 and 150 mV.

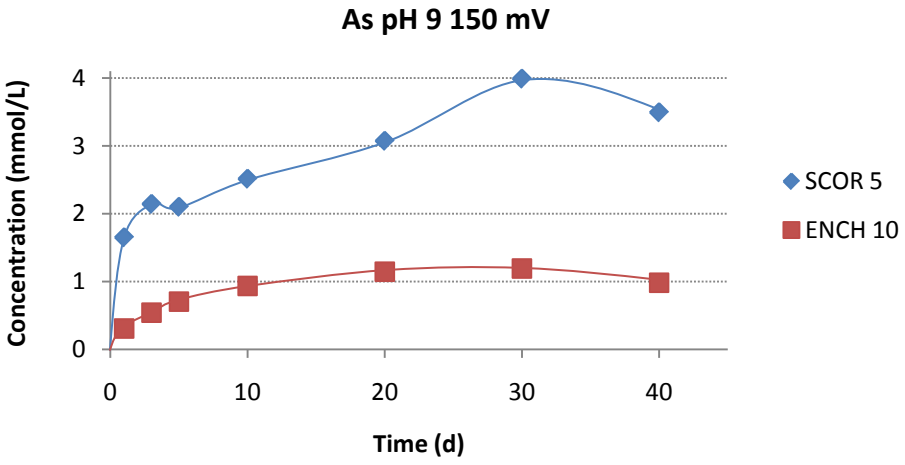

Figure 62: Arsenic release from scorodite and ENCH 10 solids at pH 9 and 150 mV.

First comparison of the oxic and anoxic stability data clearly shows that scorodite releases at least one order of magnitude more arsenic under anoxic than oxic conditions that makes its encapsulation even more necessary. Encapsulation with HAP coatings proved indeed (at least partially) successful as arsenic was reduced to ~ 30 %

of that of unprotected scorodite. For example arsenic release was ~110 mg/L after 40 days at pH 9 this being reduced to ~30 mg/L upon encapsulation. However this level of protection is not considered adequate given the current environmental regulations reviewed in Chapter 2 hence additional encapsulated materials were tested.

Thus in addition to scorodite and ENCH 10 solids, the products from ENCH 11 and ENCH 13 encapsulation tests were tested under the conditions of pH 8 and e_h of 150 mV. All the arsenic release results from these tests are presented in Figure 63 including the results from the stability testing of the physical mixture of scorodite with hydroxyapatite.

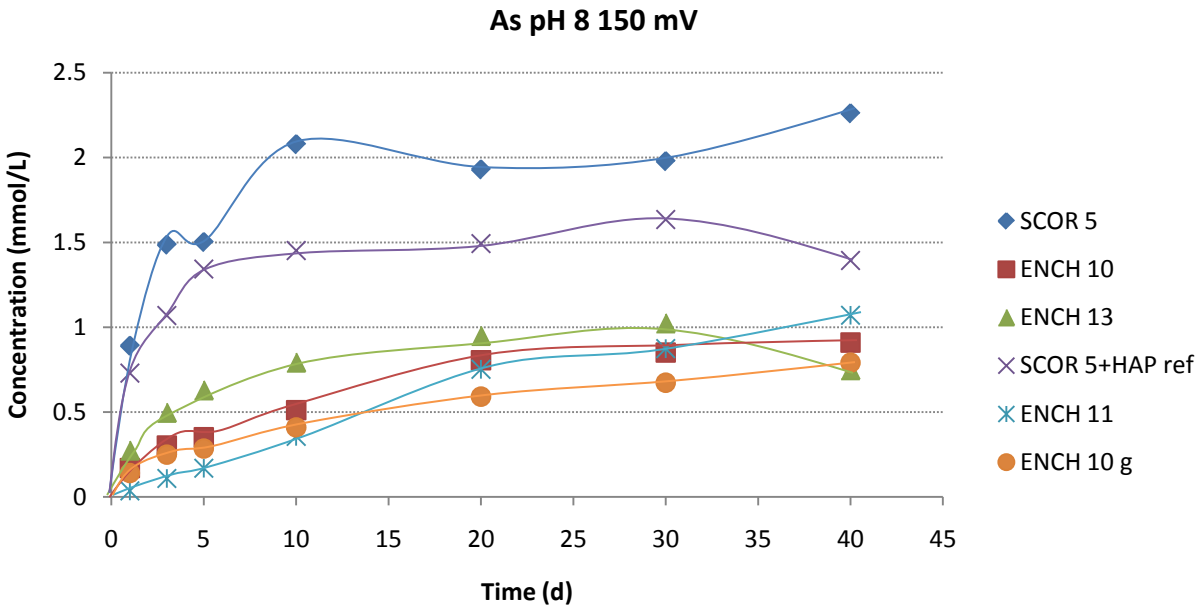

Figure 63: Arsenic release under anoxic conditions (pH 8 and 150 mV) for various materials.

According to the plotted data it is seen that all the encapsulated scorodite materials behave better than unprotected scorodite. Moreover judging from the data of the physical mixture of scorodite with hydroxyapatite it can be concluded that the observed reduction in arsenic release is not owed simply to the presence of hydroxyapatite but rather to its coating around the scorodite particles (heterogeneous deposition). All encapsulated materials (produced via the different deposition procedures-refer to Section 4.2) exhibited similar arsenic release patterns.

Unfortunately the level of protection achieved is not adequate apparently due to incomplete growth of a continuous thick layer of HAP on the surface of all scorodite particles. Furthermore the use of sulphites as reducing agent may have interfered with the stability of the HAP coatings.

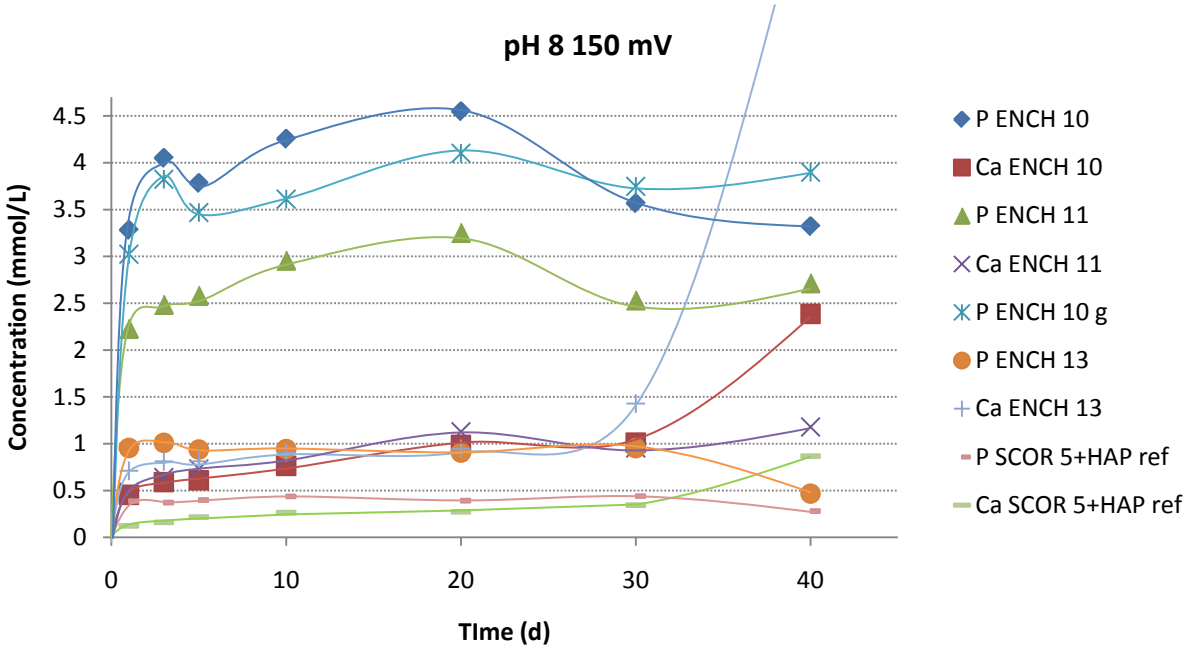

Figure 64: Release of Ca and P under anoxic conditions (pH 8 150 mV) for various materials. (The value for Ca ENCH 13 at the 40-day mark was exceptionally high and is omitted so that the rest of the values are viewed properly.)

In addition to arsenic the concentrations of P and Ca were monitored during the anoxic stability tests and are shown in Figure 63. It can be seen that the release of phosphorus is very low for ENCH 13, which consisted of conditioning the scorodite in a calcium solution and a subsequent Nancollas step, compared to ENCH 10 and 11, which consisted of several nucleation steps and a “growth” or “Nancollas” step deposition procedure. This again points to the beneficial effect of the pre-nucleation calcium conditioning step that helps build more robust HAP coating.

4.3.3 Stability of FAP-encapsulated scorodite

Due to time constrains only a few preliminary encapsulation tests were performed with fluoroapatite. These tests are summarized in Table C-1. Selected stability data collected by equilibration of solids for 40 days at pH 9 under oxic and anoxic (150mV target e_h) are presented in the Figures below.

4.3.3.1 Oxic Environment

As seen in the plotted data of Figure 65, under oxic conditions the FAP-encapsulated scorodite obtained in the ENCF 3 test yielded three times lower arsenic release than the unprotected scorodite indicating that the fluoroapatite layer effectively coated the surface of the scorodite. The respective numbers after 40 days testing are 22 mg/L As for scorodite and 7.7 mg/L As for the ENCF 3 material. By comparison the HAP-coated scorodite (Test ENCH 10) yielded 1 mg/L As, i.e. significantly lower than that of the FAP-coated material apparently reflecting better continuous growth of the HAP layer.

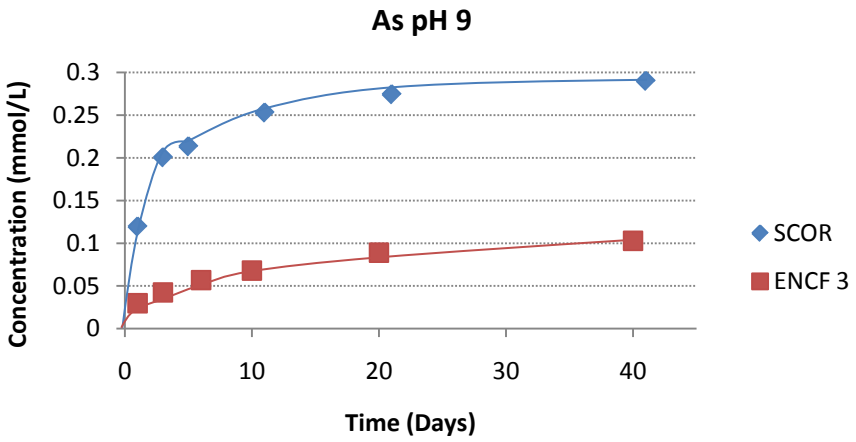

Figure 65: Oxic tests at pH 9 for reference scorodite and ENCF 3 solids.

In the following graph Figure 66 the concentrations for phosphorus and calcium during the long term stability tests for fluoroapatite encapsulated scorodite at pH 9 are presented. The concentration of phosphorus at pH 9 after 40 days was found to be 0.01 mmol/L or 0.34 mg/L P, which is close to the value found for the HAP-coated material (ENCH 10), namely 0.2 mg/L P. This may indicate that the FAP deposit is in fact in mixture with HAP not having grown fully on its own. Due to time constraints no proper

characterisation for the identification of the deposit was done. Apparently further work is needed to improve the deposition-formation of FAP on scorodite.

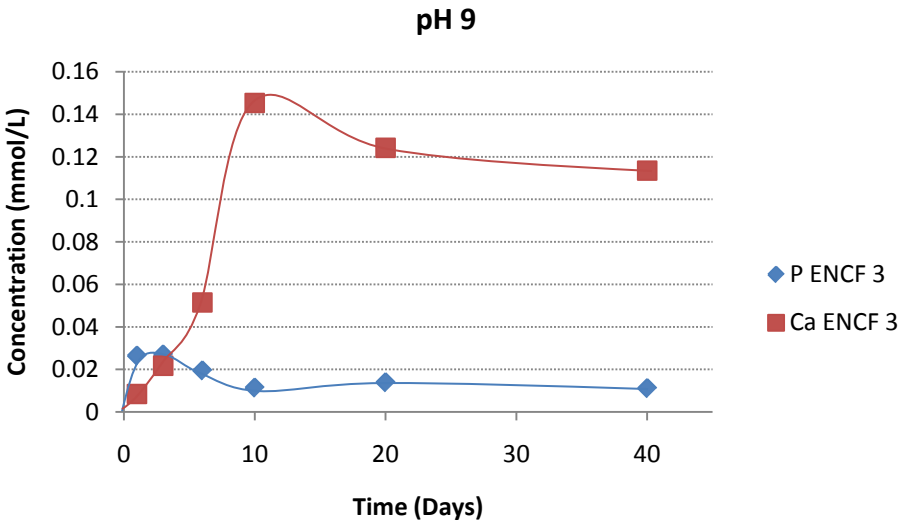

Figure 66: Phosphorus and calcium release for ENCF 3 under oxic conditions.

4.3.3.2 Anoxic Environment

The stability data of the ENCF 3 solids under anoxic conditions is plotted in Figure 67. It is clear that the concentration of arsenic for the encapsulated materials is a lot lower than that for naked scorodite, confirming once again the effectiveness of the encapsulation layer, regardless of its poor development and identification. Thus the As concentration released after 40 days dropped from 260 mg/L for the unprotected scorodite down to 12.3 mg/L for the FAP-coated material. The equivalent value for the HAP-coated material (ENCH 10) under the same conditions was higher at 73.5 mg/L. This differentiation between the two coated materials mirrors the corresponding P release data (Figure 68 and data in Appendix D) according to which the HAP-coated material released higher P content (15 mg/L after 40 d) than the FAP-coated material (0.73 mg/L). This was an unexpected result that perhaps reflects an interaction of the HAP coating with the sulphite reducing agent or some other unidentified factor.

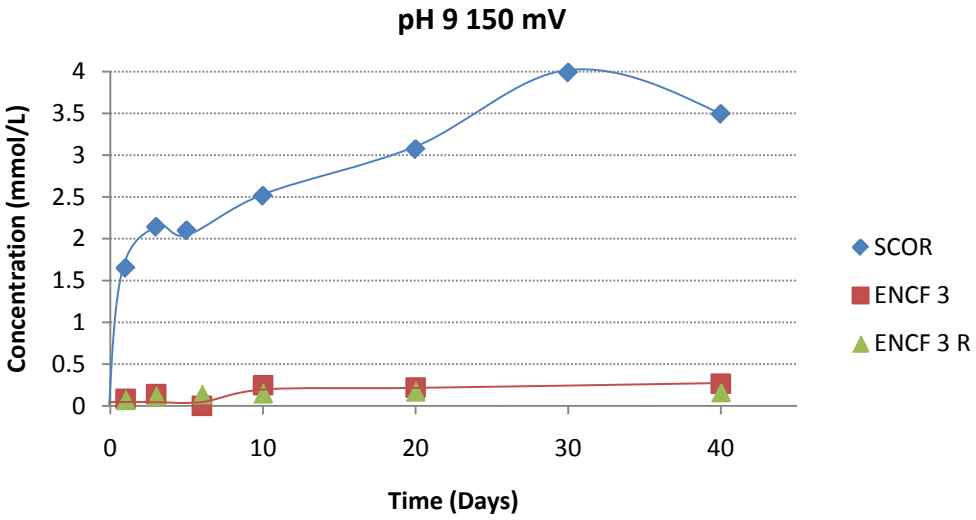

Figure 67: Arsenic release from scorodite and ENCF 1, 3 and 3 repeat, 1g at pH 9 and 150 mV

.

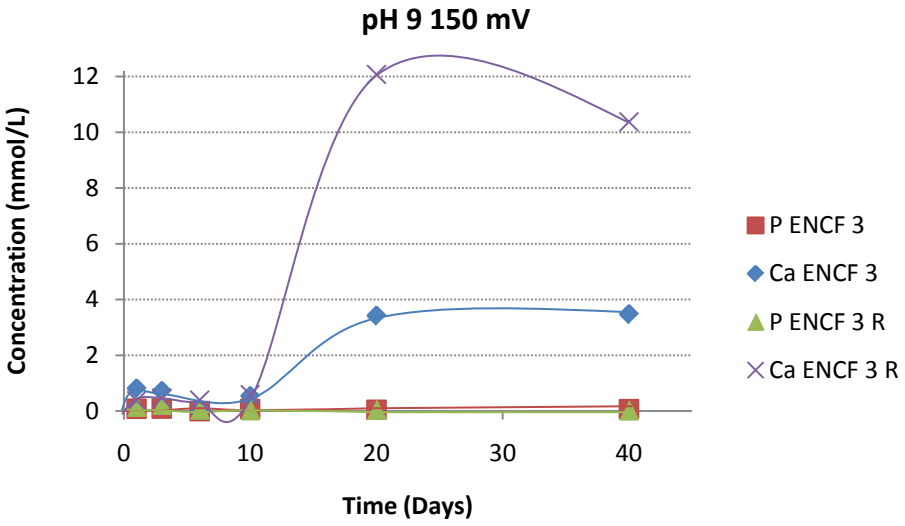

Figure 68: Phosphorus and Calcium release under anoxic conditions (pH 9 150 mV) for fluoroapatite encapsulated scorodite.

Chapter 5. Conclusions

The encapsulation of scorodite via direct precipitation of calcium phosphate coatings and the stability of the products were studied under oxic and anoxic environments.

Hydroxyapatite (HAP) powders were homogeneously precipitated initially from solutions with different concentrations (give range) and at different temperatures (22-80 ºC). The precipitation mehod involved controlled addition/mixing of two calcium and phosphate source solutions at fixed pH. Though the precipitated powders were identified as (Ca-deficient) hydroxyapatite, their crystallinity and stability were lower compared to that of the reference hydroxyapatite powder that was purchased by Sigma Aldrich. This reflects the nanocrystalline character of these solution-synthesized powders and the fact that they were not thermally treated. The precipitation of fluoroapatite (FAP) was also investigated but not as extensively as that of hydroxyapatite. All characterisation and stability evidence collected suggest that the fluoroapatite product was indeed a solid solution or mixed with hydroxyapatite. The metastable zones for both hydroxyapatite and fluoroapatite products were determined and used as guide in designing the encapsulation experiments.

Encapsulation experiments of scorodite were conducted by depositing hydroxyapatite or fluoroapatite on the particles. Different combinations of procedures were used to control supersaturation and induce the deposition of HAP/FAP on the scorodite particle surface and thus effect their coating. Heterogeneous deposition proved difficult. After trying various procedures it was determined that prior conditioning of the scorodite substrate in a calcium solution created favourable nucleation conditions. Low agitation (500 rpm) and high temperature (37 ºC) also proved beneficial as also did adaptation of the Wu and Nancollas procedure for the deposition of hydroxyapatite on titanium dioxide spheres to the encapsulation of scorodite. Nevertheless, the coating layers formed on the particles were not as robust and continuous as desired an issue that should be addressed in future research.

The long term stability of the encapsulated solids, as well as the scorodite alone and the hydroxyapatite were tested, and the results clearly demonstrated that in principle stabilisation and protection of scorodite with hydroxyapatite/fluoroapatite is possible. In all cases the solids after the encapsulation experiments behaved much better than the scorodite control sample, either under oxic or under anoxic conditions in the alkaline region. By far the best results were obtained with the HAP-coated system under anoxic conditions, which yielded 1 mg/L As release after 40 days at pH 9 compared to 7.7 mg/L for the FAP-coated material and 22 mg/L for the unprotected scorodite. At the same time the P concentration released was 0.2-0.3 mg/L for both HAP and FAP. The stability of the coatings, as well as that of scorodite, was enhanced further by the presence of gypsum. Unfortunately under anoxic conditions not similarly robust behaviour was observed. This could have been due to the use of sulphite (SO_3^{2-}) ions as reducing agent causing the release of the phosphate ions via adsorption and ion exchange or due to some other unidentified factor. Use of a different reducing agent should be tested, in order to acquire further insight to the system.

Chapter 6. References

1. Mandal, B.K.; Suzuki, K.T., *Arsenic round the world: a review.* Talanta, 2002. **58**(1): p. 201-235.
2. Federal Department of Fisheries and, Oceans; Government of Canada, *Metal Mining Effluent Regulations*. 2002, The Queen's Printer for Canada: Ottawa. p. 1246-1543.
3. Environmental Protection, Agency, *Technical Assistance Document for Complying with the TC Rule and Implementing the Toxicity Characteristic Leaching Procedure (TCLP)*, Environmental Protection Agency, Editor. 1994.
4. Le Berre, J. F.; Gauvin, R.; Demopoulos, G. P., *Synthesis, structure and stability of galium arsenate dihydrate, indium arsenate dihydrate and lanthanum arsenate.* Ind. Eng. Chem. Res., 2007. **46**: p. 7875-7882.
5. De Klerk, Richard Jack, *Investigating the continuous circuit coprecipitation of arsenic(V) with ferric iron in sulphate media*. 2008.
6. Daenzer, R., *Investigating the role of ferrous iron in the arsenic(V)-iron(II,III) coprecipitation process system*, in *Department of Mining and Materials Engineering*. 2011, McGill University: Montreal.
7. Harris, G.B. *The removal of arsenic from process solutions: Theory and industrial practice.* in *Hydrometallurgy*. 2003. Warrendale, PA: The Minerals, Metals & Materials Society.
8. Robins, R.G.; Dove, P.M.; Rimstidt, J.D.; Nordstrom, D.K.; Parks, G.A., *Solubility and stability of scorodite, FeAsO 4 .2H 2 O; discussions and replies.* American Mineralogist, 1987. **72**(7-8): p. 842-855.
9. Bluteau, M.-C.; Demopoulos, G.P., *The incongruent dissolution of scorodite -- Solubility, kinetics and mechanism.* Hydrometallurgy, 2007. **87**(3-4): p. 163-177.
10. Rochette, E.A.; Li, G.C.; Fendorf, S.E., *Stability of arsenate minerals in soil under biotically generated reducing conditions.* Soil Science Society of America, 1998. **62**: p. 1530-1537.
11. Demopoulos, G. P., *On the preparation and stability of scorodite*, in *Arsenic Metallurgy*. 2005, The Minerals, Metals and Materials Society: San Francisco.
12. Lagno, F., *Encapsulation of scorodite particles with phosphate coatings*, in *Mining, Metals and Materials Engineering*. 2005, McGill University: Montreal.
13. Leetmaa, K., *Scorodite stabilization with aluminum hydroxy-gels*. 2008, McGill University: Montreal.
14. European Chemicals, Agency, *Background document for diarsenic trioxide.* 2010.
15. Brooks, W.E., *2007 Minerals Yearbook, Arsenic*. 2008, United States Geological Survey.
16. Riveros, P.A.; Dutrizac, J. E.; Spencer, P., *Arsenic disposal practices in the Metallurgical Industry.* Canadian Metallurgical Quarterly, 2001. **40**(4): p. 395-420.
17. Filippou, D.; Demopoulos, G.P., *Arsenic immobilization by controlled scorodite precipitation.* JOM Journal of the Minerals, Metals and Materials Society, 1997. **49**(12): p. 52-55.
18. Swash, P.M.; Monhemius, A.J.; Schaekers, J.M. *Solubilities of process residues from biological oxidation pretreatments of refractory gold ores*. in *Minor Elements 2000*. 2000. Littleton, CO, USA: Society of Mineral Metal Exploration.
19. Mahoney, J., *Control of As and Ni releases from a uranium mill tailings neutralization circuit: Solution chemistry, mineralogy and geochemical modeling of laboratory study results.* Applied Geochemistry, 2007. **22**(12): p. 2758-2776.
20. Kwong, Y.T.J.; Percival, J.B.; Soprovich, E.A. *Arsenic mobilization and attenuation in near-neutral drainage - Implications for tailings and waste rock management for Saskatchewan uranium mines*. in *Uranium 2000*. 2000: Canadian Institute of Mining, Metallurgy and Petroleum, Montreal, Canada.

21. Paktunc, A.D.; Szymanski, J.T.; Lastra, R.; Laflamme, J.H.G.; Enns, V.; Soprovich, E., *Assessment of potential arsenic mobilization from the Ketza river mine tailings, Yukon, Canada*, in *Waste Characterization and Treatment*, W. Petruk, Editor. 1998, Society of Mineral Metal Exploration: Littleton, CO, USA.
22. Gomez, M.A.; Becze, L.; Bluteau, M.-C.; Le Berre, J.N.; Cutler, J.N.; Demopoulos, G.P. *Autoclave precipitation and characterization of Fe(III)-AsO4-SO4 Phases*. in *Hydrometallurgy 2008*. 2008. Phoenix, AZ, USA: TMS.
23. White, T.J.; Eaton, G.F.; Kyle, J.; Lincoln, F. *Xtaltite - A mineralogical approach to the disposal of mercury and arsenic wastes*. in *Extraction and Processing for the Treatment and Minimization of Wastes*. 1994. San Francisco, CA.
24. McCloskey, J.; Twidwell, L.G.; Lee, M.G. *Arsenic removal from mine and process waters by lime/phosphate precipitation: Pilot scale demonstration*. in *Arsenic Metallurgy*. 2005: The Minerals, Metals & Materials Society.
25. Rosengrant, L.; Fargo, L., *Final best demonstrated available technology (BDAT) background document for K031, K084, K101, K102, characteristic arsenic wastes, characteristic selenium wastes, and P and U wastes containing arsenic and selenium listing constituents*. 1990, U. S. Environmental Protection Agency: Washington, DC, USA.
26. Yia, Y.; Demopoulos, G. P.; Chen, N.; Cutler, J.;, *Co-precipitation of As(V) with Fe(III) in Sulphate Media: Solubility and speciation of Arsenic*, in *Arsenic Metallurgy*, R.G.; Ramachandran Reddy, V.;, Editor. 2005, TMS: Warrendale, PA. p. 137-148.
27. Chen, N.; Jiang, D.T.; Cutler, J.; Kotzer, T.; Jia, Y.F.; Demopoulos, G.P.; Rowson, J.W.;, *Structural characterization of poorly crystalline scorodite, Iron(III)-Arsenate co-precipitates and Uranium mill neutralized raffinate.* Geochim. Cosmochim. Acta, 2009. **73**: p. 3260-3276.
28. Le Berre, J. F.; Gauvin, R.; Demopoulos, G. P., *A study of the crystallization kinetics of scorodite via the transformation of poorly crystalline ferric arsenate in weakly acidic solution.* Colloids and Surfaces A: Physicochemical and Engineering Aspects, 2008. **315**(1-3): p. 117-129.
29. Dutrizac, J.E.; Jambor, J.L., *The synthesis of crystalline scorodite, FeAsO4 · 2H2O.* Hydrometallurgy, 1988. **19**(3): p. 377-384.
30. Harris, G.B.; Monette, S., *The disposal of arsenic solid residues*, in *Productivity and technology in the metallurtgical industries.*, M. Koch and J.C. Taylor, Editors. 1989, The Minerals, Metals and Materials Society: Warrendale, PA. p. 545-560.
31. Swash, P.M.; Monhemius, A.J., *Hydrothermal precipitation from aqueous solutions containing iron(III), arsenate and sulphate*, in *Hydrometallurgy '94*. 1994: Cambridge, UK. p. 177-190.
32. Monhemius, A.J.; Swash, P.M., *Removing and stabilizing As from Copper refining circuits by hydrothermal processing.* JOM Journal of the Minerals, Metals and Materials Society, 1999. **51**(9): p. 30-33.
33. Demopoulos, G.P., *Aqueous precipitation and crystallization for the production of particulate solids with desired properties.* Hydrometallurgy, 2008.
34. Demopoulos, G.P.; Droppert, D.J.; Van Weert, G., *Precipitation of crystalline scorodite (FeAsO4 · 2H2O) from chloride solutions.* Hydrometallurgy, 1995. **38**(3): p. 245-261.
35. Singhania, Shalabh, Wang, Qiankun, Filippou, Dimitrios and Demopoulos, George, *Acidity, valency and third-ion effects on the precipitation of scorodite from mixed sulfate solutions under atmospheric-pressure conditions.* Metallurgical and Materials Transactions B, 2006. **37**(2): p. 189-197.
36. Fujita, T.; Taguchi, R.; Abumiya, M.; Matsumoto, M.; Shibata, E.; Nakamura, T., *Novel atmospheric scorodite synthesis by oxidation of ferrous sulfate solution. Part I.* Hydrometallurgy, 2008. **90**(2-4): p. 92-102.

37. Singhania, S.; Wang, Q.; Filippou, D.; Demopoulos, G.P., *Temperature and seeding effects on the precipitation of scorodite from sulfate solutions under atmospheric-pressure conditions.* Metallurgical and Materials Transactions B, 2005. **36**(3): p. 327-333.
38. Debekaussen, R.; Droppert, D.; Demopoulos, G.P., *Ambient pressure hydrometallurgical conversion of arsenic trioxide to crystalline scorodite*. 2001, Canadian Institute of Mining, Metallurgy and Petroleum: Montreal, QC, Canada.
39. Demopoulos, G.P.; Lagno, F.; Wang, Q.; Singhania, S.;. *The atmospheric scorodite process*. in *Copper 2003-Hydrometallurgy of Copper*. 2003. Montreal: CIM.
40. Swash, P.M.; Monhemius, A.J.; Schaekers, J.M., *Solubilities of process residues from biological oxidation pretreatments of reftractory gold ores* in *Minor elements 2000: Processing and Environmental Aspects of As, Sb, Se, Te and Bi*, Young. C., Editor. 2000: Littleton, CO, USA. p. 115-123.
41. Dove, P.M.; Rimstidt, J.D., *The solubility and stability of scorodite, FeAsO 4 .2H 2 O.* American Mineralogist, 1985. **70**(7-8): p. 838-844.
42. Krause, E.; Ettel, V.A., *Solubility and stability of scorodite, FeAsO[4]•2H[2]O: new data and further discussion*. Vol. 73. 1988, Washington, DC, ETATS-UNIS: Mineralogical Society of America.
43. Koutsoukos, P.G., *Current knowledge of calcium phosphate chemistry and in particular solid surface-water interface interactions.*, in *Second International Conference on the Recovery of Phosphorus from Sewage and Animal Wastes*. 2001: Noordwijkerhout, The Netherlands.
44. Tai, C.Y.-D.; Chen, P.-C.; Chien, W.-C., *Particle Nucleation and Growth.* Encyclopedia of Surface and Colloid Science: Second Edition, 2006: p. 4452 - 4466.
45. Garside, J., *Industrial crystallization from solution.* Chemical Engineering Science, 1985. **40**(1): p. 3-26.
46. Kaschiev, D., *Nucleation: Basic Theory with Application*. 2000, Oxford, UK: Elsevier Science.
47. Brečević, L.; Kralj, D., *Kinetics and mechanisms of crystal growth in aqueous systems.* Interfacial Dynamics, Surfactant Science Series 2000. **88**: p. 435-474.
48. Dirksen, J. A.; Ring, T. A., *Fundamentals of crystallization: Kinetic effects on particle size distributions and morphology.* Chemical Engineering Science, 1991. **46**(10): p. 2389-2427.
49. Tashiro, N.; Maruyama, O., *Encapsulation method*, United States Patent and Trademark Office, Editor. 1994, Dainippon Ink and Chemicals, Inc: USA.
50. Lindsay, W.L.; Vlek, P.L.G.; Chien, S.H., *Phosphate Minerals*, in *Minerals in soil environment*, J.B.; Weed Dixon, S.B., Editor. 1989, Soil Science Society of America: Madison, WI, USA. p. 1089-1130.
51. Nancollas, G.H., *The nucleation and growth of phosphate minerals.*, in *Berlin, Germany*, J.O.; Moore Nriagu, P.B., Editor. 1984, Springer Verlag. p. 137-154.
52. Nixon, S.W., *Coastal marine eutrophication: a definition, social causes, and future concerns.* Ophelia, 1995. **41**.
53. Yeoman, S.; Stephenson, T.; Lester, J. N.; Perry, R., *The removal of phosphorus during wastewater treatment: A review.* Environmental Pollution, 1988. **49**(3): p. 183-233.
54. De Groot, K., *Bioceramics consisting of calcium phosphate salts.* Biomaterials, 1980. **1**(1): p. 47-50.
55. Ten Cate, J.M.; Featherstone, J.D.B., *Mechanistic aspects of the interactions between fluoride and dental enamel.* Critical Reviews in Oral Biology and Medicine, 1991. **2**(2): p. 283-296.
56. Mojumdar, S.C.; Kozankova, J.; Chocholousek, J.; Majling, J.; Fabryova, D., *FLUOROAPATITE - MATERIAL FOR MEDICINE. Growth, morphology and thermoanalytical properties.* Journal of Thermal Analysis and Calorimetry, 2004. **78**: p. 73-82.

57. Tung, M.S., *Calcium Phosphates: Structure, composition, solubility and stability.*, in *Calcium Phosphates in Biological and Industrial Systems*, Z. Amjad, Editor. 1998, Kluwer Academic Publishers: Norwell, MA, USA.
58. Bohner, M., *Calcium orthophosphates in medicine: from ceramics to calcium phosphate cements.* Injury, 2000. **31**(Supplement 4): p. D37-D47.
59. Williams, R.A.D.; Elliott, J.C., *Basic and Applied Dental Biochemistry*, Churchill Livingstone: Edinburgh.
60. Chow, L.C.; Markovic, M., *Physicochemical properties of fluorapatite*, in *Calcium phosphates in biological and industrial systems*, Z. Amjad, Editor. 1998, Kluwer: Boston. p. 67-83.
61. Chow, L.C., *Solubility of calcium phosphates.* Monographs in Oral Science Basel, Karger, 2001. **18**: p. 94-111.
62. Dorozhkin, S.V., *A review on the dissolution models of calcium apatites.* Progress in Crystal Growth and Characterization of Materials, 2002. **44**(1): p. 45-61.
63. *Phosphates: geochemical, geobiological, and materials importance*, ed. M.J.; Rakovan Kohn, J.; Hughes, M.J. 2002, Washington, DC, USA: Mineralogical Society of America.
64. Zhu, Y.; Zhang, X.; Chen, Y.; Xie, Q.; Lan, J.; Qian, M.; He, N., *A comparative study on the dissolution and solubility of hydroxylapatite and fluorapatite at 25 °C and 45 °C.* Chemical Geology, 2009. **268**(1-2): p. 89-96.
65. Fabian, R.; Kotsis, I.; Zimany, P.; Halmos, P., *Preparation and chemical characterization of high purity fluorapatite.* Talanta, 1998. **46**: p. 1273-1277.
66. Holand, W.; Ritzberger, C.; Apel, E.; Rheinberger, V.; Nesper, R.; Krumeich, F.; Moenster, C.; Eckert, H., *Formation and crystal growth of needle-like fluoroapatite in functional glass-ceramics.* Journal of Materials Chemistry, 2007. **18**: p. 1318-1332.
67. Pramanik, S.; Agarwal, A. K.; Rai, K. N.; Garg, A., *Development of high strength hydroxyapatite by solid-state-sintering process.* Ceramics International, 2007. **33**(3): p. 419-426.
68. Slósarczyk, A.; Stobierska, E.; Paszkiewicz, Z.; Gawlicki, M., *Calcium Phosphate Materials Prepared from Precipitates with Various Calcium:Phosphorus Molar Ratios.* Journal of the American Ceramic Society, 1996. **79**(10): p. 2539-2544.
69. Nikcevic, I.; Jokanovic, V.; Mitric, M.; Nedic, Z.; Makovec, D.; Uskokovic, D., *Mechanochemical synthesis of nanostructured fluorapatite/fluorhydroxyapatite and carbonated fluorapatite/fluorhydroxyapatite.* Journal of Solid State Chemistry, 2004. **177**: p. 2565-2574.
70. Rhee, S.-H., *Synthesis of hydroxyapatite via mechanochemical treatment.* Biomaterials, 2002. **23**(4): p. 1147-1152.
71. Willigeroth, S. F.; Beneke, K.; Hannig, M.; Zimehl, R. , *Preparation strategies for phosphate-based mineral biomaterials.* Progr Colloid Polym Sci, 2002. **121**: p. 1-6.
72. Zimehl, R.; Willingeroth, S.F.; Hannig, M.; Frahm, H. , *Nano-sized fluoroapatite particles by controlled precipitation from heterogeneous systems.* Progr Colloid Polym Sci, 2004. **129**: p. 110-118.
73. Jarudilokkul, S.; Tanthapanichakoon, W.; Boonamnuayvittaya, V, *Synthesis of hydroxyapatite nanoparticles using an emulsion liquid membrane system.* Colloids and Surfaces A: Physicochemical and Engineering Aspects, 2007. **296**(1-3): p. 149-153.
74. Koumoulidis, G.C.; Katsoulidis, A.P.; Ladavos, A.K.; Pomonis, P.J.; Trapalis, C.C.; Sdoukos, A.T.; Vaimakis, T.C., *Preparation of hydroxyapatite via microemulsion route.* Journal of Colloid and Interface Science, 2003. **259**(2): p. 254-260.
75. Panda, R. N.; Hsieh, M. F.; Chung, R. J.; Chin, T. S., *FTIR, XRD, SEM and solid state NMR investigations of carbonate-containing hydroxyapatite nano-particles synthesized by hydroxide-gel technique.* Journal of Physics and Chemistry of Solids, 2003. **64**(2): p. 193-199.

76. Liu, D.-M.; Troczynski, T.; Tseng, W.J., *Water-based sol-gel synthesis of hydroxyapatite: process development.* Biomaterials, 2001. **22**(13): p. 1721-1730.
77. Rodriguez-Lorenzo, L.M.; Hart, J.N.; Gross, K.A. , *Influence of fluorine in the synthesis of apatites. Synthesis of solid solutions of hydroxy-fluorapatite.* Biomaterials, 2003. **24**: p. 3777-3785.
78. Rodriguez-Lorenzo, L.M.; Vallet-Regi, M. , *Controlled Crystallization of Calcium Phosphate Apatites.* Chemistry of Materials, 2000. **12**: p. 2460-2465.
79. Chen, H.; Sun, K.; Tang, Z.; Law, R.V.; Mansfield, J.F.; Czajka-Jakubowska, A.; Clarkson, B.H.;, *Synthesis of fluorapatite nanorods and nanowires by direct precipitation from solution.* Crystal Growth and Design, 2006. **6**(6): p. 1504-1508.
80. Okazaki, M.; Miake, Y.; Tohda, H.; Yanagisawa, T.; Matsumoto, T.; Takahashi, J., *Functionally graded fluoridated apatites.* Biomaterials, 1999. **20**(15): p. 1421-1426.
81. Okazaki, M.; Miake, Y.; Tohda, H.; Yanagisawa, T.; Takahashi, J., *Fluoridated apatite synthesized using a multi-step fluoride supply system.* Biomaterials, 1999. **20**(14): p. 1303-1307.
82. Weng, W.; Baptista, J.L., *Preparation and Characterization of Hydroxyapatite Coatings on Ti6Al4V Alloy by a Sol-Gel Method.* Journal of the American Ceramic Society, 1999. **82**(1): p. 27-32.
83. Ramay, H.R.; Zhang, M., *Preparation of porous hydroxyapatite scaffolds by combination of the gel-casting and polymer sponge methods.* Biomaterials, 2003. **24**(19): p. 3293-3302.
84. Saiz, E.; Gremillard, L.; Menendez, G.; Miranda, P.; Gryn, K.; Tomsia, A.P., *Preparation of porous hydroxyapatite scaffolds.* Materials Science and Engineering: C, 2007. **27**(3): p. 546-550.
85. Oh, S.; Oh, N.; Appleford, M.; Ong, J.L., *Bioceramics for Tissue Engineering Applications–A Review.* American journal of biochemistry & biotechnology, 2006. **2**(2): p. 49.
86. Paschalis, E. P., Wikiel, K. and Nancollas, G. H., *Dual constant composition kinetics characterization of apatitic surfaces.* Journal of Biomedical Materials Research, 1994. **28**(12): p. 1411-1418.
87. Mobasherpour, I.; Heshajin, M. Soulati; Kazemzadeh, A.; Zakeri, M., *Synthesis of nanocrystalline hydroxyapatite by using precipitation method.* Journal of Alloys and Compounds, 2007. **430**(1-2): p. 330-333.
88. Boskey, A. L.; Posner, A. S., *Formation of hydroxyapatite at low supersaturation.* The Journal of Physical Chemistry, 1976. **80**(1): p. 40-45.
89. Gomes, J.F.; Granadeiro, C.C.; Silva, M.A.; Hoyos, M.; Silva, R.; Vieira, T., *An Investigation of the Synthesis Parameters of the Reaction of Hydroxyapatite Precipitation in Aqueous Media.* International Journal of Chemical Reactor Engineering, 2008. **6**(A103).
90. Koutsoukos, P.; Amjad, Z.; Tomson, M. B.; Nancollas, G. H., *Crystallization of calcium phosphates. A constant composition study.* Journal of the American Chemical Society, 1980. **102**(5): p. 1553-1557.
91. Verne, E.; Bosetti, M.; Brovarone, C.V.; Moisescu, C.; Lupo, F.; Spriano, S.; Cannas, M., *Fluoroapatite glass-ceramic coatings on alumina: structural, mechanical and biological characterization.* Biomaterials, 2002. **23**: p. 3395-3403.
92. Desai, S.; Bidanda, B.; Bártolo, P., *Metallic and Ceramic Biomaterials: Current and Future Developments*. 2008. p. 1-14.
93. Lee, S.-H.; Kim, H.-W.; Lee, E.-J.; Li, L.-H.; Kim, H.-E., *Hydroxyapatite-TiO2 Hybrid Coating on Ti Implants.* J Biomater Appl, 2006. **20**(3): p. 195-208.
94. Chien, C.S.; Liao, T.Y.; Hong, T.F.; Kuo, T.Y.; Wu, J.L., Cheng, Y.T., *Effects of coating fluoroapatite on Ti-6Al-4V by Nd-YAG laser cladding.*
95. Wang, D.G.; Chen, C.Z.; Ma, J.; Zhang, G., *In situ synthesis of hydroxyapatite coating by laser cladding.* Colloids and Surfaces B: Biointerfaces, 2008. **66**(2): p. 155-162.

96. Yang, Y.; Kim, K.-H.; Ong, J.L., *A review on calcium phosphate coatings produced using a sputtering process--an alternative to plasma spraying.* Biomaterials, 2005. **26**(3): p. 327-337.
97. Tsui, Y. C.; Doyle, C.; Clyne, T. W., *Plasma sprayed hydroxyapatite coatings on titanium substrates Part 1: Mechanical properties and residual stress levels.* Biomaterials, 1998. **19**(22): p. 2015-2029.
98. Klein, C.P.A.T.; De Blieck-Hogervorst, J.M.A.; Wolke, J.G.C.; De Groot, K. *A study of solubility and surface features of different calcium phosphate coatings in vitro and in vivo: A pilot study*. in *Ceramics in Substitutive and Reconstructive Surgery 7th Int.Meeting on Modern Ceramics Technologies (7th CIMTEC - World Ceramics Congress)*. 1991. Montecatini Terme.
99. Wang, J.; Chao, Y.; Wan, Q.; Zhu, Z.; Yu, H., *Fluoridated hydroxyapatite coatings on titanium obtained by electrochemical deposition.* Acta Biomaterialia, 2009. **5**(5): p. 1798-1807.
100. Wu, W.; Nancollas, G.H., *Kinetics of nucleation and crystal growth of hydroxyapatite and fluorapatite on titanium oxide surfaces.* Colloids and Surfaces B: Biointerfaces, 1997. **10**(2): p. 87-94.
101. Le Guéhennec, L.; Soueidan, A.; Layrolle, P.; Amouriq, Y., *Surface treatments of titanium dental implants for rapid osseointegration.* Dental Materials, 2007. **23**(7): p. 844-854.
102. Kuroda, K.; Ichino, R.; Okido, M.; Takai, O., *Hydroxyapatite coating on titanium by thermal substrate method in aqueous solution.* Journal of Biomedical Materials Research, 2002. **59**(2): p. 390-397.
103. American Public Health, Association, *Standard methods for the examination of water and wastewater / prepared and published jointly by the American Public Health Association, American Water Works Association, Water Pollution Control Federation ; joint editorial board, Michael J. Taras, Arnold E. Greenberg, R.D. Hoak*, ed. Arnold E. Greenberg, et al. 1971, Washington, D.C. :: American Public Health Association.
104. Gomez, M. A., Assaaoudi, H., Becze, L., Cutler, J. N. and Demopoulos, G. P., *Vibrational spectroscopy study of hydrothermally produced scorodite (FeAsO4·2H2O), ferric arsenate sub-hydrate (FAsH; FeAsO4·0.75H2O) and basic ferric arsenate sulfate (BFAS; Fe[(AsO4)1−x(SO4)x(OH)x]·wH2O).* Journal of Raman Spectroscopy, 2010. **41**(2): p. 212-221.
105. Bluteau, M.-C., Becze, L. and Demopoulos, G. P., *The dissolution of scorodite in gypsum-saturated waters: Evidence of Ca-Fe-AsO4 mineral formation and its impact on arsenic retention.* Hydrometallurgy, 2009. **97**(3-4): p. 221-227.
106. Ishikawa, K., Ducheyne, P. and Radin, S., *Determination of the Ca/P ratio in calcium-deficient hydroxyapatite using X-ray diffraction analysis.* Journal of Materials Science: Materials in Medicine, 1993. **4**(2): p. 165-168.
107. Antonakos, A.; Liarokapis, E.; Leventouri, T., *Micro-Raman and FTIR studies of synthetic and natural apatites.* Biomaterials, 2007. **28**(19): p. 3043-3054.
108. Arends, J.; Christoffersen, J.; Christoffersen, M. R.; Eckert, H.; Fowler, B. O.; Heughebaert, J. C.; Nancollas, G. H.; Yesinowski, J. P.; Zawacki, S. J., *A calcium hydroxyapatite precipitated from an aqueous solution : An international multimethod analysis.* Journal of Crystal Growth, 1987. **84**(3): p. 515-532.

Appendix A. OLI Software Calculations

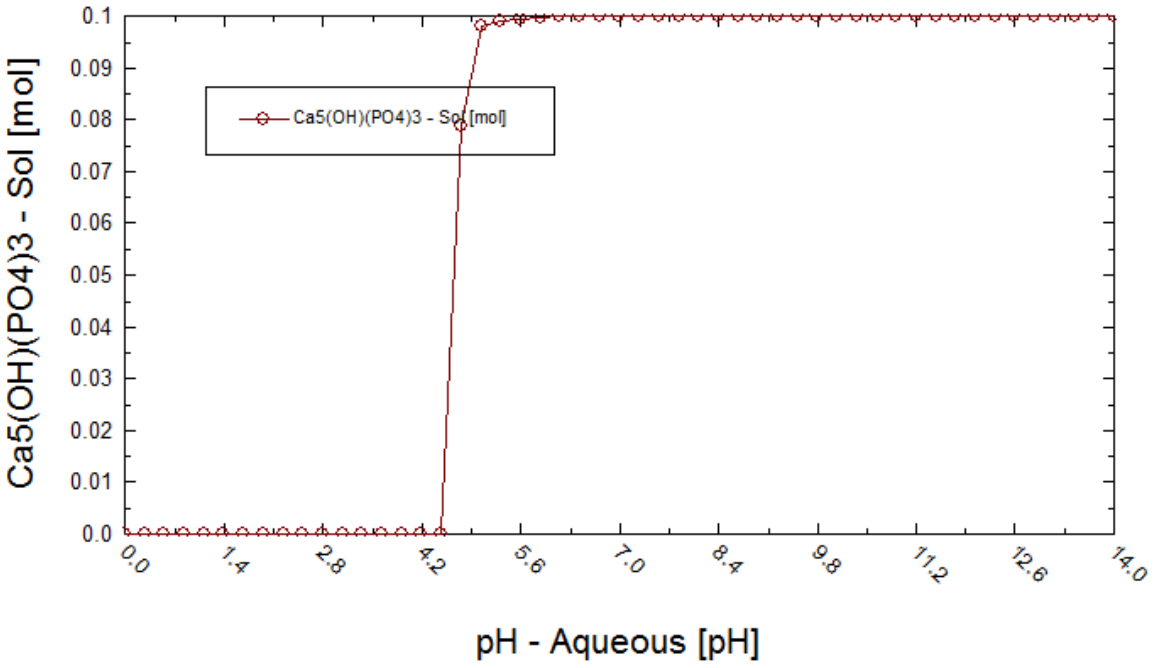

Figure A- 1: Solubility of 0.1 mol of hydroxyapatite in 1 L of water.

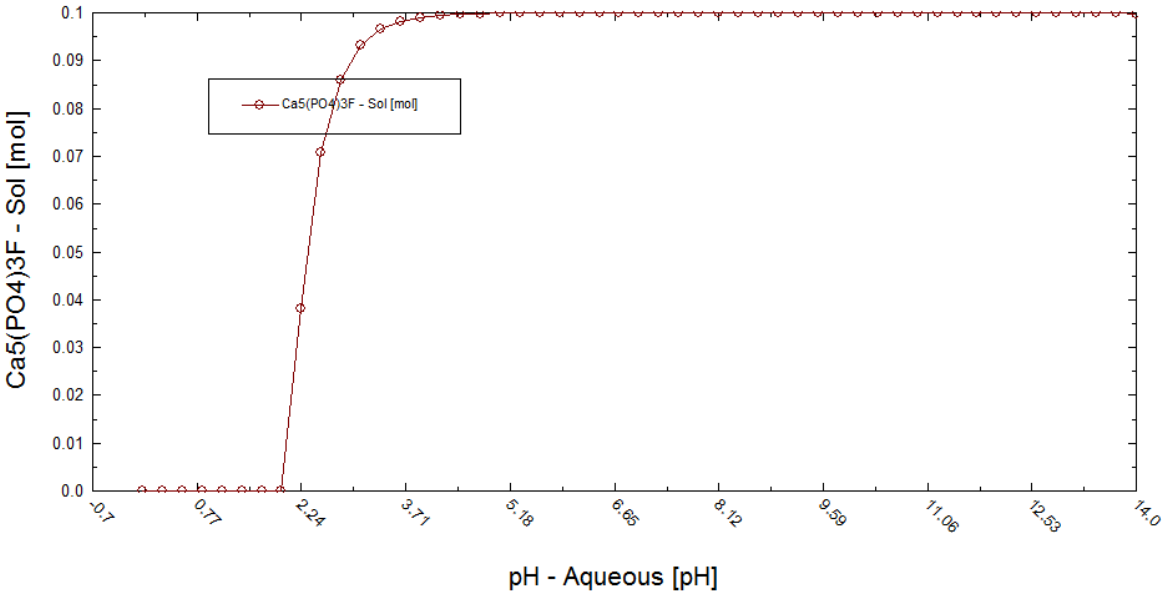

Figure A- 2: Solubility of 0.1 mol of fluoroapatite in 1 L of water.

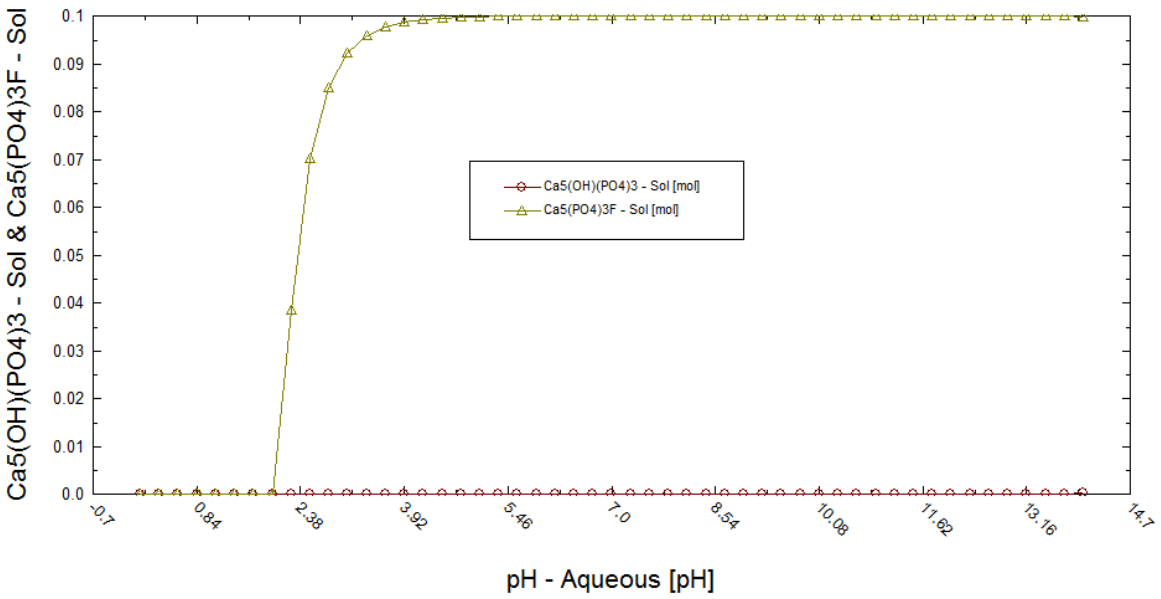

Figure A- 3: Amount of solids in solution following the introduction of hydroxyapatite in a solution containing the stoichiometric amount of fluoride ions.

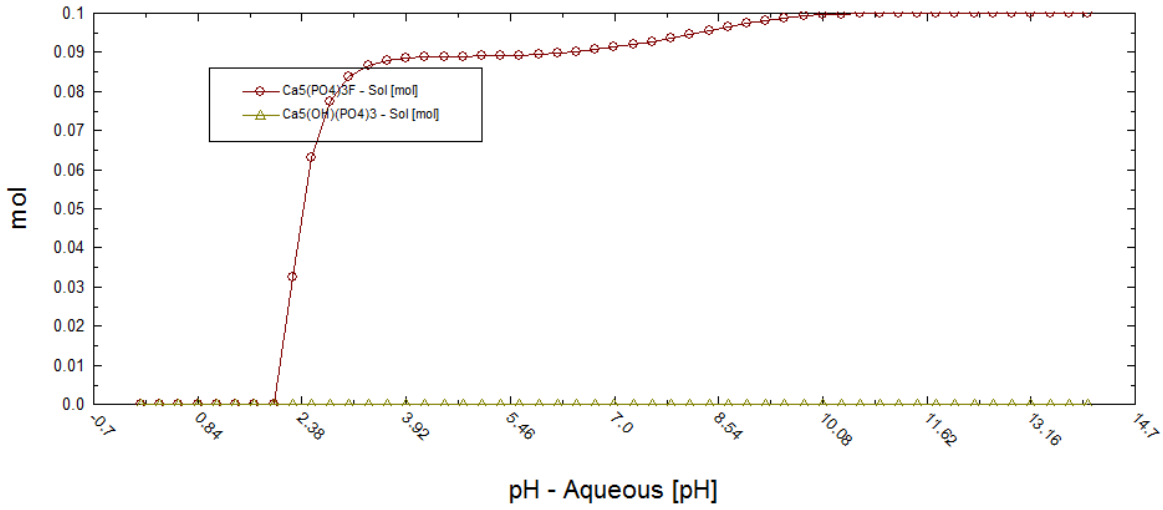

Figure A- 4: Amount of solids in solution following the introduction of hydroxyapatite in a solution containing twice the stoichiometric amount of fluoride ion.

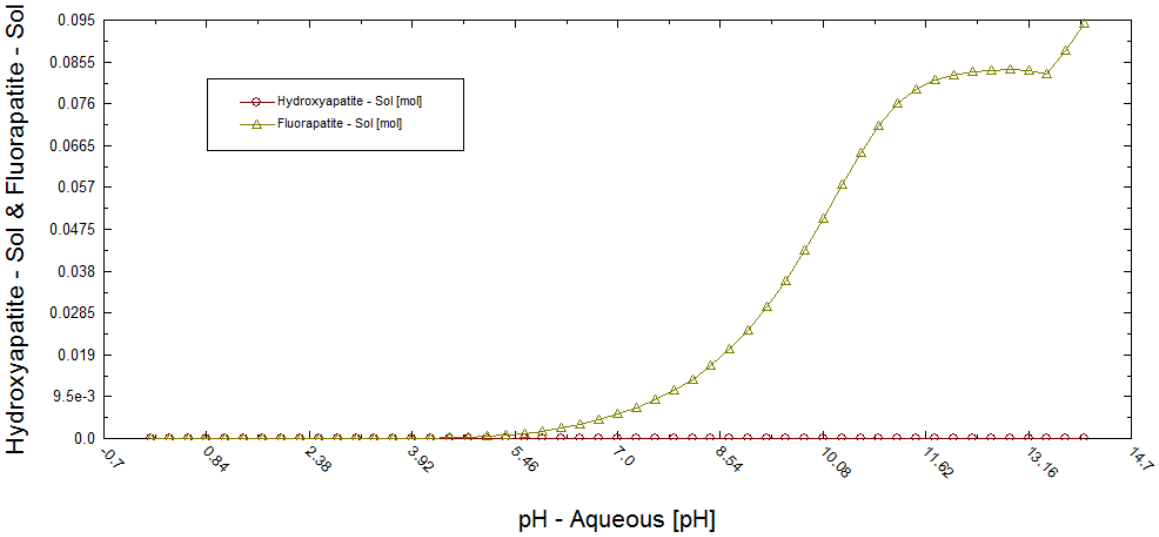

Figure A- 5: Amount of solids in solution following the introduction of hydroxyapatite in a solution containing 10 times the stoichiometric amount of fluoride ions.

Appendix B. TGA curves

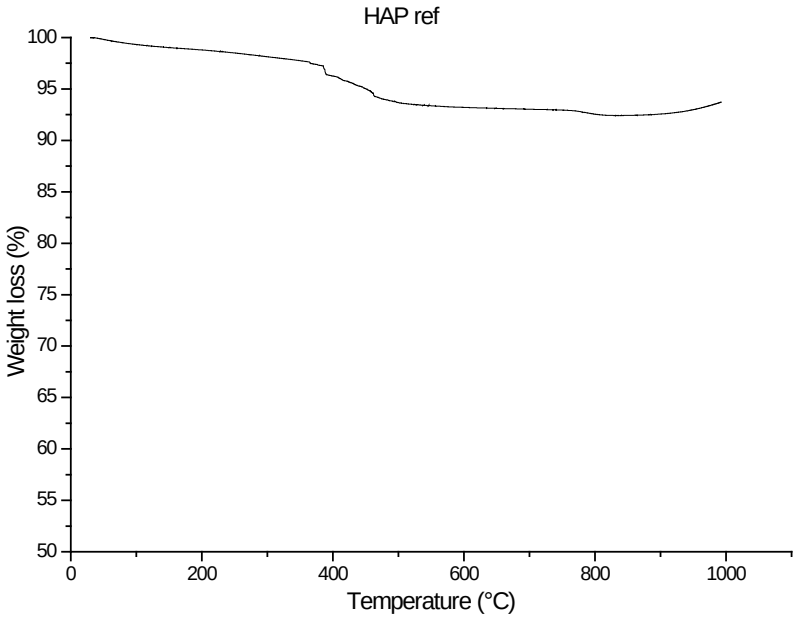

Figure B - 1: TGA curve for reference hydroxyapatite powder showing a 7.25 % weight loss.

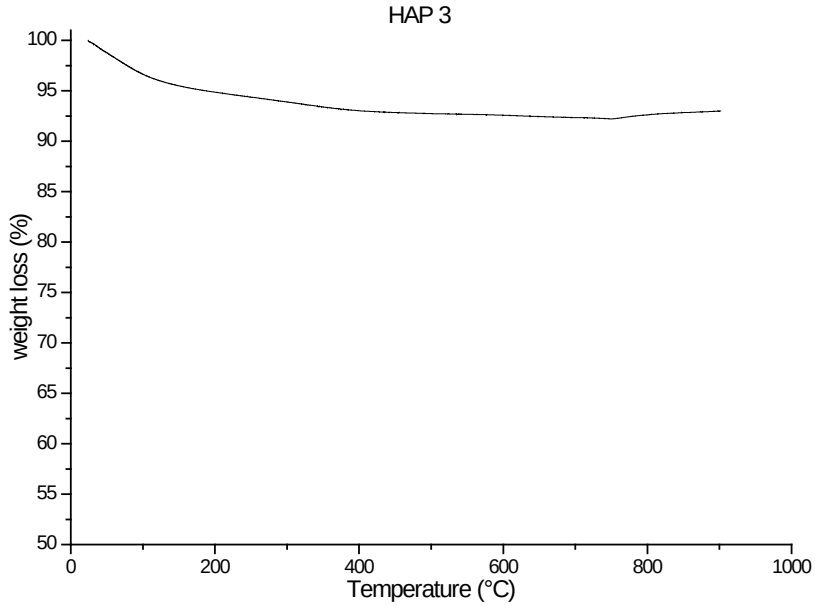

Figure B - 2: TGA curve for HAP 3 powder showing a 8 % weight loss.

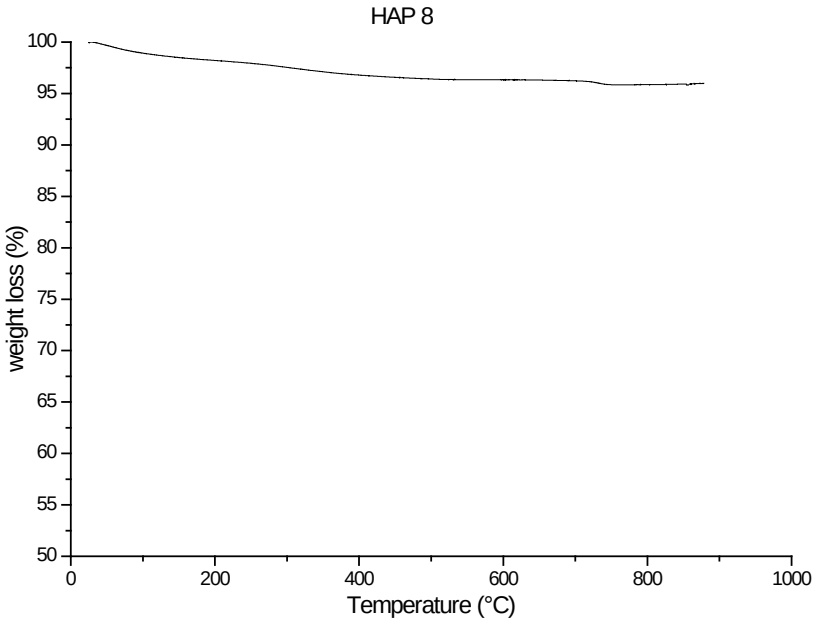

Figure B - 3: TGA curve for HAP 8 powder showing a 4 % weight loss.

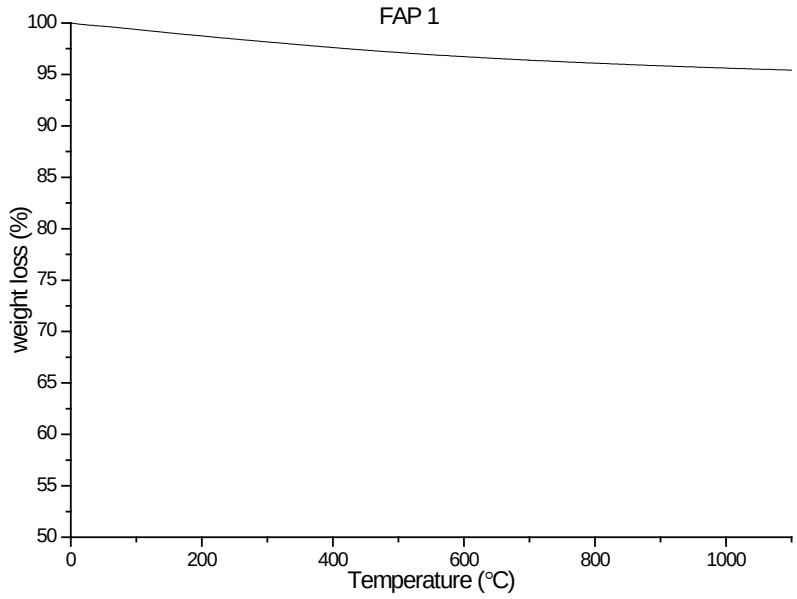

Figure B - 4: TGA curve for FAP 1 powder showing a 4.5 % weight loss.

Appendix C. Encapsulation data tables

Table C - 1: Summary of the encapsulation experiments that were conducted.

Experiment	Scorodite	Conditioning step	Nucleation step							Growth step	Nancollas step
				concentration (mmol/L)			pH	RPM	°C		
				P	Ca	F					
ENCH 1	unknown, 10 g/L wet	-	-							5x20mL/h	-
ENCH 2	SCOR 5, 5 g/L wet	-	-							5x20mL/h	-
ENCH 3	SCOR 5, 5 g/L wet	pH 7.6	1x6mL/h							3x20mL/h	-
ENCH 4	SCOR 5, 5 g/L wet	pH 7.6	5xmet	0.9	1.5	-	7.6	850	22	-	-
ENCH 5	SCOR 5, 5 g/L wet	pH 7.6	2xmet	0.9	1.5	-	7.6	850	22	-	-
ENCH 6	SCOR 5, 5 g/L wet	pH 7.6	1xmet	0.9	1.5	-	7.6	850	40	-	-
ENCH 7	SCOR 5, 5 g/L wet	pH 7.6	1xmet	0.9	1.5	-	7.6	350	22	-	-
ENCH 8	SCOR 5, 5 g/L wet	pH 7.6	1xmet	0.9	1.5	-	7.6	350	40	-	-
ENCH 10	SCOR 5, 5 g/L wet	pH 7.6	9xmet	2	3.34	-	7	500	22	1x20mL/h	-
ENCH 11	SCOR 5, 5 g/L wet	pH 7.6	9xmet	2	3.34	-	7	500	22	1x20mL/h	2
ENCH 12	SCOR 5, 5 g/L wet	pH 7.6	-			-				-	2
ENCH 13	SCOR 5, 15 g/L wet	6 M Ca, pH 6.0, 22 °C	-			-					2
ENCF 1	SCOR 1, 5 g/L wet	pH 6.0	2xmet	2	3.4	0.72	7	900	22	-	-
ENCF 2	SCOR 1, 5 g/L wet	pH 6.0	1xmet	2	3.4	0.72	7	900	22	-	-
ENCF 3	SCOR 1, 50 g/L wet	0.01 M Ca, pH 6.8, 22 °C	-							-	2
ENCF 4	SCOR 1,	-	-							-	1

For all experiments Ca:P=1.67

For all growth steps, concentrations were: 60 mmol/L P and 100 mmol/L Ca.

All Nancollas steps were 2x500 mL of feed solutions at: pH 7.4, T 37 °C, 500 RPM, 10.8 mmol/L P, 18 mmol/L NaOH, 18 mmol/L Ca, 270 mmol/L NaCl and 3.5 mmol/L F where applicable

Appendix D. Stability testing data

Table D - 1: Oxic test results for naked scorodite.

Flask No	Sample N°	C_{As} (ppm) ICP	C_{As} (ppm)	C_{As} (mmol/L)	C_{Fe} (ppm) ICP	C_{Fe} (ppm)	C_{Fe} (mmol/L)	Notes	Days	*pH*	*pH adjustment*
LTS1	S1	2.407	8.02253	0.10711	0.0051	0.017	0.0003	Scorodite pH 7	1	6.106	7.2
	S10	1.948	6.49268	0.08668	0.0014	0.00467	8.4E-05		3	7.415	7.2
	S19	1.856	6.18605	0.08259	0.0022	0.00733	0.00013		6	6.275	6.8
	S28	1.983	6.60934	0.08824	0.0012	0.004	7.2E-05		11	6.53	6.9
	S37	1.944	6.47935	0.08651	0.0164	0.05467	0.00098		21	6.34	7.0
	S46	2.037	6.78932	0.09065	0.0112	0.03733	0.00067		41	6.621	7.0
	S55	2.852	9.50572	0.12691	0.583	1.94331	0.0348		77	6.357	7.0
LTS2	S2	1.661	5.53611	0.07391	0.0022	0.00733	0.00013	Scorodite pH 8	1	6.84	8.0
	S11	2.914	9.71236	0.12967	0.0002	0.00067	1.2E-05		3	8.168	no
	S20	3.088	10.2923	0.13741	0.0009	0.003	5.4E-05		6	7.083	8.1
	S29	3.734	12.4454	0.16616	0.0042	0.014	0.00025		11	7.023	7.9
	S38	4.217	14.0553	0.18765	0.0026	0.00867	0.00016		21	7.077	8.1
	S47	4.479	14.9285	0.19931	0.0053	0.01767	0.00032		41	7.419	8.2
	S56	6.119	20.3946	0.27229	0.004	0.01333	0.00024		77	6.787	8.1
LTS3	S3	2.685	8.94911	0.11948	0.0035	0.01167	0.00021	Scorodite pH 9	1	7.25	9.0
	S12	4.507	15.0218	0.20056	0.0007	0.00233	4.2E-05		3	8.467	8.9
	S21	4.795	15.9817	0.21337	0.001	0.00333	6E-05		5	7.275	8.8
	S30	5.684	18.9448	0.25293	0.002	0.00667	0.00012		11	7.51	8.9
	S39	6.165	20.5479	0.27434	0.0009	0.003	5.4E-05		21	7.414	9.2
	S48	6.517	21.7212	0.29	0.0004	0.00133	2.4E-05		41	7.844	9.2
	S57	8.719	29.0604	0.38799	0.0017	0.00567	0.0001		77	7.447	9.2

Table D - 2: Oxic test results for ENCH 10.

Flask No	Sample N°	C_{As} (ppm)	C_{As} (ppm)	C_{As} (mmol/L)	C_{Fe} (ppm)	C_{Fe} (ppm)	C_{Fe} (mmol/L)	C_{Ca} (ppm)	C_{Ca} (mg/L)	C_{Ca} (mmol/L)	C_{P} (ppm)	C_{P} (mg/L)	C_{P} (mmol/L)	Notes	Days	*pH*	*pH adjustment*	*Ca:P ratio*
		ICP			ICP			ICP	Orig. sol. (dilution. f. 3.33)		ICP	Orig. sol. (dilution. f. 3.33)						
LTS4	S4	0.7203	2.40076	0.03205	0.0014	0.00467	8.4E-05	8.01	26.6973	0.66743	1.976	6.58601	0.21266	ENCH 10 pH 7	1.5	6.25	7.1	3.13853
	S13	0.4383	1.46085	0.0195	0.0003	0.001	1.8E-05	7.353	24.5075	0.61269	0.6214	2.07113	0.06688		3	7.75	7.2	9.16167
	S22	0.8328	2.77572	0.03706	0.0005	0.00167	3E-05	13.47	44.8955	1.12239	1.954	6.51268	0.21029		5	6.282	7.1	5.33733
	S31	0.6437	2.14545	0.02864	0.0012	0.004	7.2E-05	13.7	45.6621	1.14155	0.8033	2.6774	0.08645		10	6.521	6.9	13.2046
	S40	0.7115	2.37143	0.03166	0.0007	0.00233	4.2E-05	13.81	46.0287	1.15072	0.6251	2.08346	0.06727		22	6.617	7.0	17.1051
	S49	0.8503	2.83405	0.03784	0.0003	0.001	1.8E-05	14.19	47.2953	1.18238	0.6214	2.07113	0.06688		40	6.9	no	17.6804
	S58	2.045	6.81599	0.091	0.0008	0.00267	4.8E-05	27.3	90.9909	2.27477	1.494	4.9795	0.16078		77	6.251	7.1	14.1479
LTS5	S5	0.74	2.46642	0.03293	0.001	0.00333	6E-05	1.867	6.22271	0.15557	1.549	5.16282	0.1667	ENCH 10 pH 8	1.5	7.012	8.0	0.9332
	S14	0.6075	2.0248	0.02703	0.0006	0.002	3.6E-05	1.285	4.28291	0.10707	0.7457	2.48542	0.08025		3	8.304	7.9	1.3342
	S23	0.6081	2.0268	0.02706	0.002	0.00667	0.00012	4.03	13.432	0.3358	0.7113	2.37076	0.07655		5	6.86	7.8	4.38665
	S32	0.5556	1.85181	0.02472	0	0	0	3.67	12.2321	0.3058	0.3222	1.07389	0.03468		10	7.21	7.9	8.81905
	S41	0.8058	2.68573	0.03586	0.0021	0.007	0.00013	4.44	14.7985	0.36996	0.3901	1.3002	0.04198		22	7.043	8.0	8.81228
	S50	0.867	2.88971	0.03858	0.0016	0.00533	9.5E-05	4.671	15.5684	0.38921	0.2038	0.67927	0.02193		40	7.583	7.9	17.7454
	S59	1.411	4.70286	0.06279	0.0005	0.00167	3E-05	5.916	19.718	0.49295	0.3392	1.13055	0.0365		77	6.744	7.9	13.5037
LTS6	S6	0.0083	0.02766	0.00037	0.0058	0.01933	0.00035	7.207	24.0209	0.60052	0.0799	0.26631	0.0086	ENCH 10 pH 9	1.5	7.44	8.9	69.8375
	S15	0.044	0.14665	0.00196	0.0019	0.00633	0.00011	7.706	25.6841	0.6421	0.0495	0.16498	0.00533		3	8.708	9.0	120.533
	S24	0.0729	0.24298	0.00324	0.0016	0.00533	9.5E-05	8.23	27.4306	0.68576	0.0536	0.17865	0.00577		5	7.536	8.9	118.882
	S33	0.0712	0.23731	0.00317	0.0024	0.008	0.00014	22.8	75.9924	1.89981	0.0844	0.28131	0.00908		10	7.454	8.9	209.158
	S42	0.2673	0.89091	0.01189	0.0011	0.00367	6.6E-05	23.97	79.892	1.9973	0.0553	0.18431	0.00595		22	7.397	9.2	335.602
	S51	0.3227	1.07556	0.01436	0.0016	0.00533	9.5E-05	24.53	81.7585	2.04396	0.0664	0.22131	0.00715		40	7.716	9.0	286.029
	S60	1.166	3.88628	0.05189	0.0001	0.00033	6E-06	35.07	116.888	2.92221	0.0652	0.21731	0.00702		77	7.062	9.2	416.456

Table D - 3: Oxic test results for ENCH 10 in gypsum saturated water.

Flask No	Sample N°	C_{As} (ppm) ICP	C_{As} (ppm)	C_{As} (mmol/L)	C_{Fe} (ppm) ICP	C_{Fe} (ppm)	C_{Fe} (mmol/L)	C_{Ca} (ppm) ICP	C_{Ca} (mg/L) Orig. sol. (dilution f. 3.33)	C_{Ca} (mmol/L)	C_{P} (ppm) ICP	C_{P} (mg/L) Orig. sol. (dilution f. 3.33)	C_{P} (mmol/L)	Notes	Days	*pH*	*pH adjustment*	*Ca:P ratio*
LTS7	S7	0.4404	1.46785	0.0196	0.0001	0.00033	6E-06	137	456.621	11.4155	0.3043	1.01423	0.03275	ENCH 10 pH 7 g	1.5	6.309	7.2	348.578
	S16	0.2789	0.92957	0.01241	0.0025	0.00833	0.00015	137	456.621	11.4155	0.0913	0.3043	0.00983		3	7.616	7.0	1161.8
	S25	0.6092	2.03046	0.02711	0.0028	0.00933	0.00017	137	456.621	11.4155	0.618	2.05979	0.06651		5	6.25	7.0	171.638
	S34	0.6602	2.20045	0.02938	0.0008	0.00267	4.8E-05	137	456.621	11.4155	0.7073	2.35743	0.07612		10	6.094	7.0	149.968
	S43	0.5178	1.72583	0.02304	0.0039	0.013	0.00023	137	456.621	11.4155	0.2828	0.94257	0.03044		22	6.351	7.0	375.079
	S52	0.4468	1.48918	0.01988	0.0003	0.001	1.8E-05	137	456.621	11.4155	0.1138	0.3793	0.01225		40	6.444	7.0	932.094
	S61	0.5648	1.88248	0.02513	0.0001	0.00033	6E-06	226	753.258	18.8315	0.146	0.48662	0.01571		77	6.175	7.2	1198.5
LTS8	S8	0.238	0.79325	0.01059	0.0021	0.007	0.00013	137	456.621	11.4155	0.0001	0.00033	1.1E-05	ENCH 10 pH 8 g	1.5	6.445	8.2	1060723
	S17	0.0645	0.21498	0.00287	0.0003	0.001	1.8E-05	137	456.621	11.4155	0.0755	0.25164	0.00813		3	8.103	no	1404.93
	S26	0.1412	0.47062	0.00628	0.0027	0.009	0.00016	137	456.621	11.4155	0.054	0.17998	0.00581		5	7.006	7.8	1964.3
	S35	0.1482	0.49395	0.00659	0.002	0.00667	0.00012	137	456.621	11.4155	0.0065	0.02166	0.0007		10	7.259	8.0	16318.8
	S44	0.2265	0.75492	0.01008	0.0011	0.00367	6.6E-05	137	456.621	11.4155	0.043	0.14332	0.00463		22	7.222	8.0	2466.8
	S53	0.3113	1.03756	0.01385	0.0009	0.003	5.4E-05	137	456.621	11.4155	0.0647	0.21565	0.00696		40	7.208	8.1	1639.45
	S62	0.5477	1.82548	0.02437	0.0002	0.00067	1.2E-05	198	659.934	16.4984	0.0667	0.22231	0.00718		77	6.659	7.9	2298.37
LTS9	S9	0.0322	0.10732	0.00143	0.0007	0.00233	4.2E-05	137	456.621	11.4155	0.0803	0.26764	0.00864	ENCH 10 pH 9 g	1.5	7.055	9.2	1320.95
	S18	0.0321	0.10699	0.00143	0.0006	0.002	3.6E-05	137	456.621	11.4155	0.0666	0.22198	0.00717		3	8.633	8.8	1592.68
	S27	0.0523	0.17432	0.00233	0.0007	0.00233	4.2E-05	137	456.621	11.4155	0.0768	0.25597	0.00827		5	7.526	9.1	1381.15
	S36	0.0735	0.24498	0.00327	0.0015	0.005	9E-05	137	456.621	11.4155	0.0521	0.17365	0.00561		10	7.602	9.0	2035.94
	S45	0.1747	0.58228	0.00777	0.0038	0.01267	0.00023	137	456.621	11.4155	0.0611	0.20365	0.00658		22	7.392	9.0	1736.04
	S54	0.246	0.81992	0.01095	0.0001	0.00033	6E-06	137	456.621	11.4155	0.0183	0.06099	0.00197		40	7.434	9.0	5796.3
	S63	0.5379	1.79282	0.02394	0.0009	0.003	5.4E-05	201	669.933	16.7483	0.0418	0.13932	0.0045		77	6.949	9.1	3723.07

Table D - 4: Anoxic test results for naked scorodite.

Flask No	Sample N°	C_{As} (ppm) ICP	C_{As} (ppm)	C_{As} (mmol/L)	C_{Fe} (ppm) ICP	C_{Fe} (ppm)	C_{Fe} (mmol/L)	Notes	Days	e_h	e_h adjustment	pH	pH adjustment
LTS 10	S70	10.05	33.497	0.44722	0.0625	0.2083	0.00373	Scorodite pH 7 150 mV	1	190.1	yes	7.215	no
	S81	21.7	72.326	0.96564	0.2951	0.9837	0.01761		3	177.4	yes	7.209	no
	S92	27.27	90.891	1.2135	0.4235	1.4117	0.02528		5	177.1	no	7.168	no
	S103	33.36	111.19	1.4845	0.6987	2.329	0.0417		10	175.4	no	7.157	no
	S114	31.02	103.39	1.38037	0.7223	2.4076	0.04311		20	174.8	no	7.149	no
	S125	35.6	118.65	1.58418	0.8021	2.6736	0.04787		30	176.3	no	7.203	no
	S136	43.98	146.59	1.95708	0.8738	2.9126	0.05215		40	157.9	no	7.116	no
LTS 11	S71	20.02	66.727	0.89088	0.1971	0.657	0.01176	Scorodite pH 8 150 mV	1	171.5	no	7.97	no
	S82	33.4	111.32	1.48628	0.197	0.6567	0.01176		3	171.4	no	7.963	no
	S93	33.75	112.49	1.50185	0.2215	0.7383	0.01322		5	176	no	7.901	no
	S104	46.71	155.68	2.07856	0.4992	1.664	0.02979		10	167.1	no	7.896	no
	S115	43.37	144.55	1.92994	0.6707	2.2356	0.04003		20	164.1	no	7.865	no
	S126	44.46	148.19	1.97844	0.8356	2.7853	0.04987		30	165.2	no	7.901	no
	S137	50.8	169.32	2.26057	1.059	3.53	0.0632		40	146.4	no	7.84	no
LTS 12	S72	37.08	123.59	1.65004	0.0076	0.0253	0.00045	Scorodite pH 9 150 mV	1	169.3	no	8.493	8.86
	S83	48.14	160.45	2.1422	0.0516	0.172	0.00308		3	164.5	no	8.523	9
	S94	47.18	157.25	2.09948	0.0624	0.208	0.00372		5	167	no	8.769	8.95
	S105	56.47	188.21	2.51288	0.1161	0.387	0.00693		10	164.5	no	8.718	no
	S116	69.03	230.08	3.07179	0.232	0.7733	0.01385		20	163.2	no	8.563	no
	S127	8.961	298.7	3.98794	0.294	0.98	0.01755		30	160.1	no	8.564	8.8
	S138	7.848	261.6	3.49262	0.3737	1.2457	0.0223		40	140.6	no	8.658	no

Table D - 5: Anoxic test results for ENCH 10 in gypsum saturated water.

Flask No	Sample N°	C_{As} (ppm) ICP	C_{As} (ppm)	C_{As} (mmol/L)	C_{Fe} (ppm) ICP	C_{Fe} (ppm)	C_{Fe} (mmol/L)	C_{Ca} (ppm) ICP	C_{Ca} (mg/L) Orig. sol. (dilution f. 3.33)	C_{Ca} (mmol/L)	C_P (ppm) ICP	C_P (mg/L) Orig. sol. (dilution f. 3.33)	C_P (mmol/L)	Notes	Days	e_h	e_h adjustment	pH	pH adjustment	Ca:P ratio
LTS 13	S73	3.266	10.886	0.14533	0.0014	0.0047	8.4E-05	5.131	17.1016	0.42754	42.23	140.753	4.5448	ENCH 10 pH 7 150 mV g	1	185.1	yes	7.398	7.1	0.0941
	S84	5.194	17.312	0.23113	0.0046	0.0153	0.00027	5.418	18.0582	0.45145	60.26	200.847	6.4852		3	178.3	yes	7.369	7.2	0.0696
	S95	6.319	21.061	0.28119	0.0082	0.0273	0.00049	5.608	18.6915	0.46729	65.93	219.745	7.0954		5	181.3	yes	7.144	no	0.0659
	S106	8.59	28.63	0.38225	0.0153	0.051	0.00091	6.113	20.3746	0.50937	75.69	252.275	8.14578		10	179.3	yes	7.125	no	0.0625
	S117	11.8	39.329	0.52509	0.0314	0.1047	0.00187	6.333	21.1079	0.5277	74.87	249.542	8.05753		20	180.9	no	7.109	no	0.0655
	S128	13.52	45.062	0.60163	0.0336	0.112	0.00201	6.669	22.2278	0.55569	66.45	221.478	7.15137		30	186.3	no	7.033	no	0.0777
	S139	15.54	51.795	0.69152	0.0182	0.0607	0.00109	12.28	40.9292	1.02323	70.43	234.743	7.5797		40	172.1	no	6.828	no	0.135
LTS 14	S74	3.16	10.532	0.14062	0.0016	0.0053	9.5E-05	4.476	14.9185	0.37296	28.09	93.624	3.02305	ENCH 10 pH 8 150 mV g	1	176.8	no	8.107	no	0.1234
	S85	5.599	18.661	0.24915	0.0021	0.007	0.00013	4.951	16.5017	0.41254	35.53	118.421	3.82375		3	176.1	no	8.053	no	0.1079
	S96	6.405	21.348	0.28502	0.0006	0.002	3.6E-05	4.79	15.9651	0.39913	32.23	107.423	3.4686		5	176.2	yes	7.973	no	0.1151
	S107	9.2	30.664	0.40939	0.022	0.0733	0.00131	5.026	16.7517	0.41879	33.55	111.822	3.61066		10	173.2	no	7.997	no	0.116
	S118	13.28	44.262	0.59095	0.004	0.0133	0.00024	5.901	19.668	0.4917	38.11	127.021	4.10141		20	173.3	no	7.919	no	0.1199
	S129	15.13	50.428	0.67327	0.0051	0.017	0.0003	6.675	22.2478	0.55619	34.83	116.088	3.74841		30	175.8	no	7.839	no	0.1484
	S140	17.78	59.261	0.7912	0.0016	0.0053	9.5E-05	10.07	33.5633	0.83908	36.22	120.721	3.89801		40	162.6	no	7.759	no	0.2153
LTS 15	S75	6.908	23.024	0.3074	0.0004	0.0013	2.4E-05	4.528	15.0918	0.3773	38.07	126.887	4.0971	ENCH 10 pH 9 150 mV g	1	170.1	no	8.72	9	0.0921
	S86	12.156	40.516	0.54093	0.0023	0.0077	0.00014	4.649	15.4951	0.38738	37.39	124.621	4.02392		3	165.2	no	8.696	9	0.0963
	S97	15.81	52.695	0.70353	0.0005	0.0017	3E-05	4.935	16.4484	0.41121	26.47	88.2245	2.84871		5	167.9	no	8.949	no	0.1443
	S108	20.99	69.96	0.93404	0.0013	0.0043	7.8E-05	5.199	17.3283	0.43321	27.2	90.6576	2.92727		10	169.7	no	8.767	no	0.148
	S119	25.71	85.691	1.14408	0.0006	0.002	3.6E-05	6.986	23.2843	0.58211	24.75	82.4918	2.6636		20	172.3	no	8.532	no	0.2185
	S130	26.79	89.291	1.19214	0.0044	0.0147	0.00026	12.43	41.4292	1.03573	17.13	57.0943	1.84354		30	164.8	no	8.162	9	0.5618
	S141	22.06	73.526	0.98166	0.0015	0.005	9E-05	144.2	480.619	12.0155	4.628	15.4251	0.49807		40	198.7	no	7.733	no	24.124

Table D - 6: Anoxic test results for ENCH 10 and 11.

Flask No	Sample N°	C_{As} (ppm) ICP	C_{As} (ppm)	C_{As} (mmol/L)	C_{Fe} (ppm) ICP	C_{Fe} (ppm)	C_{Fe} (mmol/L)	C_{Ca} (ppm) ICP	C_{Ca} (mg/L) Orig. sol. (dilution f. 3.33)	C_{Ca} (mmol/L)	C_{P} (ppm) ICP	C_{P} (mg/L) Orig. sol. (dilution f. 3.33)	C_{P} (mmol/L)	Notes	Days	e_h	e_h *adjustment*	*pH*	*pH adjustment*	*Ca:P ratio*
LTS 16	S76	3.82	12.732	0.16999	0.001	0.0033	6E-05	5.453	18.1748	0.45437	30.5	101.657	3.28242	ENCH 10 pH 8 150 mV	1	175.1	no	8.106	no	0.1384
	S87	6.808	22.691	0.30295	0.0016	0.0053	9.5E-05	7.081	23.601	0.59002	37.65	125.487	4.0519		3	175.6	no	8.051	no	0.1456
	S98	7.909	26.361	0.35195	0.0009	0.003	5.4E-05	7.321	24.4009	0.61002	35.16	117.188	3.78393		5	176.6	yes	7.967	no	0.1612
	S109	11.49	38.296	0.5113	0.0012	0.004	7.2E-05	9.163	30.5403	0.76351	39.55	131.82	4.25638		10	177.3	yes	7.943	no	0.1794
	S120	18.1	60.327	0.80544	0.0045	0.015	0.00027	11.85	39.4961	0.9874	42.28	140.919	4.55019		20	179.5	no	7.886	no	0.217
	S131	19.12	63.727	0.85083	0.0052	0.0173	0.00031	12.13	40.4293	1.01073	33.15	110.489	3.56761		30	181.3	no	7.661	no	0.2833
	S142	20.44	68.127	0.90957	0.0013	0.0043	7.8E-05	28.64	95.4571	2.38643	30.87	102.89	3.32224		40	179.4	no	7.524	no	0.7183
LTS 17	S77	0.7951	2.6501	0.03538	0.0006	0.002	3.6E-05	5.771	19.2347	0.48087	20.7	68.9931	2.22774	ENCH 11 pH 8 150 mV	1	186	yes	8.039	no	0.2159
	S88	2.439	8.1292	0.10853	0.0022	0.0073	0.00013	7.66	25.5308	0.63827	23.09	76.959	2.48495		3	181.1	yes	8.019	no	0.2569
	S99	3.799	12.662	0.16905	0.0033	0.011	0.0002	8.772	29.2371	0.73093	23.99	79.9587	2.58181		5	164.8	no	8.014	no	0.2831
	S110	8.014	26.711	0.35662	0.0028	0.0093	0.00017	10.16	33.8633	0.84658	27.47	91.5575	2.95633		10	169.9	no	7.962	no	0.2864
	S121	16.91	56.361	0.75248	0.006	0.02	0.00036	13.53	45.0955	1.12739	30.23	100.757	3.25336		20	175.1	no	7.875	no	0.3465
	S132	19.64	65.46	0.87397	0.0091	0.0303	0.00054	11.46	38.1962	0.9549	23.53	78.4255	2.53231		30	175.3	no	7.796	no	0.3771
	S143	24.06	80.192	1.07065	0.0022	0.0073	0.00013	14.14	47.1286	1.17822	25.23	84.0916	2.71526		40	165	no	7.719	no	0.4339
LTS 18	S78	1.176	3.9196	0.05233	0.0015	0.005	9E-05	5.929	19.7614	0.49403	30.85	102.823	3.32009	ENCH 11 pH 8 150 mV	1	180.6	yes	8.046	no	0.1488
	S89	2.954	9.8457	0.13145	0.0012	0.004	7.2E-05	7.644	25.4775	0.63694	36.12	120.388	3.88724		3	176.1	no	7.99	no	0.1639
	S100	4.261	14.202	0.18961	0.0017	0.0057	0.0001	8.606	28.6838	0.71709	35.16	117.188	3.78393		5	169.2	no	7.957	no	0.1895
	S111	7.861	26.201	0.34981	0.003	0.01	0.00018	10.21	34.0299	0.85075	38.28	127.587	4.1197		10	171.6	no	7.903	no	0.2065
	S122	13.9	46.329	0.61854	0.0015	0.005	9E-05	12.93	43.0957	1.07739	40.45	134.82	4.35324		20	177	no	7.818	no	0.2475
	S133	18.22	60.727	0.81078	0.0052	0.0173	0.00031	12.86	42.8624	1.07156	37.12	123.721	3.99486		30	177.2	no	7.729	no	0.2682
	S144	23.64	78.792	1.05196	0.0037	0.0123	0.00022	16.2	53.9946	1.34987	36.79	122.621	3.95935		40	167.8	no	7.633	no	0.3409

Table D - 7: Results for oxic and anoxic tests for ENCH 1.

Flask No	Sample N°	C_{As} (ppm) ICP	C_{As} (ppm)	C_{As} (mmol/L)	C_{Fe} (ppm) ICP	C_{Fe} (ppm)	C_{Fe} (mmol/L)	C_{Ca} (ppm) ICP	C_{Ca} (mg/L) Orig. sol. (dilution f. 3.33)	C_{Ca} (mmol/L)	C_{P} (ppm) ICP	C_{P} (mg/L) Orig. sol. (dilution f. 3.33)	C_{P} (mmol/L)	Notes	Days	e_h	e_h adjustment	pH	pH adjustment	Ca:P ratio
LTS 19	S79	43.94	146.45	1.9553	0.0042	0.014	0.00025	9.92	33.0634	0.82658	59.42	198.047	6.3948	ENCH 1 pH 8 150 mV	1	185.4	yes	7.96	no	0.1293
	S90	60.99	203.28	2.71401	0.0076	0.0253	0.00045	7.595	25.3141	0.63285	65.93	219.745	7.0954		3	176.5	no	7.927	no	0.0892
	S101	64.93	216.41	2.88934	0.0058	0.0193	0.00035	7.099	23.661	0.59152	65.04	216.778	6.99962		5	174.9	yes	7.848	7.93	0.0845
	S112	81.05	270.14	3.60667	0.0136	0.0453	0.00081	6.468	21.5578	0.53895	59.79	199.28	6.43462		10	172.1	no	7.917	no	0.0838
	S123	84.86	282.84	3.77621	0.0322	0.1073	0.00192	6.468	21.5578	0.53895	59.25	197.48	6.3765		20	173.2	no	7.839	no	0.0845
	S134	12.27	409	5.46056	0.0452	0.1507	0.0027	6.899	22.9944	0.57486	60.9	202.98	6.55407		30	172.8	no	7.765	no	0.0877
	S145	12.71	423.66	5.65637	0.0422	0.1407	0.00252	8.051	26.834	0.67085	55.83	186.081	6.00844		40	157.3	no	7.705	no	0.1117
LTS 20	S80	0.7427	2.4754	0.03305	0.0002	0.0007	1.2E-05	8.703	29.0071	0.72518	0.096	0.31997	0.01033	ENCH 1 pH 8	1	-	-	7.331	8	70.191
	S91	0.8454	2.8177	0.03762	0.0002	0.0007	1.2E-05	8.026	26.7507	0.66877	0.0654	0.21798	0.00704		3	-	-	7.383	8.1	95.017
	S102	0.7739	2.5794	0.03444	0.0008	0.0027	4.8E-05	7.876	26.2507	0.65627	0.0505	0.16832	0.00543		5	-	-	7.405	8.1	120.75
	S113	0.4957	1.6522	0.02206	0.0009	0.003	5.4E-05	32.59	108.622	2.71556	0.0284	0.09466	0.00306		10	-	-	7.518	8	888.48
	S124	0.7759	2.5861	0.03453	0.0004	0.0013	2.4E-05	35.25	117.488	2.93721	0.0332	0.11066	0.00357		20	-	-	7.241	8.1	822.06
	S135	0.8916	2.9717	0.03968	0.0063	0.021	0.00038	32.48	108.256	2.7064	0.0387	0.12899	0.00416		30	-	-	7.529	8.1	649.81
	S146	1.174	3.9129	0.05224	0	0	0	35.23	117.422	2.93554	0.0564	0.18798	0.00607		40	-	-	7.547	no	483.63

Table D - 8: Anoxic test results for ENCH 13 and mixtures of naked scorodite and hydroxyapatite powders.

Flask No	Sample N°	C_{As} (ppm) ICP	C_{As} (ppm)	C_{As} (mmol/L)	C_{Fe} (ppm) ICP	C_{Fe} (ppm)	C_{Fe} (mmol/L)	C_{Ca} (ppm) ICP	C_{Ca} (mg/L) Orig. sol. (dilution f. 3.33)	C_{Ca} (mmol/L)	C_{P} (ppm) ICP	C_{P} (mg/L) Orig. sol. (dilution f. 3.33)	C_{P} (mmol/L)	Notes	Days	e_h	e_h adjustment	*pH*	pH adjustment	Ca:P ratio
LTS 21	S150	6.158	20.5246	0.27403	0.0059	0.01967	0.00035	8.527	28.4205	0.71051	8.872	29.5704	0.95481	ENCH 13 pH 8 150 mV	1	177.2	yes	8.137	no	0.74414
	S154	11.17	37.2296	0.49706	0.0191	0.06367	0.00114	9.746	32.4834	0.81209	9.383	31.2735	1.0098		3	170.5	no	7.965	no	0.8042
	S158	14.14	47.1286	0.62922	0.0306	0.102	0.00183	9.753	32.5067	0.81267	8.71	29.0304	0.93737		5	170.6	no	7.893	no	0.86696
	S162	17.82	59.3941	0.79298	0.0354	0.118	0.00211	10.85	36.1631	0.90408	8.759	29.1937	0.94265		10	168.5	no	7.735	no	0.95908
	S166	21.35	71.1596	0.95006	0.0459	0.153	0.00274	11.34	37.7962	0.94491	8.406	28.0172	0.90466		20	169.2	no	7.565	no	1.04449
	S170	23.02	76.7257	1.02437	0.0448	0.14933	0.00267	17.14	57.1276	1.42819	8.85	29.4971	0.95244		30	165.3	no	7.22	8.1	1.49951
	S174	16.81	56.0277	0.74803	0.0211	0.07033	0.00126	106.9	356.298	8.90744	4.338	14.4586	0.46686		40	304.3	no	6.745	no	19.0796
LTS 22	S151	5.592	18.6381	0.24884	0.0023	0.00767	0.00014	6.303	21.0079	0.5252	153.4	511.282	16.509	ENCH 13 pH 8 150 mV	1	175.2	yes	8.062	no	0.03181
	S155	11.86	39.5294	0.52776	0.004	0.01333	0.00024	7.212	24.0376	0.60094	147.8	492.617	15.9063		3	174	no	7.941	no	0.03778
	S159	16.22	54.0613	0.72178	0.0069	0.023	0.00041	7.584	25.2775	0.63194	153.9	512.949	16.5628		5	174.6	yes	7.87	no	0.03815
	S163	18.31	61.0272	0.81478	0.0109	0.03633	0.00065	7.183	23.9409	0.59852	141.5	471.62	15.2283		10	175.4	no	7.779	no	0.0393
	S167	22.48	74.9258	1.00034	0.0159	0.053	0.00095	6.906	23.0177	0.57544	126.8	422.624	13.6463		20	174.3	no	7.774	no	0.04217
	S171	25.98	86.5913	1.15609	0.0032	0.01067	0.00019	5.104	17.0116	0.42529	14.14	47.1286	1.52175		30	337.2	yes	6.117	7.8	0.27947
	S175	36.51	121.688	1.62467	0.015	0.05	0.0009	32.18	107.256	2.6814	150.1	500.283	16.1538		40	168.4	no	7.744	no	0.16599
LTS 23	S152	14.66	48.8618	0.65236	0.0024	0.008	0.00014	6.133	20.4413	0.51103	28.37	94.5572	3.05319	SCOR 5 + HAP 3 pH 8 150 mV	1	176	yes	7.946	no	0.16738
	S156	22.29	74.2926	0.99189	0.0059	0.01967	0.00035	7.883	26.274	0.65685	28.64	95.4571	3.08224		3	170.5	no	7.831	no	0.21311
	S160	25.3	84.3249	1.12583	0.0061	0.02033	0.00036	8.026	26.7507	0.66877	28.39	94.6239	3.05534		5	172	no	7.768	no	0.21888
	S164	32.58	108.589	1.44979	0.0139	0.04633	0.00083	10.58	35.2631	0.88158	31	103.323	3.33623		10	174.4	no	7.663	no	0.26424
	S168	36.79	122.621	1.63713	0.0151	0.05033	0.0009	10.41	34.6965	0.86741	26.32	87.7246	2.83257		20	165.2	no	7.653	no	0.30623
	S172	40.25	134.153	1.7911	0.017	0.05667	0.00101	12.37	41.2292	1.03073	27.67	92.2241	2.97785		30	168.7	no	7.455	yes	0.34613
	S176	45.39	151.285	2.01982	0.0175	0.05833	0.00104	16.32	54.3946	1.35986	24.69	82.2918	2.65714		40	181.3	no	7.552	no	0.51178
LTS 24	S153	16.39	54.6279	0.72934	0.0155	0.05167	0.00093	1.476	4.91951	0.12299	3.597	11.9888	0.38711	SCOR 5 + HAP ref pH 8 150 mV	1	177.2	yes	7.901	no	0.31771
	S157	24.02	80.0587	1.06887	0.0362	0.12067	0.00216	1.921	6.40269	0.16007	3.449	11.4955	0.37118		3	171.8	no	7.778	no	0.43124
	S161	30.18	100.59	1.34299	0.0452	0.15067	0.0027	2.593	8.64247	0.21606	3.704	12.3454	0.39863		5	175.8	no	7.69	no	0.54202
	S165	32.63	108.756	1.45201	0.0674	0.22466	0.00402	3.164	10.5456	0.26364	4.059	13.5286	0.43683		10	177.3	no	7.606	no	0.60353
	S173	33.55	111.822	1.49295	0.0761	0.25366	0.00454	3.281	10.9356	0.27339	3.641	12.1355	0.39185		20	169.4	no	7.59	no	0.6977
	S169	36.74	122.454	1.63491	0.0032	0.01067	0.00019	4.127	13.7553	0.34388	4.093	13.642	0.44049		30	170.5	no	7.375	8.1	0.78068
	S177	31.32	104.39	1.39372	0.0984	0.328	0.00587	10.41	34.6965	0.86741	2.608	8.69246	0.28067		40	179.5	no	7.676	no	3.09047

Table D - 9: Oxic and anoxic test results for hydroxyapatite prepared in the lab and hydroxyapatite purchased from Sigma Aldrich.

Flask No	Sample N°	C_{Ca} (ppm)	C_{Ca} (mg/L)	C_{Ca} (mmol/L)	C_P (ppm)	C_P (mg/L)	C_P (mmol/L)	Notes	Days	e_h	e_h adjustment	pH	pH adjustment
		ICP	Orig. sol. (dilution f. 3.33)		ICP	Orig. sol. (dilution f. 3.33)							
LTS25	S180	2.808	9.35906	0.23398	17.59	58.6275	1.89304	HAP ref pH 8 150 mV	1	167.8	no	8.061	0.1236
	S186	3.674	12.2454	0.30614	23.94	79.792	2.57643		4	163.3	no	7.951	0.11882
	S192	4.132	13.772	0.3443	25.85	86.1581	2.78198		6	148.4	no	7.818	0.12376
	S198	4.881	16.2684	0.40671	30.22	100.723	3.25228		8	157.5	no	7.674	0.12505
LTS26	S181	5.007	16.6883	0.41721	119.7	398.96	12.8821	HAP 3 pH 8 150 mV g	1	175.5	no	8.113	0.03239
	S187	5.185	17.2816	0.43204	133.5	444.956	14.3673		4	163.9	no	7.962	0.03007
	S193	5.895	19.648	0.4912	132.5	441.623	14.2597		6	157.5	no	7.839	0.03445
	S199	7.868	26.224	0.6556	13.81	460.329	14.8637		8	163.4	no	7.662	0.04411
LTS27	S182	5.47	18.2315	0.45579	131.9	439.623	14.1951	HAP 3 pH 8 150 mV	1	165.2	no	8.192	0.03211
	S188	5.343	17.8082	0.44521	137.3	457.621	14.7763		4	156.4	no	8.071	0.03013
	S194	5.291	17.6349	0.44087	139	463.287	14.9592		6	152.5	no	7.996	0.02947
	S200	5.585	18.6148	0.46537	16.06	535.328	17.2854		8	158.4	no	7.866	0.02692
LTS28	S183	9.507	31.6868	0.79217	3.218	10.7256	0.34632	HAP ref pH 8	1	-	-	5.568	2.28738
	S189	8.86	29.5304	0.73826	2.273	7.57591	0.24462		4	-	-	6.074	3.01797
	S195	7.558	25.1908	0.62977	0.5565	1.85481	0.05989		6	-	-	6.521	10.5153
	S201	18.25	60.8273	1.52068	0.1783	0.59427	0.01919		8	-	-	6.714	79.2488
LTS29	S184	153.9	512.949	12.8237	1.117	3.72296	0.12021	HAP 3 pH 8 g	1	-	-	6.048	106.676
	S190	154.1	513.615	12.8404	0.362	1.20655	0.03896		4	-	-	6.336	329.591
	S196	154	513.282	12.8321	0.0594	0.19798	0.00639		6	-	-	6.858	2007.31
	S202	144.8	482.618	12.0655	0.0883	0.2943	0.0095		8	-	-	7.038	1269.66
LTS30	S185	0.9675	3.22468	0.08062	25.35	84.4916	2.72817	HAP 3 pH 8	1	-	-	7.131	0.02955
	S191	0.6002	2.00047	0.05001	23.78	79.2587	2.55921		4	-	-	7.179	0.01954
	S197	0.3482	1.16055	0.02901	20.37	67.8932	2.19223		6	-	-	7.565	0.01323
	S203	1.466	4.88618	0.12215	18.81	62.6937	2.02434		8	-	-	7.669	0.06034

Table D - 10: Oxic and anoxic test results for scorodite 1.

Flask No	Sample N°	C_{As} (ppm) ICP	C_{As} (ppm)	C_{As} (mmol/L)	C_{Fe} (ppm) ICP	C_{Fe} (ppm)	C_{Fe} (mmol/L)	C_{Ca} (ppm) ICP	C_{Ca} (mg/L)	C_{Ca} (mmol/L)	C_{P} (ppm) ICP	C_{P} (mg/L)	C_{P} (mmol/L)	Notes	Days
LTS 31	SD1-1	0.4176	4.176	0.05568	0.0063	0.063	0.001128	2.112	21.12	0.528	0.0294	0.294	0.009484	SCOR 1 pH 5	1
	SD3-1	1.601	5.336666	0.071156	0.0144	0.048	0.000859	6.789	22.63	0.56575	0.0155	0.051667	0.001667		3
	SD6-1	1.921	6.403333	0.085378	0.0144	0.048	0.000859	7.234	24.11333	0.602833	0.0008	0.002667	8.6E-05		6
LTS 32	SD1-2	1.891	6.303333	0.084044	0.015	0.05	0.000895	3.771	12.57	0.31425	0.0047	0.015667	0.000505	SCOR 1 pH 7	1
	SD3-2	2.317	7.723333	0.102978	0.0155	0.051667	0.000925	1.157	3.856666	0.096417	0.0075	0.025	0.000806		3
	SD6-2	2.107	7.023333	0.093644	0.0079	0.026333	0.000472	5.116	17.05333	0.426333	0.0113	0.037667	0.001215		6
LTS 33	SD1-3	1.272	4.24	0.056533	0.0181	0.060333	0.00108	58.86	196.2	4.905	0.0123	0.041	0.001323	SCOR 1 pH 9	1
	SD3-3	1.563	5.209999	0.069467	0.0167	0.055667	0.000997	60.26	200.8666	5.021666	0.0428	0.142667	0.004602		3
	SD6-3	2.105	7.016666	0.093556	0.0065	0.021667	0.000388	51.67	172.2333	4.305833	0.0023	0.007667	0.000247		6
LTS 34	SD1-4	9.723	32.41	0.432133	0.2986	0.995333	0.017822	0.0859	0.286333	0.007158	0.1591	0.530333	0.017108	SCOR 1 pH 5 150 mV	1
	SD3-4	15.24	50.79999	0.677333	1.354	4.513333	0.080812	0.3619	1.206333	0.030158	0.1839	0.613	0.019774		3
	SD6-4	17.96	59.86666	0.798222	2.024	6.746666	0.1208	5.861	19.53666	0.488417	0.1098	0.366	0.011806		6
LTS 35	SD1-5	11.01	36.7	0.489333	0.2452	0.817333	0.014634	0.0361	0.120333	0.003008	0.0966	0.322	0.010387	SCOR 1 pH 7 150 mV	1
	SD3-5	9.732	32.44	0.432533	0.0389	0.129667	0.002322	0.4866	1.622	0.04055	0.0869	0.289667	0.009344		3
	SD6-5	6.548	21.82666	0.291022	0.0384	0.128	0.002292	75.81	252.7	6.317499	0.0257	0.085667	0.002763		6
LTS 36	SD1-6	13.15	43.83333	0.584444	0.0037	0.012333	0.000221	17.81	59.36667	1.484167	0.0863	0.287667	0.00928	SCOR 1 pH 9 150 mV	1
	SD3-6	18.22	60.73333	0.809778	0.0123	0.041	0.000734	4.094	13.64667	0.341167	0.0735	0.245	0.007903		3
	SD6-6	22.69	75.63333	1.008444	0.0589	0.196333	0.003515	4.599	15.33	0.38325	0.0699	0.233	0.007516		6
LTS 37	SD1-7	0.8118	2.706	0.03608	0.017	0.056667	0.001015	141.1	470.3333	11.75833	0.0185	0.061667	0.001989	SCOR 1 pH 7 g	1
	SD3-7	0.8056	2.685333	0.035804	0.0188	0.062667	0.001122	141	470	11.75	0.0264	0.088	0.002839		3
	SD6-7	0.848	2.826666	0.037689	0.01	0.033333	0.000597	131.8	439.3333	10.98333	0.0184	0.061333	0.001978		6
LTS 38	SD1-8	10.53	35.1	0.468	0.1255	0.418333	0.00749	3.9737	13.24567	0.331142	0.1195	0.398333	0.012849	SCOR 1 pH 7 150 mV g	1
	SD3-8	12.57	41.9	0.558667	0.1399	0.466333	0.00835	5.818	19.39333	0.484833	0.0738	0.246	0.007935		3
	SD6-8	11.33	37.76666	0.503556	0.943	3.143333	0.056282	94.72	315.7333	7.893333	0.0775	0.258333	0.008333		6

Table D - 11: Oxic and anoxic test results for fluoroapatite encapsulated scorodite.

Flask No	Sample N°	C_{As} (ppm) ICP	C_{As} (ppm) ICP	C_{As} (mmol/L) ICP	C_{Fe} (ppm) ICP	C_{Fe} (ppm) ICP	C_{Fe} (mmol/L) ICP	C_{Ca} (ppm) ICP	C_{Ca} (mg/L) Orig. sol. (dilution f. 3.33)	C_{Ca} (mmol/L)	C_P (ppm) ICP	C_P (mg/L) Orig. sol. (dilution f. 3.33)	C_P (mmol/L)	Notes	Days
LTS 39	SD1-9	2.413	8.043333	0.107244	0.0629	0.209667	0.003754	2.36	7.866667	0.196667	2.589	8.63	0.278387	ENCF 4 pH 7	1
	SD3-9	3.557	11.85667	0.158089	0.0079	0.026333	0.000472	3.3	11	0.275	2.867	9.556666	0.30828		3
	SD6-9	4.98	16.6	0.221333	0.0018	0.006	0.000107	4.601	15.33667	0.383417	2.827	9.423332	0.303978		6
LTS 40	SD1-10	1.946	6.486667	0.086489	0.0164	0.054667	0.000979	5.689	18.96333	0.474083	1.168	3.893333	0.125591	ENCF 4 pH 9	1
	SD3-10	2.455	8.183333	0.109111	0.0163	0.054333	0.000973	6.163	20.54333	0.513583	1.767	5.889999	0.19		3
	SD6-10	3.049	10.16333	0.135511	0.0013	0.004333	7.76E-05	6.397	21.32333	0.533083	1.667	5.556666	0.179247		6
LTS 41	SD1-11	10.92	36.4	0.485333	0.0589	0.196333	0.003515	4.309	14.36333	0.359083	7.165	23.88333	0.77043	ENCF 4 pH 7 150 mV g	1
	SD3-11	14.16	47.2	0.629333	0.057	0.19	0.003402	5.021	16.73666	0.418417	7.075	23.58333	0.760753		3
	SD6-11	13.1	43.66666	0.582222	0.0247	0.082333	0.001474	131.9	439.6666	10.99167	5.664	18.88	0.609032		6
LTS 42	SD1-12	10.8	36	0.48	0.0003	0.001	1.79E-05	30.14	100.4667	2.511667	6.613	22.04333	0.711075	ENCF 4 pH 9 150 mV	1
	SD3-12	19.07	63.56666	0.847555	0.0066	0.022	0.000394	4.536	15.12	0.378	6.967	23.22333	0.74914		3
	SD6-12	25.71	85.69999	1.142667	0.0387	0.129	0.00231	4.182	13.94	0.3485	5.961	19.87	0.640968		6
LTS 43	SD1-13	1.713	5.71	0.076133	0.0183	0.061	0.001092	141	470	11.75	0.8546	2.848667	0.091892	ENCF 4 pH 7 g	1
	SD3-13	1.856	6.186666	0.082489	0.0198	0.066	0.001182	141.2	470.6666	11.76667	0.944	3.146666	0.101505		3
	SD6-13	2.359	7.863333	0.104844	0.0023	0.007667	0.000137	131.8	439.3333	10.98333	0.988	3.293333	0.106237		6
LTS 44	SD1-14	9.757	32.52333	0.433644	0.2182	0.727333	0.013023	15.18	50.6	1.265	8.353	27.84333	0.898172	ENCF 4 pH 7 150 mV	1
	SD3-14	13.41	44.7	0.596	0.2306	0.768667	0.013763	7.133	23.77666	0.594417	8.362	27.87333	0.89914		3
	SD6-14	16.87	56.23333	0.749778	0.1845	0.615	0.011012	5.509	18.36333	0.459083	7.191	23.97	0.773226		6
LTS 45	SD1-15	0.6285	2.095	0.027933	0.016	0.053333	0.000955	0.1627	0.542333	0.013558	0.5209	1.736333	0.056011	ENCF 3 pH 7	1
	SD3-15	0.87	2.9	0.038667	0.0143	0.047667	0.000853	0.1265	0.421667	0.010542	0.4671	1.557	0.050226		3
	SD6-15	1.198	3.993333	0.053244	0.0012	0.004	7.16E-05	0.5679	1.893	0.047325	0.4307	1.435667	0.046312		6
	SD10-15	1.273	4.243333	0.056578	0.0112	0.037333	0.000668	1.446	4.82	0.1205	0.296	0.986667	0.031828		10
	SD20-15	0.9628	3.209333	0.042791	0.0006	0.002	3.58E-05	3.292	10.97333	0.274333	0.1635	0.545	0.017581		20
	SD40-15	1.127	3.756666	0.050089	0.0148	0.049333	0.000883	3.002	10.00667	0.250167	0.0998	0.332667	0.010731		40

Table D - 12: Oxic and anoxic test results for fluoroapatite encapsulated scorodite.

Flask No	Sample N°	C_{As} (ppm)	C_{As} (ppm)	C_{As} (mmol/L)	C_{Fe} (ppm)	C_{Fe} (ppm)	C_{Fe} (mmol/L)	C_{Ca} (ppm)	C_{Ca} (mg/L)	C_{Ca} (mmol/L)	C_{P} (ppm)	C_{P} (mg/L)	C_{P} (mmol/L)	Notes	Days
		ICP			ICP			ICP	Orig. sol. (dilution f. 3.33)		ICP	Orig. sol. (dilution f. 3.33)			
LTS 46	SD1-16	0.6706	2.235333	0.029804	0.0151	0.050333	0.000901	0.1014	0.338	0.00845	0.2464	0.821333	0.026495	ENCF 3 pH 9	1
	SD3-16	0.9543	3.181	0.042413	0.0154	0.051333	0.000919	0.2607	0.869	0.021725	0.2514	0.838	0.027032		3
	SD6-16	1.279	4.263333	0.056844	0.0019	0.006333	0.000113	0.6178	2.059333	0.051483	0.1816	0.605333	0.019527		6
	SD10-16	1.53	5.099999	0.068	0.0099	0.033	0.000591	1.744	5.813333	0.145333	0.1063	0.354333	0.01143		10
	SD20-16	2.001	6.669999	0.088933	0.0011	0.003667	6.57E-05	1.491	4.97	0.12425	0.1297	0.432333	0.013946		20
	SD40-16	2.313	7.709999	0.1028	0.0127	0.042333	0.000758	1.362	4.54	0.1135	0.104	0.346667	0.011183		40
LTS 47	SD1-17	1.877	6.256667	0.083422	0.1329	0.443	0.007932	5.231	17.43667	0.435917	1.724	5.746667	0.185376	ENCF 3 pH 7 150 mV	1
	SD3-17	2.947	9.823332	0.130978	0.0644	0.214667	0.003844	7.437	24.79	0.61975	2.461	8.203333	0.264624		3
	SD6-17	3.984	13.28	0.177067	0.1726	0.575333	0.010301	7.537	25.12333	0.628083	2.443	8.143333	0.262688		6
	SD10-17	5.022	16.74	0.2232	0.1962	0.654	0.01171	7.576	25.25333	0.631333	2.737	9.123332	0.294301		10
	SD20-17	6.197	20.65666	0.275422	0.0794	0.264667	0.004739	17.15	57.16666	1.429167	3.507	11.69	0.377097		20
	SD40-17	23.7	78.99999	1.053333	0.4109	1.369667	0.024524	124.4	414.6666	10.36667	150.8	502.6666	16.21505		40
LTS 48	SD1-18	1.882	6.273333	0.083644	0.0093	0.031	0.000555	9.735	32.45	0.81125	0.7967	2.655667	0.085667	ENCF 3 pH 9 150 mV	1
	SD3-18	3.166	10.55333	0.140711	0.0067	0.022333	0.0004	8.655	28.85	0.72125	0.8411	2.803666	0.090441		3
	SD6-18		0	0		0	0		0	0		0	0		6
	SD10-18	5.551	18.50333	0.246711	0.0114	0.038	0.00068	6.481	21.60333	0.540083	0.683	2.276666	0.073441		10
	SD20-18	4.914	16.38	0.2184	0.0012	0.004	7.16E-05	41.04	136.8	3.42	0.4355	1.451667	0.046828		20
	SD40-18	5.966	19.88666	0.265156	0.0109	0.036333	0.000651	41.69	138.9667	3.474166	0.641	2.136666	0.068925		40
LTS 49	SD1-19	1.718	5.726667	0.076356	0.0167	0.055667	0.000997	2.541	8.47	0.21175	0.9884	3.294667	0.10628	ENCF 1 pH 7	1
	SD3-19	2.219	7.396666	0.098622	0.0141	0.047	0.000842	1.815	6.049999	0.15125	1.088	3.626666	0.116989		3
	SD6-19	2.466	8.219999	0.1096	0.0024	0.008	0.000143	4.651	15.50333	0.387583	0.839	2.796666	0.090215		6
	SD10-19	2.696	8.986666	0.119822	0.0114	0.038	0.00068	5.539	18.46333	0.461583	0.7293	2.431	0.078419		10
	SD20-19	3.071	10.23667	0.136489	0.0009	0.003	5.37E-05	6.1	20.33333	0.508333	0.7126	2.375333	0.076624		20
	SD40-19	3.35	11.16667	0.148889	0.004	0.013333	0.000239	5.798	19.32666	0.483167	0.5282	1.760666	0.056796		40

Table D - 13: Oxic and anoxic test results for fluoroapatite encapsulated scorodite.

Flask No	Sample N°	C_{As} (ppm) ICP	C_{As} (ppm)	C_{As} (mmol/L)	C_{Fe} (ppm) ICP	C_{Fe} (ppm)	C_{Fe} (mmol/L)	C_{Ca} (ppm) ICP	C_{Ca} (mg/L) Orig. sol. (dilution f. 3.33)	C_{Ca} (mmol/L)	C_{P} (ppm) ICP	C_{P} (mg/L) Orig. sol. (dilution f. 3.33)	C_{P} (mmol/L)	Notes	Days
LTS 50	SD1-20	1.525	5.083333	0.067778	0.0186	0.062	0.00111	140.9	469.6667	11.74167	0.6715	2.238333	0.072204	ENCF 1 pH 7 g	1
	SD3-20	1.527	5.089999	0.067867	0.0158	0.052667	0.000943	140.8	469.3333	11.73333	0.5674	1.891333	0.061011		3
	SD6-20	1.444	4.813333	0.064178	0.0015	0.005	8.95E-05	131.8	439.3333	10.98333	0.3635	1.211667	0.039086		6
	SD10-20	1.323	4.41	0.0588	0.0125	0.041667	0.000746	132	440	11	0.368	1.226667	0.03957		10
	SD20-20	1.389	4.63	0.061733	0.001	0.003333	5.97E-05	145.1	483.6666	12.09167	0.3247	1.082333	0.034914		20
	SD40-20	1.492	4.973333	0.066311	0.0118	0.039333	0.000704	124.4	414.6666	10.36667	0.2705	0.901667	0.029086		40
LTS 51	SD1-21	6.054	20.18	0.269067	0.0995	0.331667	0.005939	0.1908	0.636	0.0159	2.443	8.143333	0.262688	ENCF 1 pH 7 150 mV	1
	SD3-21	8.324	27.74666	0.369956	0.176	0.586667	0.010504	0.2689	0.896333	0.022408	2.607	8.689999	0.280323		3
	SD6-21	10.75	35.83333	0.477778	0.1551	0.517	0.009257	0.9428	3.142666	0.078567	2.424	8.079999	0.260645		6
	SD10-21	7.032	23.44	0.312533	0.218	0.726667	0.013011	112.9	376.3333	9.408332	1.417	4.723333	0.152366		10
	SD20-21	3.924	13.08	0.1744	0.1524	0.508	0.009096	144.8	482.6666	12.06667	0.7215	2.405	0.077581		20
	SD40-21	3.917	13.05667	0.174089	0.0948	0.316	0.005658	124.5	415	10.375	0.6377	2.125666	0.06857		40
LTS 52	SD1-22	5.252	17.50667	0.233422	0.0181	0.060333	0.00108	3.8	12.66667	0.316667	1.796	5.986667	0.193118	ENCF 1 pH 7 150 mV g	1
	SD3-22	7.737	25.79	0.343867	0.0621	0.207	0.003706	4.577	15.25667	0.381417	2.117	7.056666	0.227634		3
	SD6-22	10.79	35.96666	0.479556	0.2771	0.923667	0.016538	5.634	18.78	0.4695	2.03	6.766666	0.21828		6
	SD10-22	8.021	26.73666	0.356489	0.2016	0.672	0.012032	131.9	439.6666	10.99167	1.77	5.899999	0.190323		10
	SD20-22	6.025	20.08333	0.267778	0.0496	0.165333	0.00296	0.7128	2.376	0.0594	0.7128	2.376	0.076645		20
	SD40-22	5.199	17.33	0.231067	0.0394	0.131333	0.002352	124.4	414.6666	10.36667	0.5135	1.711666	0.055215		40
LTS 53	SD1-2R	0.9476	3.158667	0.042116	0.0166	0.055333	0.000991	3.525	11.75	0.29375	0.006	0.02	0.000645	SCOR 1 pH 7	1
	SD3-2R	1.843	6.143333	0.081911	0.0152	0.050667	0.000907	2.861	9.536666	0.238417	0.0029	0.009667	0.000312		3
	SD6-2R	2.387	7.956666	0.106089	0.0019	0.006333	0.000113	3.43	11.43333	0.285833	0.0055	0.018333	0.000591		6
LTS 54	SD1-5R	11.07	36.9	0.492	0.2897	0.965667	0.01729	0.141	0.47	0.01175	0.1155	0.385	0.012419	SCOR 1 pH 7 150 mV	1
	SD3-5R	9.604	32.01333	0.426844	0.0328	0.109333	0.001958	1.214	4.046666	0.101167	0.1979	0.659667	0.02128		3
	SD6-5R	8.901	29.67	0.3956	0.0953	0.317667	0.005688	131.8	439.3333	10.98333	0.054	0.18	0.005806		6
LTS 55	SD1-18R	1.579	5.263333	0.070178	0.1212	0.404	0.007234	4.494	14.98	0.3745	1.446	4.82	0.155484	ENCF 3 pH 9 150 mV	1
	SD3-18R	2.651	8.836666	0.117822	0.163	0.543333	0.009728	5.631	18.77	0.46925	2.126	7.086666	0.228602		3
	SD6-18R	3.115	10.38333	0.138444	0.0016	0.005333	9.55E-05	4.739	15.79667	0.394917	0.5071	1.690333	0.054527		6
	SD10-18R	3.365	11.21667	0.149556	0.0106	0.035333	0.000633	7.091	23.63666	0.590917	0.2731	0.910333	0.029366		10
	SD20-18R	3.868	12.89333	0.171911	0.0007	0.002333	4.18E-05	144.9	483	12.075	0.4114	1.371333	0.044237		20
	SD40-18R	3.7	12.33333	0.164444	0.0074	0.024667	0.000442	124.5	415	10.375	0.2207	0.735667	0.023731		40

Appendix E. pH and e_h variation graphs for stability tests

The adjustment of pH or e_h was limited to cases when the measured value had extremely deviated from the initial value or the immediate last. Otherwise the addition of reagents was avoided so as to not interfere with the equilibrium of the solution.

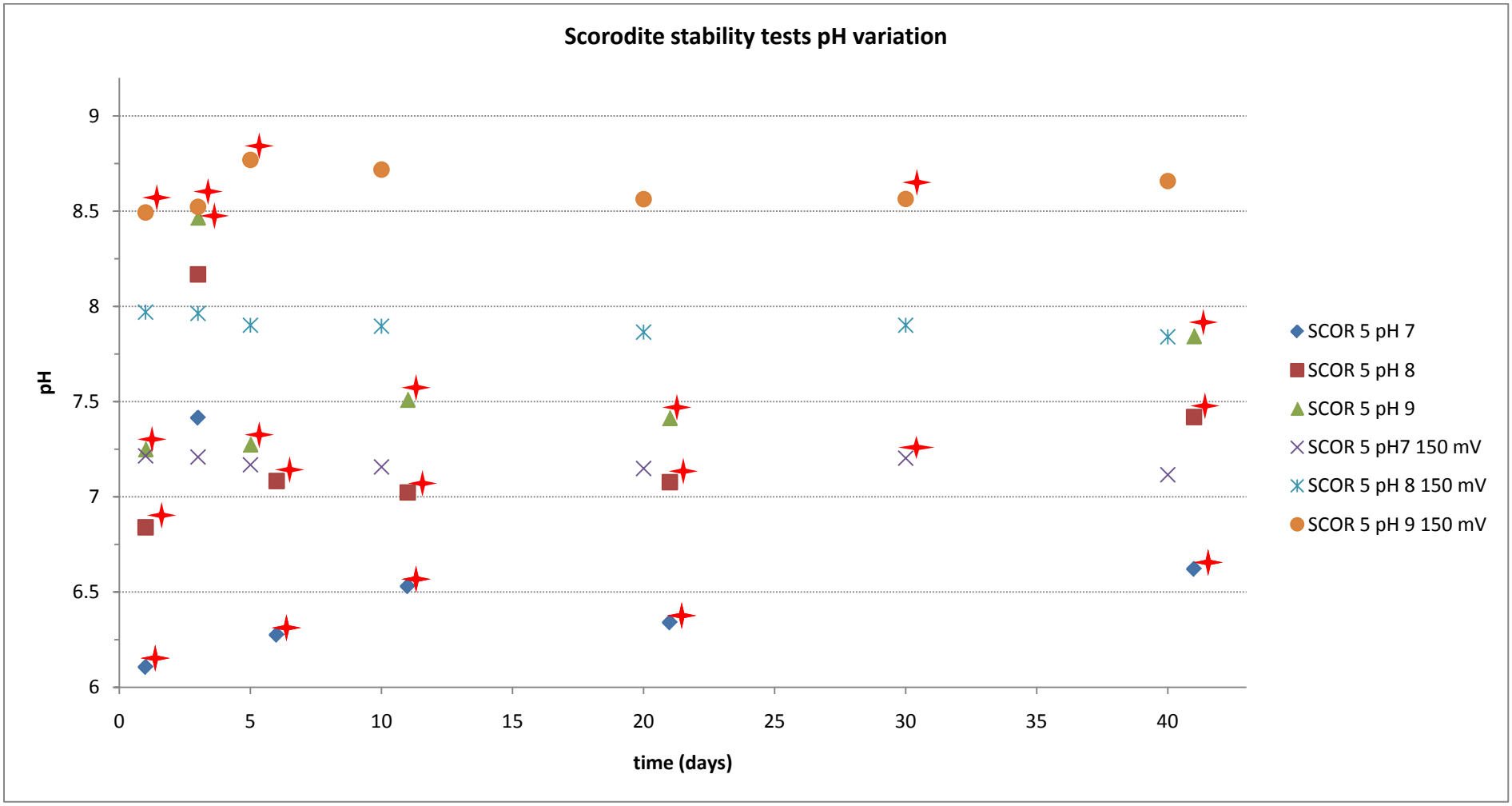

Figure E - 1: pH values measured for the scorodite stability tests. With a four-point red star on the top right are marked the measurements for which the pH was adjusted so that it would be closer to the starting value.

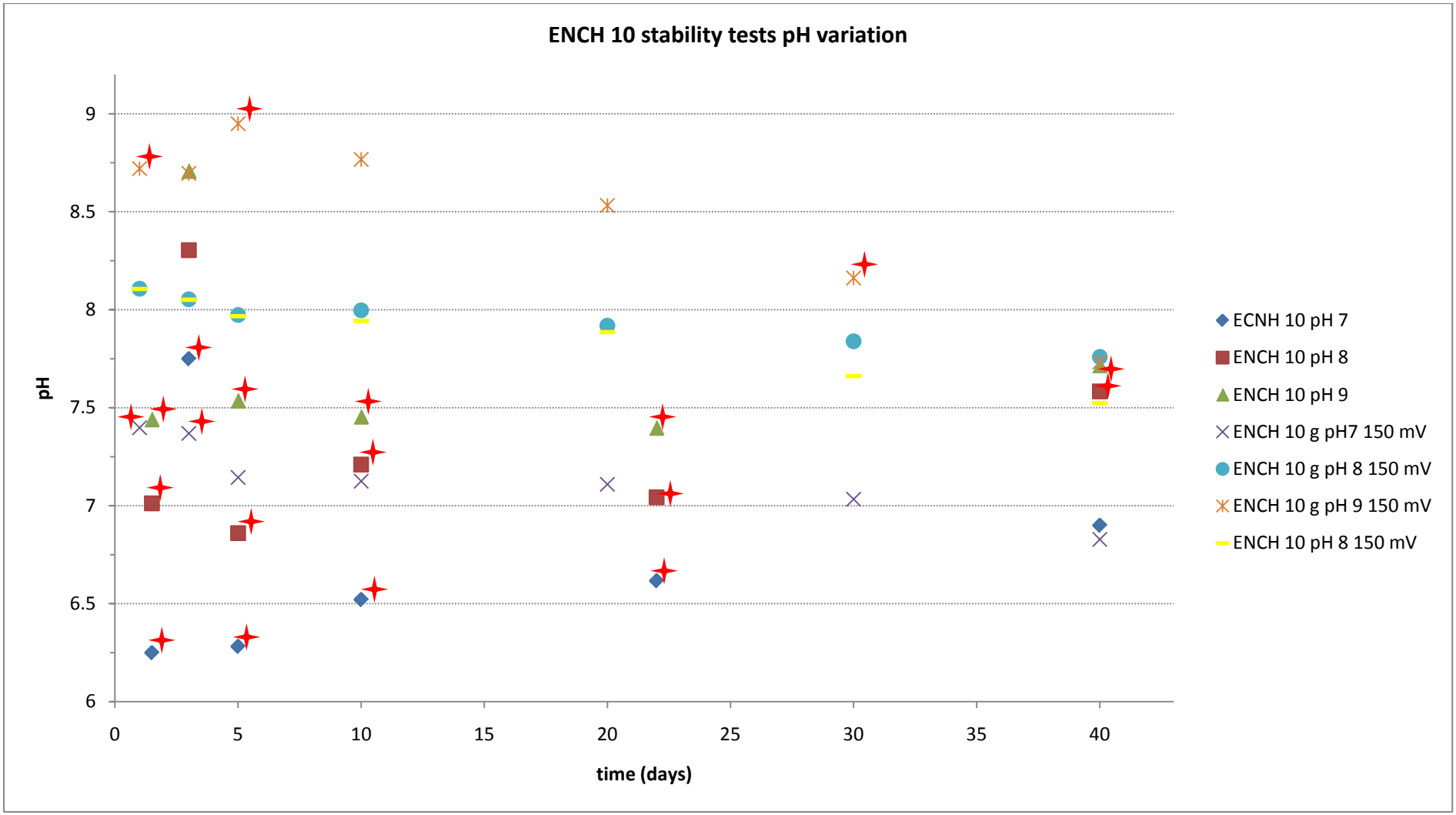

Figure E - 2: pH values measured for the ENCH 10 stability tests. With a four-point red star on the top right are marked the measurements for which the pH was adjusted so that it would be closer to the starting value.

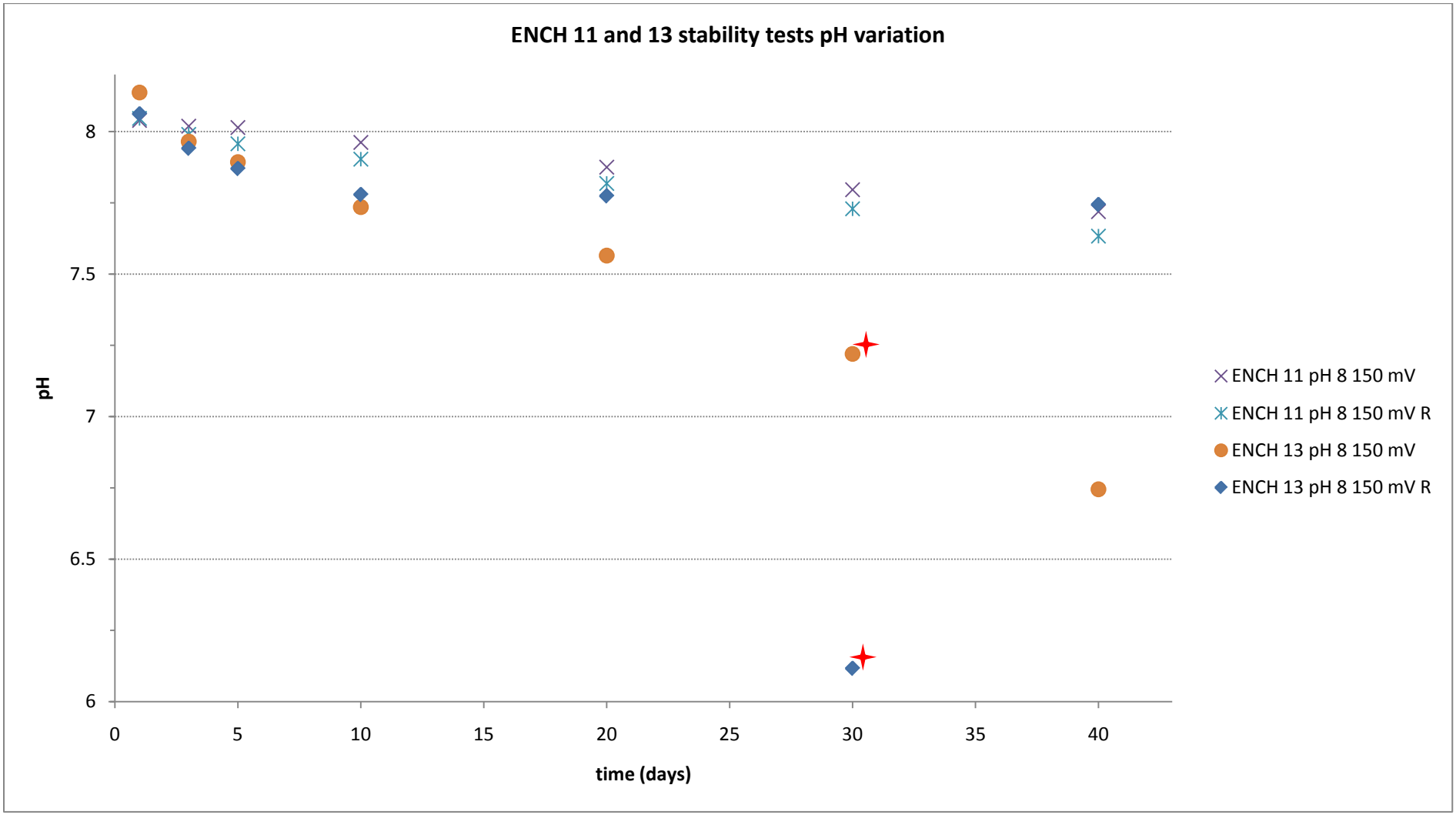

Figure E - 3: pH values measured for the ENCH 11 and 13 stability tests. With a four-point red star on the top right are marked the measurements for which the pH was adjusted so that it would be closer to the starting value.

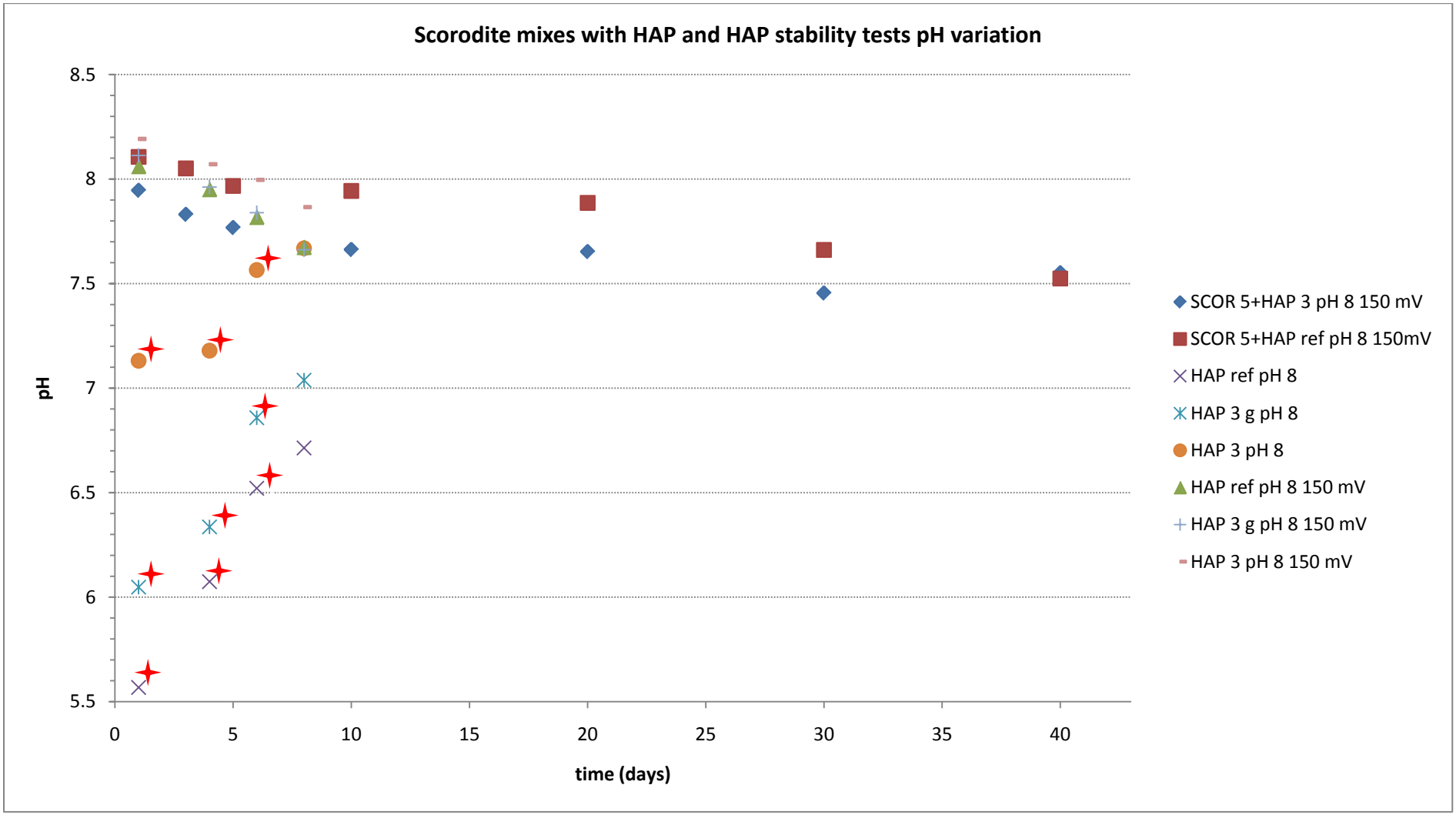

Figure E - 4: pH values measured for the scorodite mixtures with HAP and HAP only stability tests. With a four-point red star on the top right are marked the measurements for which the pH was adjusted so that it would be closer to the starting value.

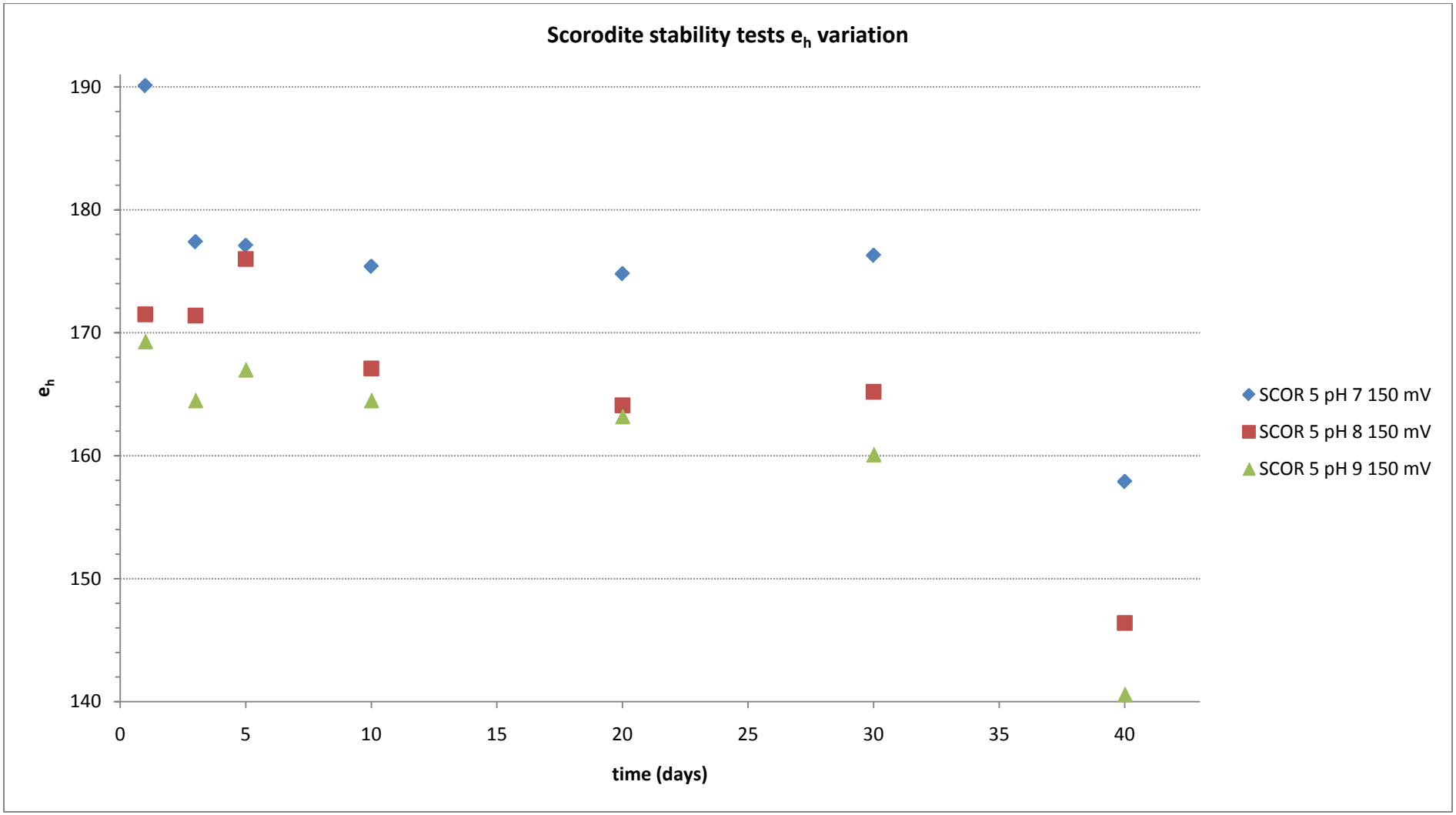

Figure E - 5: e_h values measured for the scorodite stability tests.

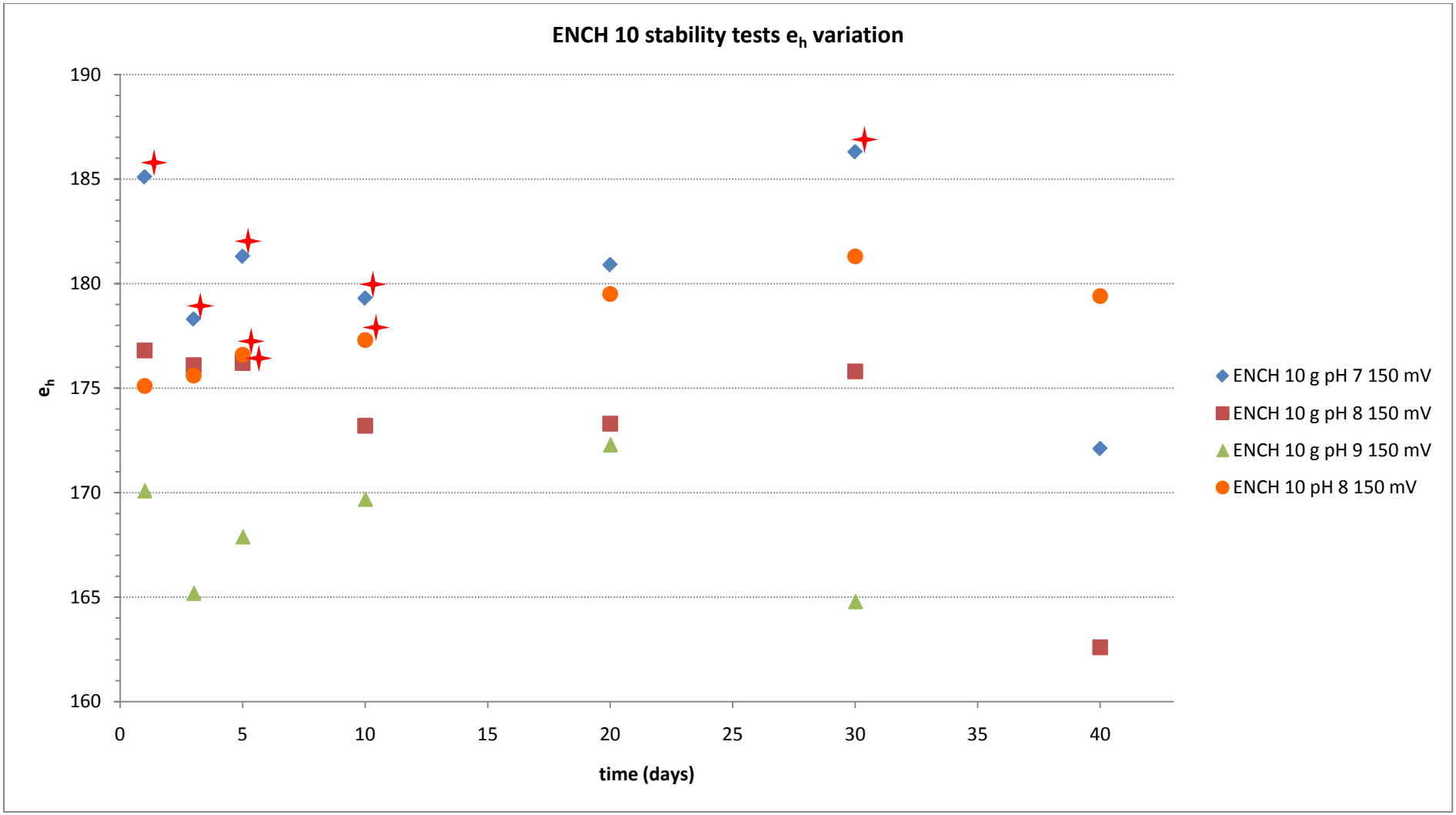

Figure E - 6: e_h values measured for the ENCH 10 stability tests. With a four-point red star on the top right are marked the measurements for which the pH was adjusted so that it would be closer to the starting value.

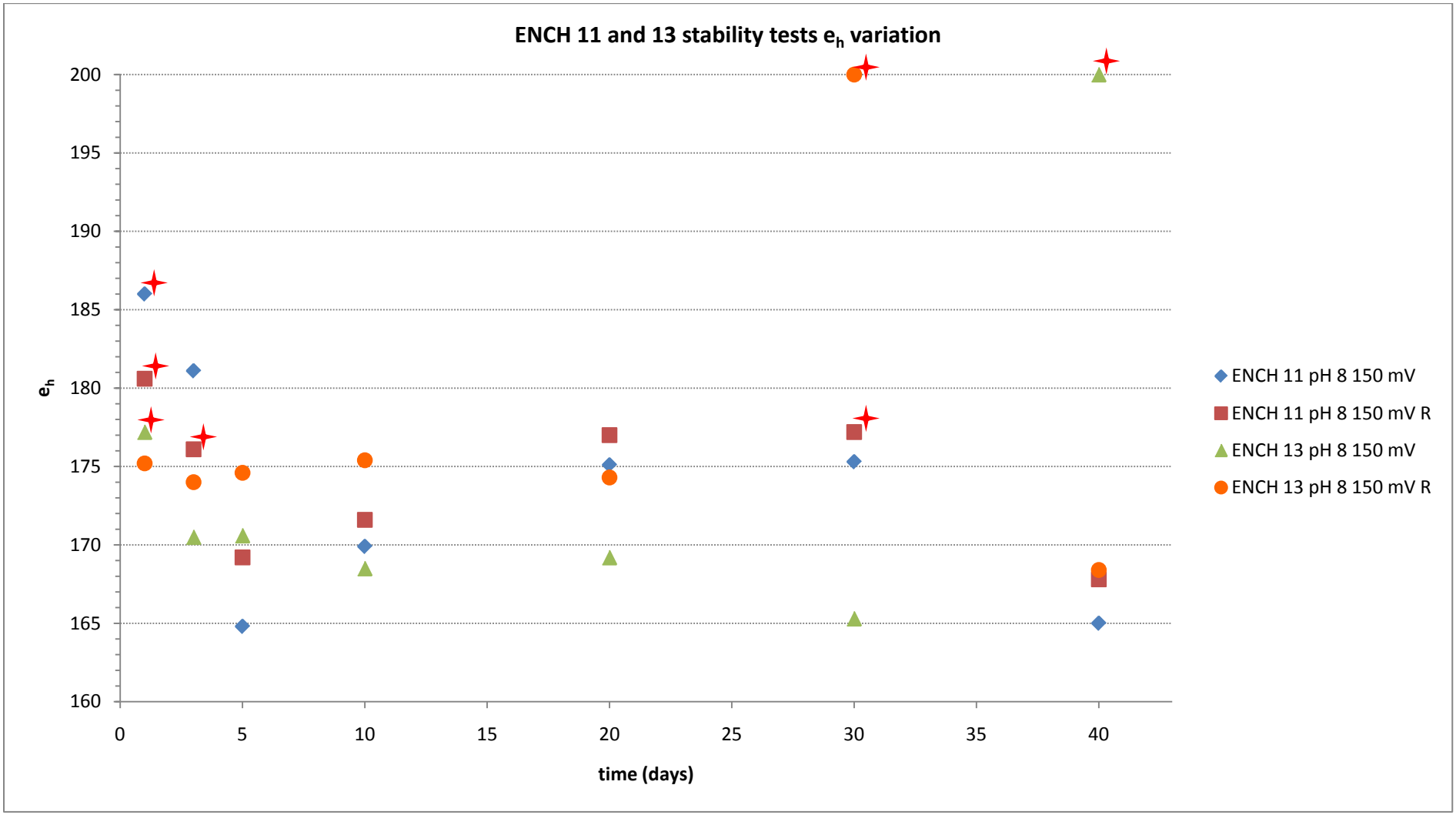

Figure E - 7: e_h values measured for the ENCH 11 and 13 stability tests. With a four-point red star on the top right are marked the measurements for which the pH was adjusted so that it would be closer to the starting value.

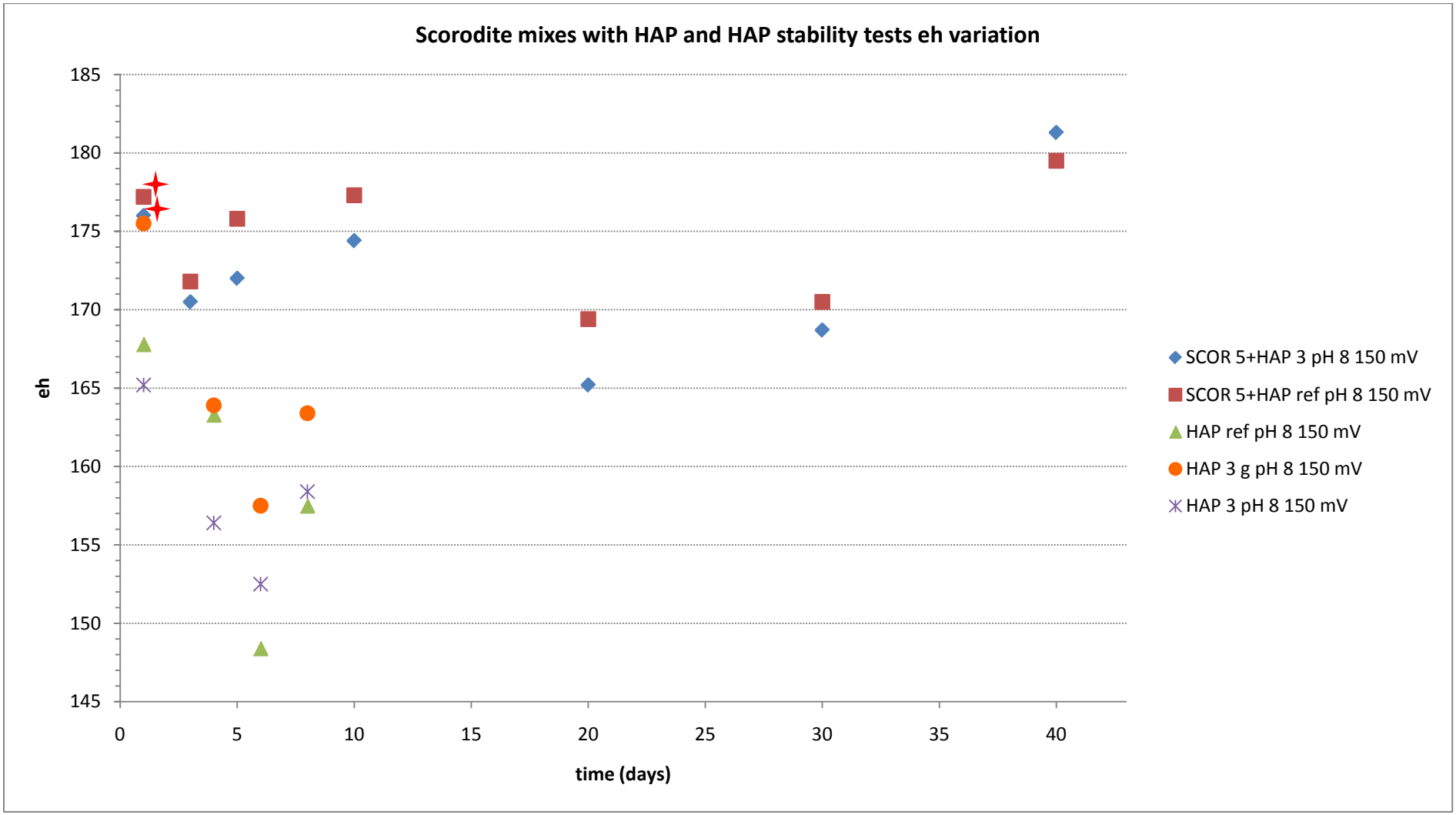

Figure E - 8: e_h values measured for the scorodite mixtures with HAP and HAP only stability tests. With a four-point red star on the top right are marked the measurements for which the pH was adjusted so that it would be closer to the starting value.

Appendix F. Onomatology and organisation of the experiments

For the homogeneous precipitation experiments the first word is the compound that is meant to be precipitated in the experiment:

- HAP for hydroxyapatite
- FAP for fluoroapatite
- SCOR for scorodite

Then a number follows. Example: HAP 3 is the 3rd experiment for the homogeneous precipitation of hydroxyapatite.

The encapsulation experiments are denoted by the letters ENC followed by the letter H or F, that represent the use of hydroxyapatite or fluoroapatite for the encapsulation respectively. Then the increasing number correspondent to the number of the experiment follows. When the experimental set is made up of multiple experimental steps a dot and the number of the step follow the first number. For example: ENCH 10.5 is the 5th step of the 10th experimental set of encapsulation with hydroxyapatite. For each experimental set the scorodite used is the same throughout the set. Therefore the scorodite used for ENCH 10.1, was separated from the liquid and used for ENCH 10.2, etc., but for ENCH 11 fresh scorodite was used.